TABLE OF CONTENTS

TABLE OF CONTENTS
(Continued)

TABLE OF CONTENTS
(Continued)

LIST OF TABLES

LIST OF FIGURES

LIST OF FIGURES (Continued)

3 REACTOR

3.1 DESIGN BASIS

3.1.1 PERFORMANCE OBJECTIVES.

The reactor core is a three-region cycled core. The fuel rods are cold worked partially annealed Zircaloy tubes containing slightly enriched uranium dioxide fuel. All fuel rods are pressurized with helium during fabrication to reduce stresses and strains and to increase fatigue life. A more detailed discussion is given in Reference 1.

The fuel assembly consists of the rod cluster control (RCC) guide thimbles fastened to the grids and the top and bottom nozzles. The fuel rods are held in this assembly at seven points along their length by spring-clip grids which provide a very stiff support for the fuel rods.

The Turkey Point Units are loaded with Westinghouse 15 x 15 Optimized Fuel Assemblies (OFA). Previously, Westinghouse Low Parasitic Fuel (LOPAR) was used. The main design difference is the use of Zircaloy-4 in the manufacture of the five intermediate support grids in the OFA. The top and bottom grids (non-mixing) will continue to be manufactured using Inconel which has been used for all seven grids in the LOPAR assemblies. Beginning with Unit 3 Cycle 12 and Unit 4 Cycle 13, Debris Resistant Fuel Assemblies (DRFA) have been loaded. DRFA's are essentially the same as OFA's, except for a long end plug on the bottom of each fuel rod. This longer end plug prevents debris from fretting through the fuel rod cladding below the bottom spacer grid. Details and analysis of the DRFA design are provided in Reference 8.

Full length rod cluster control assemblies (RCCA), secondary sources, thimble plug devices and burnable poison rods are inserted into the guide thimbles of the fuel assemblies. The absorber sections of the control rods are fabricated of silver-indium-cadmium alloy sealed in stainless steel tubes. The absorber material in the fixed burnable poison rods is in the form of borosilicate glass sealed in stainless steel tubes.

Three other types of burnable poison rods and absorbers are employed:

a) Wet Annular Burnable Absorbers (WABA)[2], each consisting of an aluminum oxide-boron carbide annulus sealed in Zircaloy, and

b) Reduced length Annular Hafnium Vessel Flux Depression (HVFD) absorbers which may be placed in peripheral assemblies as part of the flux reduction program.[3]

c) Integral Fuel Burnable Absorbers (IFBA)[4], consisting of a Zirconium diboride coating on the surface of the fuel pellets.

Evaluations [5] have been performed to support the complete or partial removal of thimble plugs from Turkey Point Units 3 & 4. These evaluations have addressed the effect of thimble plug removal on core design, core thermal hydraulics, reactor pressure vessel system thermal hydraulics and the non-LOCA and LOCA safety analyses. Based on these evaluations, it has been determined that it is acceptable to remove all or any combination of thimble plugs from Turkey Point Units 3 & 4. In addition, the secondary sources have been removed from Turkey Point Units 3 & 4 (References 6 and 7, respectively)

The control rod drive mechanisms for the RCC assemblies are of the magnetic latch type. The latches are controlled by three magnetic coils. They are so designed that upon a loss of power to the coils, the RCC assembly is released and falls by gravity to shut down the reactor.

The mechanisms for the former part length rod cluster control assemblies have been immobilized in a fully withdrawn position. Two of these positions have been modified to accommodate the installation of heated junction thermocouple probes for the Reactor Vessel Level Monitoring System (RVLMS).

Turkey Point Units 3 & 4 have made a transition from all-LOPAR fuel cores to all-OFA/DRFA fuel cores with the exception that LOPAR fuel assemblies, once removed from the reactor core, may be re-inserted to meet cycle specific energy requirements and to enhance fuel efficiency.

REFERENCES, SECTION 3.1.1

1. WCAP-9002 (2/69), "Use of Internally Pressurized Fuel Rods in Westinghouse Pressurized Water Reactors", PROPRIETARY. A NON-PROPRIETARY version of this report is WCAP-7855.

2. Letter from Thomas, C.D., NRC, to Rahe, E.P., Westinghouse, Subject: Acceptance for Referencing of Licensing Topical Report WCAP-10021 (P), Revision 1, and WCAP-10377 (NP), "Westinghouse Wet Annular Burnable Absorber Evaluation Report", August 9, 1983.

3. Letter from Uhrig, R.E., FP&L to Varga, S.A., NRC, Subject: Pressurized Thermal Shock, Letter No L-83-180, March 25, 1983.

4. WCAP-10444 Addendum 1 (NP) "Reference Core Report Vantage 5 Fuel Assembly," via Westinghouse transmittal letter NS-NRC-85-3090, December 23, 1985, to Standardization and Special Projects Directorate, U.S.N.R.C.

5. Westinghouse Letter #87FP*-G-0052, "Evaluation Report for Thimble Plug Removal for Turkey Point Units 3 & 4", December 18, 1987.

6. PCM-91-072, "Turkey Point Unit 3 Removal of Startup Sources," July 11. 1991.

7. PCM-91-043, "Turkey Point Unit 4 Removal of Startup Sources," July 11, 1991.

8. WCAP-12346, Turkey Point Units 3 and 4, 15x15 Debris Resistant Fuel Assembly Design Report, July 1989.

3.1.2 PRINCIPAL DESIGN CRITERIA

Reactor Core Design

Criterion: The reactor core with its related controls and protection systems shall be designed to function throughout its design lifetime without exceeding acceptable fuel damage limits which have been stipulated and justified. The core and related auxiliary system designs shall provide this integrity under all expected conditions of normal operation with appropriate margins for uncertainties and for specified transient situations which can be anticipated (1967 Proposed GDC 6)

The reactor core, with its related control and protection system, is designed to function throughout its design lifetime without exceeding fuel limits specified to preclude damage. The core design, together with reliable process and decay heat removal systems, provides for this capability under all expected conditions of normal operation with appropriate margins for uncertainties and anticipated transient situations, including, as examples, the effects of the loss of reactor coolant flow (Section 14.1.9), loss of external electrical load (Section 14.1.10), loss of normal feedwater flow (Section 14.1.11) and loss of non-emergency A.C. power to the plant auxiliaries (Section 14.1.12).

The Reactor Control and Protection system is designed to actuate a reactor trip for any anticipated combination of plant conditions, when necessary, to ensure a minimum Departure from Nucleate Boiling (DNB) ratio greater than or equal to the DNBR limit of the applicable DNB correlation. The integrity of the fuel cladding is ensured by preventing excessive fuel swelling, excessive clad heating, and excessive cladding stress and strain. This is achieved by designing the fuel rods so that the following conservative limits are not exceeded during normal operation or any anticipated transient condition:

a) Minimum DNB ratio equal to or greater than the DNBR limit of the applicable DNB correlation.

b) Fuel Center temperature below melting point of UO_2.

c) Clad stresses less than the Zircaloy yield strength (as irradiated).

d) Clad strain less than 1%.

e) Cumulative fatigue life shall not exceed the design failure life design strain (as irradiated).

f) The internal gas pressure of the lead rod in the reactor is maintained below a value that could cause (1) the diametral gap to increase due to outward clad creep during steady-state operations and (2) extensive DNB propagation DNB propagation to occur.

The ability of fuel designed and operated to these criteria to withstand postulated normal service conditions is described in this chapter. Abnormal service conditions as shown by analyses are presented in Chapter 14 to substantiate that the demands of plant operation are well within applicable regulatory limits.

The reactor coolant pumps have sufficient rotational inertia to maintain an adequate flow coastdown in the event of a simultaneous loss of power to all pumps. The flow coastdown inertia is sufficient such that the reduction in heat flux obtained with a low flow reactor trip prevents core damage.

In the unlikely event of a turbine trip from full power without immediate reactor trip, the subsequent reactor coolant temperature increase and volume insurge to the pressurizer results in a high pressurizer pressure trip and thereby prevents fuel damage from this transient. A loss of external electrical load is controlled by RCCA insertion together with a controlled steam dump to the condenser and atmosphere to prevent a large temperature and pressure increase in the Reactor Coolant System. In this case, trip signals due to overpower delta-T, overtemperature delta-T, high pressurizer pressure or water lever, and low-low steam generator water level would guard against any combination of pressure, temperature and power which could result in a DNB ratio less than the DNBR limit of the applicable DNB correlation during the course of the transient. Details of this event are described in FSAR Section 14.1.10.

In neither the turbine trip nor the loss-of-flow events do the changes in coolant conditions cause a nuclear power excursion because of the large system thermal inertia and relatively small void fraction. Protection circuits actuated directly by the coolant conditions identified with core limits will prevent core damage.

Suppression of Power Oscillations

Criterion: The design of the reactor core with its related controls and protection systems shall ensure that power oscillations, the magnitude of which could cause damage in excess of acceptable fuel damage limits, are not possible or can be readily suppressed. (1967 Proposed GDC 7)

The potential for possible spatial oscillations of power distribution for this core has been reviewed. It is concluded that low frequency xenon oscillations, which may occur in the axial direction, can be controlled by control rod movement. The core is expected to be stable to xenon oscillations in the X-Y dimension. Excore instrumentation is provided to obtain necessary information concerning power distribution. This instrumentation is adequate to enable the operator to monitor and control xenon induced oscillations. (Incore instrumentation is used to periodically calibrate and verify the information provided by the excore instrumentation). The analysis, detection and control of these oscillations is discussed in reference (3) of Section 3.2.1.

Redundancy of Reactivity Control

Criterion: Two independent reactivity control systems, preferably of different principles, shall be provided. (1967 Proposed GDC 27)

Two independent reactivity control systems are provided, one involving rod cluster control assemblies (RCCA) and the other involving chemical shimming. The control rod system provides the minimum shutdown margin under Condition I events and is capable of making the core subcritical rapidly enough to prevent exceeding acceptable fuel damage limits assuming that the highest worth control rod is stuck in the fully withdrawn position.

The boron system can compensate for all xenon burnout reactivity changes and will maintain the reactor in cold shutdown.

Reactivity Hot Shutdown Capability

Criterion: The reactivity control systems provided shall be capable of making and holding the core subcritical from any hot standby or hot operating condition. (1967 Proposed GDC 28)

The two reactivity control systems provided are capable of making and holding the core subcritical from any hot standby or hot operating condition, including those resulting from power changes. The maximum excess reactivity expected for the core occurs for the cold, clean condition at the beginning of life of the initial core.

The Rod Cluster Control Assemblies (RCCA) are divided into two categories comprising control and shutdown groups. The control banks used in combination with chemical shim control provide control of the reactivity changes of the core throughout the life of the core at power conditions. This group of RCCA's is used to compensate for short term reactivity changes at power that might be produced due to variations in reactor power level or in coolant temperature. The chemical shim control is used to compensate for the more slowly occurring changes in reactivity throughout core life such as those due to fuel depletion and fission product buildup.

Reactivity Shutdown Capability

Criterion: One of the reactivity control systems provided shall be capable of making the core subcritical under any anticipated operating condition (including anticipated operational transients) sufficiently fast to prevent exceeding acceptable fuel damage limits. Shutdown margin should assure subcriticality with the most reactive control rod fully withdrawn. (1967 Proposed GDC 29)

The reactor core, together with the reactor control and protection system is designed so that the minimum allowable DNBR is greater than or equal to the DNBR limit of the DNB correlation being used, and there is no fuel melting during normal operation including anticipated transients.

The shutdown groups are provided to supplement the control groups of RCCA's to make the reactor at least one percent subcritical at the hot, zero power condition (k_{eff} = 0.99) following a trip from the most credible operating condition assuming the most reactive RCCA remains in the fully withdrawn position.

The negative reactivity worth of all the RCCAs, assuming the most reactive RCCA remains in the fully withdrawn position, is not sufficient to maintain the core subcritical for the most severe anticipated cooldown transient associated with a single active failure e.g., accidental opening of a steam bypass, or a safety valve stuck open. In this transient the core may become critical and return to power; however, the core is ultimately shutdown with a combination of RCCA's and automatic boron addition via the emergency core cooling system with the most reactive RCCA's assumed to be fully withdrawn. Manually controlled boric acid addition is used to maintain the shutdown margin for the long term conditions of xenon decay and plant cooldown.

Reactivity Holddown Capability

Criterion: The reactivity control systems provided shall be capable of making the core subcritical under credible accident conditions with appropriate margins for contingencies and limiting any subsequent return to power such that there will be no undue risk to the health and safety of the public. (1967 Proposed GDC 30)

Initial reactivity shutdown capability is provided within 2.4 seconds following a trip signal by control rods with boric acid injection used to limit any subsequent return to power and to compensate for the long term xenon decay transient and for plant cooldown. As discussed in the previous paragraph the combined shutdown capability of the RCCAs and boron addition limits the return to power and results in no undue risk to the health and safety of the public as a result of the cooldown associated with a safety valve stuck fully open.

Any time that the reactor is at power, the quantity of boric acid retained in the boric acid tanks and ready for injection always exceeds that required to support a cooldown to cold shutdown conditions without letdown. Under these conditions, adequate boration can be achieved simply by providing makeup for coolant contraction from a boric acid tank and the refueling water storage tank. The minimum volume maintained in the boric acid tanks, therefore, is that volume necessary to increase the RCS boron concentration during the early phase of the cooldown of each unit such that subsequent use of the refueling water storage tank for contraction makeup will maintain the required shutdown margin throughout the remaining cooldown. In addition, the boric acid tanks have sufficient boric acid solution to achieve cold shutdown for each unit if the most reactive RCCA is not inserted. This quantity also exceeds that required to bring the reactor to hot standby and to compensate for subsequent xenon decay.

Boric acid is pumped from the boric acid tanks by one of two boric acid transfer pumps to the suction of one of three charging pumps which inject boric acid into the reactor coolant. Any charging pump and either boric acid transfer pump can be operated from diesel generator power on loss of offsite power. Boric acid can be injected by one pump at a rate which takes the reactor to hot standby with no rods inserted in less than forty minutes when a feed and bleed process is utilized (less than 30 minutes when the available pressurizer volume is utilized). In forty additional minutes, enough boric acid can be injected to compensate for xenon decay although xenon decay below the equilibrium operating level does not begin until approximately 15 hours after shutdown. If two boric acid pumps are available, these time periods are reduced. Additional boric acid injection is employed if it is desired to bring the reactor to cold shutdown conditions.

On the basis of the above, the injection of boric acid is shown to afford backup reactivity shutdown capability, independent of control rod clusters which normally serve this function in the short term situation. Shutdown for long term and reduced temperature conditions can be accomplished with boric acid injection using redundant components, thus achieving the measure of reliability implied by the criterion.

Alternately, boric acid solution at lower concentration can be supplied from the refueling water tank. This solution can be transferred directly by the charging pumps. The reduced boric acid concentration lengthens the time required to achieve equivalent shutdown.

If pressure is reduced in the primary system, a second alternative method comprises the injection of boric acid solution by operation of the safety injection pumps, taking suction from the refueling water storage tank.

Reactivity Control Systems Malfunction

Criterion: The reactor protection systems shall be capable of protecting against any single malfunction of the reactivity control system, such as unplanned continuous withdrawal (not ejection or dropout) of a control rod, by limiting reactivity transients to avoid exceeding acceptable fuel damage limits. (1967 Proposed GDC 31)

The reactor protection systems are capable of protecting against any single anticipated malfunction of the reactivity control system, by limiting reactivity transients to avoid exceeding fuel limits specified to preclude damage. (1967 Proposed GDC 6).

Reactor shutdown with rods is completely independent of the normal rod control functions since the trip breakers completely interrupt the power to the latch type rod mechanisms regardless of existing control signals.

Details of the effects of continuous withdrawal of a control rod and continuous deboration are described in Sections 14.1.1, 14.1.2 and 14.1.5, respectively.

Maximum Reactivity Worth of Control Rods

Criterion: Limits, which include reasonable margin, shall be placed on the maximum reactivity worth of control rods or elements and on rates at which reactivity can be increased to ensure that the potential effects of a sudden or large change of reactivity cannot (a) rupture the reactor coolant pressure boundary or (b) disrupt the core, its support structures, or other vessel internals sufficiently to lose capability of cooling the core. (1967 Proposed GDC 32)

Limits, which include margin, are placed on the maximum reactivity worth of control rods or elements and on rates at which reactivity can be increased to ensure that the potential effects of a sudden or large reactivity change cannot (a) rupture the reactor coolant pressure boundary, or (b) disrupt the core, its support structures, or other vessel internals so as to lose capability to cool the core.

The reactor control system employs RCCA's approximately half of which are fully withdrawn during power operation, serving as shutdown rods. The remaining rods comprise the control groups which are used to control load and reactor coolant temperature. The full length rod cluster drive mechanisms are wired into preselected groups, and are therefore prevented from being withdrawn in other than their respective groups. The rod drive mechanism is of the magnetic latch type and the coil actuation is sequenced to provide variable speed rod travel.

The maximum reactivity insertion rate assumed in the RCCA Withdrawal safety analysis bounds the rate corresponding to the maximum differential rod worth for two overlapping groups moving together in the highest worth region of the core. The assumed maximum reactivity insertion rate is well within the capability of the overpower-overtemperature protection circuits to prevent core damage.

No single mechanical or electrical control system malfunction can cause a rod cluster to be withdrawn at a speed greater than 77 steps per minute (48 inches per minute). This represents the maximum theoretical limit. However, the nominal maximum design limit of 72 steps per minute is used in the design calculation.

3.1.3 DESIGN OBJECTIVES

The reactor is capable of meeting the performance objectives throughout core life under both steady state and transient conditions without violating the integrity of the fuel cladding. Thus the release of unacceptable amounts of fission products to the coolant is prevented.

The limiting conditions discussed below are the highest functional capacity or performance levels for the nuclear, control, thermal and hydraulic, and mechanical aspects of design permitted to assure safe operation of the facility.

Nuclear

At a full power level (license application power) the nuclear heat flux hot channel factor, F, specified in Table 3.2.1-1, Line 18, is not exceeded.

The nuclear axial peaking factor F, and the nuclear enthalpy rise hot channel factor $F^N_{\Delta H}$ are limited in their combined relationship so as not to exceed the F_q or DNBR limits.

The limiting nuclear hot channel factors are higher than those calculated at full power for the range from all control rods fully withdrawn to maximum allowable control rod insertion. Control rod insertion limits as a function of power are delineated in the Core Operating Limits Report in Appendices 14A and 14B for Units 3 and 4 respectively to ensure that hot channel factors do not exceed those specified in Table 3.2.1-1 at lower power levels due to control rod insertion and that the DNB ratio is always greater at part power than at full power.

The protection system ensures that the nuclear core limits are not exceeded.

Reactivity Control

The control system and the operational procedures provide adequate control of the core reactivity and power distribution. The following criteria are met:

a) Sufficient control is available to produce a hot shutdown margin of at least 1% Δ k/k. The minimum hot shutdown margin required by Technical Specifications is available assuming at least a 7% uncertainty in control rod worth.

b) The shutdown margin is maintained with the most reactive RCCA stuck in the fully withdrawn position.

c) The shutdown margin is maintained at ambient temperature by the use of soluble poison.

Thermal and Hydraulic

The reactor core is designed to meet the following limiting thermal and hydraulic criteria:

a) At least a 95 percent probability with 95% confidence that the minimum DNBR of the limiting rod during normal operations and anticipated transients is greater than or equal to the DNBR limit of the DNB correlation being used.

b) No fuel melts during normal operation, including anticipated transients.

To maintain fuel rod integrity and prevent fission product release, it is necessary to prevent overheating of the fuel and possible cladding perforation which would result in the release of fission products to the reactor coolant. Overheating of the fuel cladding is prevented by restricting fuel operation to within the nucleate boiling regime where the heat transfer coefficient is large and the cladding surface temperature is slightly above the coolant saturation temperature.

Operation above the upper boundary of the nucleate boiling regime could result in excessive cladding temperatures because of the onset of departure from nucleate boiling (DNB) and the resultant sharp reduction in heat transfer coefficient. DNB is not a directly measurable parameter during operation and therefore THERMAL POWER and Reactor Coolant Temperature and Pressure have been related to DNB. This relation has been developed to predict the DNB flux and the location of DNB for axially uniform and non-uniform heat flux distributions. The local DNB heat flux ratio, DNBR, defined as the ratio of the heat flux that would cause DNB at a particular core location to the local heat flux, is indicative of the margin to DNB. The correlation DNBR limit is established based on the entire applicable experimental data set such that there is a 95 percent probability with 95 percent confidence that DNB will not occur when the minimum DNBR is at the DNBR limit.

Mechanical

Reactor Internals

The reactor internal components are designed to withstand the stresses resulting from startup, steady state operation with any number of pumps running, and shutdown conditions. No damage to the reactor internals occurs as a result of a loss of pumping power.

Lateral deflection and torsional rotation of the lower end of the core barrel is limited to prevent excessive movements resulting from seismic disturbances and thus prevent interference with rod cluster control assemblies (See Appendix 5A). Core drop in the event of failure of the normal supports is limited so that the RCCA's do not disengage from the fuel assembly guide thimbles.

The structural internals are designed to maintain their functional integrity in the event of a major loss-of-coolant accident or a maximum hypothetical earthquake. The dynamic loading resulting from the pressure oscillations because of a loss-of-coolant accident does not prevent rod cluster control assembly insertion.

The following components of the reactor internals were checked for buckling under the combined effect of design earthquake and a double ended pipe break: upper barrel during hot leg break, upper and lower support columns, and fuel assemblies thimbles, for both cold and hot leg break.

The internals were analyzed by applying to each component the excitation forces due to the transient postulated condition. Maximum stresses and deflections were obtained from the structural response and compared with allowable values. The stress analysis was performed obtaining the maximum dynamic response for each component and computing the corresponding stress intensity using standard strength of materials formulas.

Resulting stresses were then combined in the most unfavorable manner with the seismic stresses and the maximum stress intensities were obtained for each component. The dynamic analysis has been performed using the following conservative assumptions:

1. The mechanical and hydraulic analyses were performed separately without including the effect of the water-solid interaction. Peak pressures obtained from the hydraulic analysis will be attenuated by the deformation of the structures.

2. When applying the hydraulic forces no credit was taken for the stiffening effect of the fluid environment which will reduce the deflections and stresses in the structure.

3. The multi-mass model was considered to have enough degrees-of-freedom to represent the most important modes of vibration in the vertical direction. This model is conservative in the sense that further mass-spring resolution of the system would lead to further attenuation of the shock effects obtained with the present model.

To assure that the components will not fail, an allowable stress criterion was established as explained in Section 14.3.3. This criterion limits the maximum strain to percentages of the material uniform strain which is an indication of the adopted margin.

Uncertainties in the dynamic loads have increased the margin contained in the maximum stresses. The major factor of conservatism is the assumption that the double ended break will occur in 0.001 sec.; larger breaking times will reduce all the stresses. The hydraulic analysis, with which the loads were computed, is performed by the MULTIFLEX Code which solves hydraulic equations by the method of characteristics.

Uncertainties in the geometric modeling technique, when applied to a full scale reactor, have been also determined analytically by studying the same reactor using models of different complexity. Results indicate that the loads obtained with the present model are conservative.

Fuel Assemblies

The fuel assemblies are designed to perform satisfactorily throughout their lifetime. The loads, stresses, and strains resulting from the combined effects of flow induced vibrations, earthquakes, reactor pressure, fission gas pressure, fuel growth, thermal strain, and differential expansion during both steady state and transient reactor operating conditions have been considered in the design of the fuel rods and fuel assembly. The assembly is also structurally designed to withstand handling and shipping loads prior to irradiation, and to maintain sufficient integrity at the completion of design burnup to permit safe removal from the core and subsequent handling during cooldown, storage and shipment.

The fuel rods are supported at several locations along their length within the fuel assemblies by brazed grid assemblies which are designed to maintain control of the lateral spacing between the fuel rods throughout the design life of the assemblies. The magnitude of the support loads provided by the grids are established to minimize possible fretting without overstressing the cladding at the points of contact between the grids and fuel rods. The grid assemblies also allow axial thermal expansion of the fuel rods without imposing restraint of sufficient magnitude to result in buckling or distortion of the rods.

The fuel rod cladding is designed to withstand operating pressure loads without collapse or rupture and to maintain encapsulation of the fuel throughout the design life.

Rod Cluster Control Assemblies

he criteria used for the design of the cladding on the individual absorber rods in the RCCA's are similar to those used for the fuel rod cladding. The cladding is designed to be free standing under all operating conditions and will maintain encapsulation of the absorber material throughout the absorber rod design life. Allowance for wear during operation is included in the RCCA cladding thickness.

Adequate clearance is provided between the absorber rods and the fuel assembly guide thimbles which position the rods within the fuel assemblies so that coolant flow along the length of the absorber rods is sufficient to remove the heat generated without overheating of the absorber cladding. The clearance is also sufficient to compensate for any misalignment between the absorber rods and fuel assembly guide thimbles and to prevent mechanical interference between the absorber rods and fuel assembly guide thimbles under any operating and accident conditions.

Control Rod Drive Assembly

Each control rod drive assembly is designed as a hermetically sealed unit to prevent leakage of reactor coolant. All pressure-containing components are designed to meet the requirements of the ASME Code, Section III, Nuclear Vessels for Class A vessels.

The control rod drive assemblies provide RCCA insertion and withdrawal rates consistent with the required reactivity changes for reactor operational load changes. The maximum reactivity addition rate is specified to limit the magnitude of a possible nuclear excursion resulting from a control system malfunction or operator error.

Also, the control rod drive assemblies for the full length rods provide a fast insertion rate during a "trip" of the RCCA's which results in a rapid shutdown of the reactor for conditions that cannot be handled by the reactor control system. This rate is based on the results of various reactor emergency analyses, including instrument and control delay times and the amount of reactivity that must be inserted before deceleration of the RCCA's occurs.

3.2 REACTOR DESIGN

3.2.1 NUCLEAR DESIGN AND EVALUATION

This section presents the nuclear characteristics of the core and an evaluation of the characteristics and design parameters which are significant to design objectives. The capability of the reactor to achieve these objectives while performing safely under normal operational modes, including both transient and steady state, is described.

Nuclear Characteristics of the Design

For historical purposes, a summary of the reactor nuclear design characteristics is presented in Table 3.2.1-1. This table includes design parameters for Cycle 1 only. Subsequent cycle specific values are calculated and their impact on plant operation and safety analyses is evaluated prior to each cycle. The results of these evaluations for the current cycles are presented in Appendices 14A and 14B for Units 3 and 4, respectively. The cycle specific design parameters for the current reloads are documented in nuclear design reports that are used for design verification and operational guidance.

Reactivity Control Aspects

Reactivity control is provided by neutron absorbing RCCA and by a soluble chemical neutron absorber (boric acid) in the reactor coolant. The concentration of boric acid is varied as necessary during the life of the core to compensate for: (1) changes in reactivity which occur with change in temperature of the reactor coolant from cold shutdown to hot operating, zero power conditions; (2) changes in reactivity associated with changes in the fission product poisons xenon and samarium; (3) reactivity losses associated with the depletion of fissile inventory and buildup of long-lived fission product poisons (other than xenon and samarium); and (4) changes in reactivity due to burnable poison burnup.

The RCCAs provide reactivity control for: (1) fast shutdown; (2) reactivity changes associated with changes in the average coolant temperature above hot zero power (core average coolant temperature is increased with power level); (3) reactivity associated with any void formation; and (4) reactivity changes associated with the power coefficient of reactivity.

Chemical Shim Control

Control to render the reactor subcritical at temperatures below the operating range is provided by a chemical neutron absorber (boron). The boron concentration during refueling has been established for Cycle 1 as shown in Table 3.2.1-1, line 29. This concentration together with the RCCA provides approximately 10 percent shutdown for these operations. In Reference 17 of Section 3.2.1, the refueling shutdown margin has been revised to 5 percent $\Delta K/k$. The concentration is also sufficient to maintain the core shutdown without any RCCA during refueling. For historical purposes, for cold shutdown in Cycle 1, at the beginning of core life, a concentration (shown in Table 3.2.1-1, line 37) is sufficient for one percent shutdown with all but one stuck rod inserted. The boron concentration (Table 3.2.1-1, line 29) for refueling is equivalent to less than two percent by weight of boric acid (H_3BO_3) and is well within solubility limits at ambient temperature. This concentration is also maintained in the spent fuel pit since it is directly connected with the refueling canal during refueling operations.

For historical purposes, the initial full power boron concentration for Cycle 1 without equilibrium xenon and samarium is specified in Table 3.2.1-1, line 34. As these fission product poisons are built up, the boron concentration is reduced to that specified in Table 3.2.1-1, line 36.

This initial boron concentration is that which permits the withdrawal of the control banks to their operational limits. The xenon-free hot zero power shutdown (k = 0.99) with all but one stuck rod inserted, can be maintained with the boron concentration specified in Table 3.2.1-1, line 38 (Cycle 1). This concentration is less than the full power operating value with equilibrium xenon.

Control Rod Requirements

Neutron-absorbing RCCA provide control to compensate for more rapid variations in reactivity. The rods are divided into two categories according to their function. Some rods compensate for changes in reactivity due to variations in operating conditions of the reactor such as power or temperature. These rods comprise the control group of rods. The remaining rods, which provide shutdown reactivity, are termed shutdown rods. The total shutdown worth of all the rods is also specified to provide adequate shutdown with the most reactive rod stuck out of the core.

For historical purposes, RCCA reactivity requirements at beginning and end of life are summarized in Table 3.2.1-2. The installed worth of the RCCA is shown in Table 3.2.1-3. The difference is available for excess shutdown upon reactor trip. Summaries of the calculated reactivity requirements and shutdown margins for the current cycles are presented in appendices 14A and 14B for Units 3 and 4, respectively.

Total Power Reactivity Defect

RCCA must be available to compensate for the reactivity change incurred with a change in power level due to the Doppler effect. The magnitude of this change has been established by correlating the experimental results of numerous operating cores.

The average temperature of the reactor coolant is increased with power level in the reactor. Since this change is actually a part of the power dependent reactivity change, along with the Doppler effect and void formation, the associated reactivity change must be controlled by rods. The largest amount of reactivity that must be controlled is at the end of life when the moderator temperature coefficient has its most negative value. For historical purposes, the moderator temperature coefficient range for Cycle 1 is given in Table 3.2.1-1, line 42, while the cumulative reactivity change is shown in the first line of Table 3.2.1-2. By the end of the fuel cycle, the nonuniform axial depletion causes a severe power peak at low power. The reactivity associated with this peak is part of the power defect. The moderator temperature coefficient range for the current cycles is given in Appendices 14A and 14B for Units 3 and 4, respectively.

Control Rod Bite

If sufficient boron is present in a chemically-shimmed core, the inherent operational control afforded by the negative moderator temperature coefficient is lessened to such a degree that the major control of transients resulting from load variations must be compensated for by control rods. The ability of the unit to accept major load variations is distinct from safety considerations, since the reactor would be tripped and shutdown safely if the rods could not follow the imposed load variations. In order to meet required reactivity ramp rates resulting from load changes, the control rods must be inserted a given distance into the core. The reactivity worth of this insertion has been defined as control rod bite.

The reactivity insertion rate must be sufficient to compensate for reactivity variation due to changes in power and temperature caused either by a ramp load change of five percent per minute, or by a step load change of ten percent. To obtain this minimum ramp rate during load change, one control bank of rods must remain inserted at least 10 percent into the core at the beginning of life. The reactivity associated with this bite is less than 0.1 percent.

The control rod bite position for D bank in steady state operation is about 210 steps withdrawn to about 220 steps withdrawn. Temperature control is still adequate at the bite position. Should an unscheduled rapid load rejection occur, the differential worth available at the bite position is adequate for the control systems to respond as designed. The consequences of withdrawing the rods farther than the bite position are quite minor.

The apparent advantages of leaving rods farther inserted than the bite position are outweighed by the disadvantages. The ability to add reactivity to the core quickly by withdrawing rods is not required during long term steady state operation. The ability to change flux difference in the positive direction is similarly not required; indeed, the flux difference is more stable with the rods fully withdrawn.

The major disadvantages of operation with rods more deeply inserted than the bite position is the shadowing of fuel burnup in the top of the core. This leads to relatively worse axial power distributions in the subsequent fuel cycles and will restrict the permissible flux difference operating band. A small effect is a loss of reactivity and therefore of cycle lifetime in the current cycle due to less than optimum axial burnup distribution. Further, the consequences of many accidents are actually worse starting from deep rod insertion, even though these worst cases have already been assumed in the accident analysis.

Xenon Stability Control

Excore instrumentation is provided to obtain necessary information concerning power distribution. This instrumentation is adequate to enable the operator to monitor xenon induced power oscillations. Extensive analysis, with confirmation of methods by spatial transient experiments at Haddam Neck, has shown that any induced radial or diametral xenon transients would die away naturally. A full discussion of xenon stability control can be found in Reference 1.

Excess Reactivity Insertion Upon Reactor Trip

The control rod requirements have been based on providing one percent shutdown at hot zero power (HZP) conditions with the highest worth rod stuck in its fully withdrawn position. The condition where excess reactivity insertion is most critical is at the end of a cycle when the steam break accident is considered.

Calculated Rod Worths

The complement of 45 full length rods arranged in the pattern shown in Figure 3.2.1-1 meets the shutdown requirements. Table 3.2.1-3 lists the calculated worths of this rod configuration for beginning and end of the first cycle. In order to be sure of maintaining a conservative margin between calculated and required rod worths the calculated reactivity worths listed are decreased in the design by at least 7 percent to account for any errors or uncertainties in the calculation. This worth is established for the condition that the highest worth rod is stuck in the fully withdrawn position in the core. The reactivity requirements and shutdown margins evaluation presented in Appendices 14A and 14B lists the calculated worths for beginning and end of the current cycles for Units 3 and 4, respectively.

A comparison between calculated and measured rod worths in the operating reactor shows the calculation to be well within the allowed uncertainty of at least 7 percent. (Reference 19)

Reactor Core Power Distribution

In order to meet the performance objectives, without violating safety limits, the peak to average power density must be within the limits set by the nuclear

hot channel factors. For the peak power point in the core, the nuclear heat flux hot channel factor, F^N_q, was established as specified for Cycle 1 in Table 3.2.1-1, Line 18. For the hottest channel the nuclear enthalpy rise hot channel factors, $F_{\Delta H}{}^N$, was established as specified in Table 3.2.1-1, Line 19. Variation in hot channel factors is illustrated for typical rod configurations for the first cycle in Figures 3.2.1-3 and 3.2.1-5. The calculations shown in these figures do not include the power flattening effect of equilibrium xenon and non-uniform Doppler broadening. Reactivity feedback effects associated with non-uniform xenon, water boron density and Doppler broadening are discussed in detail in Reference 1. Nuclear hot channel factors for the current cycles are provided in Appendices 14A and 14B for Units 3 and 4, respectively.

Incore instrumentation is employed to check the power distributions throughout core lifetime.

The excore nuclear instrumentation system supplies the information on core power distribution. This information is derived from four independently operating channels. Each channel employs a dual section long ion chamber for monitoring the upper and lower section of the core. Current signals from these detectors are summed, conditioned and calibrated against incore power distribution obtained from the movable incore detector system so that the eight individual signals are directly related to the power generated in the adjacent section of the core. This essentially divides the core into eight sections, four in the upper half, and four in the lower half.

The relationship between core power distribution and excore nuclear instrumentation reading is established during the startup testing program. Incore flux measurements are made for reactor power in the range of 25 to 100 percent. These measurements, together with long ion chamber currents, are processed to yield the relationships between power distribution parameters calculated with an incore flux map and those calculated with excore nuclear instrumentation. These relationships can be checked during operation to assess the effect of core burnup on the sensitivity between incore power distribution and excore readings.

Power Distribution Control

Limits placed on the axial flux difference are designed to assure that the heat flux hot channel factor Fq is maintained within acceptable limits. The Constant Axial Offset Control (CAOC) operating procedure described in Reference 1 requires control of the axial flux difference at all power levels within a permissible operational band about a target value corresponding to the equilibrium full power value. The Relaxed Axial Offset Control (RAOC) procedures which were implemented in Unit 3 Cycle 13, Unit 4 Cycle 14, and beyond (described in Reference 18) were developed to provide wider control bands and, consequently, more operating flexibility. These wider operating limits, particularly at lower power levels, can increase plant availability by allowing quicker plant startups and increased maneuvering flexibility without trip or reportable occurrences.

In the standard CAOC analysis described in Reference 1, the generation of the normal operation power distribution is constrained by the Rod Insertion Limit (RIL) and the axial flux difference (AFD) band limits. The purpose of the RAOC is to find the widest possible AFD-power operating space by analyzing a wide range of axial flux differences. Therefore, the generation of normal operation power distribution is constrained only by the RIL.

For a CAOC analysis, load follow simulations were performed covering the allowed CAOC operating space to generate a typical range of allowed axial xenon distributions, which in turn were used to calculate axial power distribution in both normal operation and Condition II accident conditions. For an RAOC analysis, however, as described in Reference 18 a more practical method is used to create an axial xenon distribution covering the wider AFD-power operating space allowed with RAOC operation. Each resulting power shape is analyzed to determine if LOCA constraints are met or exceeded. The total peaking factor, $F^T q$, is determined using standard synthesis methods as described in Reference 1.

Following the guidance of Generic Letter 88-16, the RAOC AFD limits were removed from the Technical Specifications and placed in the Core Operating Limits Report (COLR). These reports are presented in Appendix 14A and 14B for Units 3 and 4, respectively.

Developments with regard to Emergency Core Cooling System (ECCS) criteria for LOCA have imposed new requirements on allowable kw/ft conditions. A schematic demonstration of the various limits and their effect on allowable local power densities (kw/ft), and hence operational flexibility, is presented in Figure 3.2.1-6. This figure shows that there are many limits that must be met, but also that these limits are, in general, a function of the elevation in the core. Allowable local kw/ft limits are lower near the top of the core because of, for example, the axial power shape dependence on DNB and the reduced heat transfer upon re-flood for a large break LOCA near the top of the core.

Reactivity Coefficients

The response of the reactor core to unit conditions or operator adjustments during normal operation, as well as the response during abnormal or accidental transients, is evaluated by means of a detailed plant simulation. In these calculations, reactivity coefficients are required to couple the response of the core neutron multiplication to the variables which are set by conditions external to the core. Since the reactivity coefficients change during the life of the core, a range of coefficients is established to determine the response of the unit throughout life.

Moderator Temperature Coefficient

The moderator temperature coefficient relates a change in neutron multiplication to the change in reactor coolant temperature. Reactors employing soluble boron as a means of reactivity control possess less negative moderator temperature coefficients than cores controlled solely by RCCA's. There are two reasons for this:

a) Soluble poison density is decreased with the water density when the coolant temperature rises; and

b) In a chemical shim core the control rods are only partially inserted. A deep insertion tends to increase effective length of the core and thus causing moderator coefficient to become more negative.

In order to reduce the dissolved poison requirement for control of excess reactivity, burnable poison rods can be incorporated in the core design. The result is that changes in the coolant density will have less effect on the density of poison and the moderator temperature coefficient will become less positive.

For historical purposes, in Cycle 1 there were 816 of the borosilicate glass rods in the form of clusters distributed throughout the core in vacant rod cluster control guide tubes as illustrated in Figures 3.2.1-7 and 3.2.1-8. Information regarding research, development and nuclear evaluation of the burnable poison rods can be found in Reference 3 and 4. These rods initially controlled the installed excess reactivity shown on lines 40 and 41 of Table 3.2.1-1, and their addition resulted in a reduction of the initial hot zero power boron concentration in the coolant to the value shown on line 34. The moderator temperature coefficient was negative at the operating coolant temperature with this boron concentration and with burnable rods installed.

In a typical reload cycle, several hundreds of Wet Annular Burnable Absorber (WABA) rods in the form of clusters are distributed throughout the core in vacant rod cluster control guide tubes. Additionally, recent cores utilize several thousands of Integral Fuel Burnable Absorbers (IFBAs) in the form of a zirconium diboride coating on the surface of the fuel palette. The number and distribution of these burnable absorbers for the current cycles are presented in Appendices 14A and 14B for Units 3 and 4, respectively.

The effect of burnup on the moderator temperature coefficient is calculated and the coefficient becomes more negative with increasing burnup. This is due to the buildup of fission products with burnup and dilution of the boron concentration with burnup. The latter effect is considerably more important. However, the buildup of equilibrium xenon contributes a positive increment to the coefficient for a constant boron concentration. For historical purposes, the calculated net effect and the predicted unrodded moderator temperature coefficient with equilibrium xenon at BOL for Cycle 1 is shown in table 3.2.1-1, Line 42. With core burnup, the coefficient will become more negative as boron is removed because of a shift in the neutron energy spectrum due to the buildup of plutonium and fission products. For Cycle 1 at end of life with no boron or rods in the core, the moderator coefficient is specified in Table 3.2.1-1, Line 42.

The current Technical Specifications allows a +5 pcm/◦F (+5 x 10^{-5} $\Delta K/K/◦F$) MTC below 70 percent of rated power, ramping to a 0 pcm/◦F MTC at 100 percent power and above. A power-level dependent MTC was chosen to minimize the effect of the specification on postulated accidents at high power levels.

Moreover, as the power level is raised, the average core water temperature becomes higher as allowed by programmed average temperature for the plant,

tending to bring the moderator coefficient more negative. Also, the boron concentration can be reduced as xenon builds into the core. Thus, there is less need to allow a positive coefficient as full power is approached. As fuel burnup is achieved, boron is further reduced and the moderator coefficient will become negative over the entire operating power range.

The control rods provide a negative contribution to the moderator temperature coefficient as can be seen in Figure 3.2.1-9 for Cycle 1. Moderator temperature coefficients for current cycles are given in Appendices 14A and 14B for Units 3 and 4, respectively.

Moderator Pressure Coefficient

The moderator pressure coefficient has an opposite sign to the moderator temperature coefficient. The effect on the total coefficient is small because the pressure coefficient is 100 times smaller. For historical purposes the calculated beginning and end of life pressure coefficients for Cycle 1 are specified in Table 3.2.1-1, Line 43.

Moderator Density Coefficient

A uniform moderator density coefficient is defined as a change in the neutron multiplication per unit change in moderator density. The range of the moderator density coefficient from BOL to EOL for Cycle 1 is specified in Table 3.2.1-1, Line 44. The most positive moderator density coefficient is calculated as part of the reload safety analyses evaluation for each cycle and compared to the limit included in Appendices 14A and 14B for Unit 3 and 4, respectively.

Doppler and Power Coefficients

The Doppler coefficient is defined as the change in neutron multiplication per degree change in fuel temperature. The coefficient is obtained by calculating neutron multiplication as a function of effective fuel temperature. The results are shown in Figure 3.2.1-10 for BOL conditions for the first cycle. The coefficient becomes slightly more negative with increasing fuel burnup. Doppler coefficients for current cycles are given in Appendices 14A and 14B for Units 3 and 4, respectively.

In order to know the change in reactivity with power, it is necessary to know the change in the effective fuel temperature with power as well as the Doppler coefficient. It is very difficult to predict the effective temperature of the

fuel using a conventional heat transfer model because of uncertainties in predicting the behavior of the fuel pellets. Therefore, an empirical approach is taken to calculate the power coefficient, based on operating experience of existing Westinghouse cores. For historical purposes, Figure 3.2.1-11 shows the power coefficient as a function of power obtained by this method for non-collapsed helium filled rods for Cycle 1. The results presented for BOL do not include any moderator coefficient even though the moderator temperature changes with power level, and the coefficient becomes slightly more negative with increasing fuel burnup.

As the fuel pellet temperature increases with power, the absorption in U-238 increases due to Doppler broadening of the resonances. A large temperature drop occurs across the fuel pellet-clad gap. Under certain conditions, this gap may be closed, thus resulting in lower pellet temperature. The net effect is a lower effective fuel temperature, a higher Doppler coefficient, and a lower power coefficient than that which exists with a pellet-clad gap. The power coefficient, which is determined using a closed gap model, is shown in Figure 3.2.1-12 for Cycle 1.

Calculations indicate the stability of the reactor to Xenon oscillations is relatively insensitive to the thermal model used to obtain the power coefficient. The damping factor associated with the fuel Doppler effect is

$$\alpha_f = \frac{\partial K_{eff}}{\partial T} \frac{\partial T}{\partial P}$$

where

T = fuel temperature
P = power
K_{eff} = reactivity

The quantity $\frac{\partial T}{\partial P}$ is larger for the gap model than for the no gap case but since the Doppler coefficient varies as $T^{-1/2}$ the term $\frac{\partial K_{eff}}{\partial T}$ is smaller. The net effect is that α_f is relatively insensitive to the thermal model in the range of power 0.5 to 1.5 of core average which is the range of interest for stability.

Nuclear Evaluation

The basis for confidence in the procedures and design methods comes from the comparison of these methods with many experimental results and actual measured data from Turkey Point over numerous cycles of operation (Reference 19). These experiments include criticals performed at the Westinghouse Reactor Evaluation Center (WREC) and other facilities, and also measured data from operating power reactors. A summary of the results and discussion of the agreement between calculated and measured values is given in the following paragraphs and also documented in References 19 and 20.

Reactivity Analysis

Data from 55 oxide and 56 metal lattice critical and exponential experiments have been evaluated[5]. The results of these studies are summarized in Table 3.2.1-4. The values of neutron multiplication k are computed using experimentally measured material bucklings, and should equal unity. Table 3.2.1-4 demonstrates that much of the scatter can be attributed to variations in results from one experimental laboratory to another, whereas the evaluation demonstrates that errors do not develop with variations of certain significant parameters. As the calculational accuracy is independent of variations in hydrogen to uranium ratio, uranium enrichment, pellet diameter and buckling, extrapolation from experiments to operating cores or extrapolation from one operating core to another does not lead to any significant error.

It can be seen from Table 3.2.1-4 that if only WAPD experimental results are considered, the computational method predicts k to a standard deviation of 0.36 percent which is a better estimate of the accuracy of the method because of the more detailed information available. Much of the additional scatter in the standard deviation for the other cases can be attributed to insufficient information on the dimensions and results of many of the cases published.

Depletion Analysis

Data from the Yankee Core Evaluation Program have been compared with calculated data using the design techniques. The results are summarized in Figures 3.2.1-13 through 3.2.1-15. Uranium depletion and net plutonium production have a direct bearing on the core lifetime. The figures show the comparison between calculations (solid lines) and measured concentrations of the various isotopes. Although some small deviations can be observed between analysis and experiment, they are considered negligible.

Power Peaking Analysis

A series of critical experiments were carried out at the Westinghouse Reactor Evaluation Center (WREC) to determine the power peaking in fuel rods adjacent to water holes and to determine the effects of voids on power distribution.

The power peaking experiment was performed in a 30 x 30 array of 2.72 percent enriched fuel with a water-to-uranium ratio of 3.5 with and without boron in the moderator. The pattern of 16 water holes was symmetrical about the center of the core. The core arrangement and pattern of fuel rods scanned are shown in Figure 3.2.1-16 for the unborated core and Figure 3.2.1-17 for the same core with 479 ppm boron in the water.

The analysis consists of PDQ calculations using two-group constants obtained from LEOPARD. Mixed Number Density thermal constants are used, and "soft spectrum" microscopic constants are used in the reflector and water holes. In the PDQ analysis, two mesh spacings per fuel rod are used. Also, in the unborated core a calculation is performed for one mesh space per fuel rod. The experimental data are normalized to the PDQ results using the average of the four central rods. The experimental and calculated results for the borated and unborated cores with two mesh spacers per fuel rod are shown in Figures 3.2.1-18 and 3.2.1-19, respectively, and in Figure 3.2.1-20 for the unborated core calculated with one mesh spacer per fuel rod. Each block in the figures represents a fuel rod. The experimental values correspond to the average values of counts taken at five positions on the fuel rod.

The agreement between analysis and experiment is within 2 to 3 percent and is of the same order as the scatter in the experimental data. There is no consistent difference in over-estimating or underestimating peaking using the one mesh per fuel rod or two mesh per fuel rod representation.

The void experiments were performed for two different core configurations. The first series of experiments was carried out in a 47 x 47 square core of 2.7% enriched fuel with a W/U of 2.9, with no boron. The second series was performed using a 53 x 53 square core of 3.7% enriched fuel with a W/U of 2.9, and with 1046 ppm boron in the water. In both cores voids were simulated by empty 0.1875 inch O.D. 0.022 inch wall aluminum tubes inserted between fuel rods. The moderator in the voided region consisted of 11.52% aluminum, 16.29% void and 72.19% water. Data were taken for the following cases:

1. No void tubes
2. Four void tubes (2x2) located around the central fuel rod
3. Sixteen void tubes (4x4) at core center
4. One hundred ninety-six void tubes (14x14) are core center

The analysis again consisted of PDQ using two-group constants from LEOPARD, with MND thermal constants and "soft spectrum" water hole and reflector constants. The calculated power distribution is compared with the experimental power scans in Figure 3.2.1-21 and 3.2.1-22 for the unborated and borated cores for the four cases examined. The agreement between experiment and calculation is good except at the transition region between voided and non-voided regions. Here the calculated peaks are higher than those obtained by experimental measurements.

The reactivity effects of the void tubes were calculated assuming a constant axial reflector savings. Calculation and experiment for each case examined are compared in Table 3.2.1-5. Calculations overestimate the reactivity effect of the voids by approximately 10%, which is good agreement in view of the small magnitude of the effects being studied.

The adequacy of the current methods for peaking factor analysis is demonstrated in the Turkey Point specific evaluations of Reference 19 by comparison of prediction to actual measured values obtained using the flux map analysis code, INCORE. The nuclear enthalpy rise hot channel factor ($F_{\Delta H}$) and the heat flux hot channel factor (F_Q) were measured using the INCORE code. Predicted peaking factors were obtained from three-dimensional ANC calculations performed for core conditions similar to those at the time of the measurements. Power peaking factors measured during Unit 4 Cycles 12, 13, and 14 are compared to predicted values in Reference 19. For $F_{\Delta H}$ the mean difference between the measured and predicted values for the three cycles is 2.02% with a standard deviation of 1.27%; for F_Q the mean difference is 3.33% with a standard deviation of 1.86%.

Gross Power Distribution Analysis

The ability to evaluate power distributions in multiregion critical cores with no burnup has been evaluated in detail.(6) Agreement for all situations, including those with large enrichment variation and small regions, is found to be good as is illustrated in Figure 3.2.1-23. The ability to evaluate power distributions in depleted cores at power has been demonstrated by core evaluation programs using in-core instrumentation data from Yankee, Saxton and SELNI.

As an example of such a comparison, a power distribution is shown in Figure 3.2.1-24 for the end of life in Yankee Core I, which was not controlled by chemical shim. A comparison of the burnup distribution is also presented in Figure 3.2.1-25.

In both cases two calculated values are given which show the effect of a rod program interchange during life.(2)

The ability to evaluate power distributions in complex designs is demonstrated in the Reference 20 qualification of advanced design methods. These methods have been qualified against actual measured power distributions from the moveable incore detector system. The qualification report of Reference 20 indicates good agreement of average assembly power distribution between measured and predicted results.

RCC Assembly Worth Analysis

In the control rod calculations performed by PDQ, the RCC assemblies are represented by internal boundary conditions (α's) in the fast and thermal groups. These boundary conditions applied to the unit cell in which the absorber rod, its clad and the associated water are homogenized. The values of these α's are

determined to make the calculated rod worth of a single fuel assembly equal to that calculated by a more refined model. The better model represents each absorber rod explicitly and is used to analyze an extensive set of critical measurements. Approximately 30 different critical measurements were made for uniform and cluster arrays of absorber rods with different enrichments, rod diameters, water-to-uranium ratios and boron concentrations.

In the analysis of these measurements, the rods were represented by a theoretically determined thermal boundary condition and by a diffusion region in the single fast group. The fast absorption cross section was empirically determined from the measured rod worth to give agreement between analytical and experimental results. The development of this calculation scheme for rod worth and a description of the measurements is given in Reference 8. Figures 3.2.1-26 and 3.2.1-27 are reproduced from this reference to show the fast absorption cross section as a function of the radius of the absorber which fits the experimental measurements for cluster and uniform cases, respectively. The solid lines were obtained by at least square fitting of the experimental data.

The ability of the current design methods to accurately predict control rod worth is demonstrated in References 19 and 20. Reference 19 compares measured and predicted worths for Turkey Point Unit 4 Cycles 12,13,and 14; while Reference 20 presents similar comparisons for four different plants with a total of seven cycles. The mean difference between measured and predicted worth in the operating reactor shows the calculation to be well within the uncertainty of 7 percent.

Moderator Coefficient Analysis

Inasmuch as the safe operation of any nuclear unit is closely associated with the ability to predict the behavior of that unit, correlation of analysis with experiment is presented to show that the moderator temperature coefficient is quite predictable. Measurements were made during the startup and operation of the SELNI core to get data for a core controlled by chemical shim. During the startup, the core was heated from room to operating temperature at a constant boron concentration of 1600 ppm. Figure 3.2.1-28 shows the results of the moderator coefficient measurements taken during this core heatup, and also the comparable calculated values. The calculations were performed with the one-dimensional AIM-5 code with LEOPARD input constants as described for neutron multiplication calculations. The agreement between calculation and experiment is good over the entire temperature range.

In order to measure the moderator coefficient at different boron concentrations, control rods were traded for boron during the hot, no power startup tests. This procedure permitted moderator coefficient measurements to be made over a range of boron concentrations from 1300 to 1800ppm. The method of analysis for the case of trading rods for boron is, of necessity, different from the method discussed above. The AIM-5 code was again used, but an axial calculation was performed with an homogenized bank of absorber used to represent the moving RCCA. The results of analysis and measurement are shown in Figure 3.2.1-29. The calculations were performed in the same manner as the measurement; i.e., the control group was inserted as boron was removed.

When the control group was fully inserted, further boron removal was compensated for by insertion of all rods banked. PDQ analyses were also performed for the all rods in and all rods out end points and the results are given in Figure 3.2.1-29. It can be seen that the one-dimensional calculations in which rods are represented by a homogenized absorber predict the measured data very well.

The effect of burnup on the moderator coefficient has been measured in the core evaluation program performed on Yankee Core I.[9] Yankee Core I was controlled by cruciform blade rods, and so it was necessary to separate the effect of control rods from the effect of burnup on the moderator coefficient. Figure 3.2.1-30 illustrates these components and the agreement between analysis and measurement. The effect of rods was evaluated by treating the rods as an equivalent absorption area (approximation 1 in Figure 3.2.1-30) with a correlation for the effects of resonance absorption (approximation 2 in Figure 3.2.1-30). The results of the analysis lie within the experimental uncertainty and the burnup effect on the moderator coefficient results in a more negative coefficient with increasing burnup.

The isothermal temperature coefficient (ITC) is defined as the change in reactivity per ^{0}F change in moderator and fuel temperature. This quantity is significant in HZP measurements because it can be measured directly and it is used to determine compliance with the moderator temperate coefficient Technical Specification.

The ITCs are measured by a series of heatup and cooldown sequences over a small change in reactor coolant system temperature. ITCs were predicted by uniformly varying the core temperature by $\pm 5^0$ F about the HZP temperature in the PHOENIX-P/ANC design methods of Reference 20. The qualification presented in this reference analyzed a variety of control rod positions in addition to the basic ARO configuration. Specific comparisons for Turkey Point are presented in Reference 19.

Doppler and Power Coefficient Analysis

As the fuel pellet temperature increases with power, the resonance absorption in U-238 increases due to Doppler broadening of the resonances. In order to predict the reduction in reactivity caused by this effect, it is necessary to

know the temperature of the fuel as a function of power level, the position of burnup of fuel in the core, as well as the radial distribution of temperature within the individual fuel rods. However, uncertainties arise during operation at power which make it difficult to predict accurately the temperature of the fuel pellet. For example, pellets do not remain intact (i.e., uncracked) and in a concentric relationship with the clad, as has been observed from the Yankee spent fuel analysis.[10] In addition, the composition of gases in the gap changes with the burnup because of diffusion of fission product gases to the gap. This generally results in an uncertainty in the temperature drop across the gap as a function of power level and burnup.

A semi-empirical model has been developed for calculating the effective fuel temperature (T_{eff}) based on fitting the measured power coefficients of the Yankee, Saxton, BR-3 and SELNI reactor cores. The measured power coefficient $1/k\ \delta k/\delta P$ can be written

$$\frac{1}{k}\frac{\delta k}{\delta p} = \frac{1}{k}\frac{\delta k}{\delta T_{eff}} \bullet \frac{\delta T_{eff}}{\delta P} \qquad (1)$$

The first term in the product on the right side of the Equation (1) is the Doppler coefficient which can be computed without knowing the heat transfer behavior of the fuel pellet or the relationship of T_{eff} and power. The second term on the right side of Equation (1) can then be related to the measured values of power coefficients. In this manner an empirical expression for the effective fuel temperature is obtained which makes it possible to relate T_{eff} to power, and thus calculate the power coefficient.

The method of analysis described in the preceding paragraph assumes accuracy of prediction of the Doppler coefficient as a function of the effective fuel temperature. This assumption indicates that the behavior of the U-238 resonance integral with a change in the fuel temperature is well known. Data is presented here to support this

assumption. A correlation has been developed for the U-238 resonance integral which is known as the metal-oxide correlation.[5] This correlation has been found to agree with Hellstrand's uranium metal[11] and uranium dioxide[12] correlations for isolated rods. The correlation is also consistent with Hellstrand's temperature correlations.[13] Thus, a single correlation replaces the four Hellstrand correlations. The metal-oxide correlation is

$$R.I.^{28} = 2.16X + 1.48 + (0.0279X - 0.0537)\ T_{eff}^{1/2}$$

where T_{eff} is in degrees Kelvin and

$$x = \left[\frac{\sum so}{N_o^{28}}\ P_o + \frac{D}{1_o N_o^{28}} \right]^{1/2}$$

Σso = scattering cross section of the fuel (10.7 barns for uranium and 3.8 barns for oxygen)

N_o^{28} = U-238 number density in the fuel region

1_o = mean chord length in the fuel

D = shielding factor (calculated by Sauer's Method)[14]

P_o = 1 - P_c (P_c is tabulated in Reference 15)

This form of the resonance integral is not strictly rigorous, but its validity is demonstrated in Figure 3.2.1-31 where it is compared with Hellstrand's results for different temperatures.[5]

An extensive evaluation of power coefficient measurements has been made for the Yankee, Saxton, Br-3 and SELNI cores. The results of these measurements are given in Figure 3.2.1-32 which shows the change in the effective fuel temperature per kw/ft as a function of core average kw/ft. From this data an empirical equation for T_{eff} has been developed which will predict T_{eff} as a function of power level.[16] This equation for T_{eff} is given below.

$T_{eff}(P/P_o) = 0.55\ \Delta T_{fuel} + \alpha(\bar{q}'')\ \delta\bar{q}'' + 1.571\ P/P_o\ \Delta T_o\ (clad + film) + T_{coolant}$

where

P/P_o = fraction of full power

ΔT_{fuel} = difference between maximum and surface fuel pellet temperature (function of power)

$\alpha(\bar{q}'')$ = Empirical parameter dependent upon average heat flux

δ = ratio of the cold diametral gap to the inner diameter of the clad

$\bar{q}''$ = average surface heat flux to the pellet

ΔT_o (clad + film) = temperature drop across clad and film (function of power)

$T_{coolant}$ = average temperature of the coolant (function of power)

The empirically determined α is given in Figure 3.2.1-33 as a function of pellet surface heat flux. The difference in the effective temperature obtained from the experimental data of Figure 3.2.1-32 and from the correlation employing Figure 3.2.1-33 is shown in Figure 3.2.1-34 as a function of surface heat flux. It can be seen that even though there is some scatter in the experimental data (Figure 3.2.1-32), all the experimental points fall into a small band when the T_{eff} correlation is used. The most scattered experimental data points deviate from the predicted value (solid line) by no more than $\pm$ 80◦F. It is concluded that the T_{eff} correlation can predict T_{eff} at any power level to within $\pm$80◦F which constitutes less than $\pm$5% of the effective fuel temperature at full power. Although the experimental data discussed above continues to be the basis for currents methods, enhanced modeling schemes have been developed for the calculation of the effective fuel temperatures used in the PHOENIX-P/ANC nuclear design system. The model also includes elastic deflection of the cladding, and a pellet-clad gap conductance which depends on the kind of initial fill gas, the hot open gap dimension, and the fraction of the pellet circumference over which the gap is effectively closed due to pellet cracking. The effective temperatures of U-238 and Pu-240 are obtained by appropriate radial weighting of the temperature distribution. These modeling enhancements have lead to overall high accuracy of the PHOENIX-P/ANC nuclear design system as demonstrated in Reference 20.

Comparison of Predicted and Measured Boron Concentrations

For historical purposes, core startup data obtained from operating power reactors Prior to Turkey Point operation are shown in Table 3.2.1-6. Comparison of the predicted and measured critical boron concentration indicates differences of about 50 to 150 ppm boron, or approximately a 5% overestimate, for which allowance has been made in design calculations.

To demonstrate the ability of the current design methods, measured boron concentration at startup was collected from operating reactors. The analysis included in Reference 20 used data from four different reactors with a total of seven cycles. Specific comparisons for Turkey Point Unit 4 are presented in Reference 19. Differences between measured and predictions for the HZP, ARO critical boron concentration are within the review criteria of 50 ppm for this parameter.

3.2.1 REFERENCES

1. WCAP-7208 (1968), "Power Distribution Control in Westinghouse Pressurized Water Reactors," PROPRIETARY. A NON-PROPRIETARY version of this report is WCAP-7811.

2. McGaugh, J.D., and Chastain, R.H., "Power Density vs. Burnup Distribution in Yankee Core I," WCAP-6051 (1963), NON-PROPRIETARY.

3. Wood, P.M. Bassler, E.A., et al, "Use of Burnable Poison Rods in Westinghouse Pressurized Water Reactors," WCAP-7113 (October 1967), NON-PROPRIETARY.

4. WCAP-9000 (1968), "Nuclear Design of Westinghouse Pressurized Water Reactor with Burnable Poison Rods", PROPRIETARY. A NON-PROPRIETARY version of this report is WCAP-7806, Rev. 1.

5. Strawbridge, L.E., "Calculations of Lattice Parameters and Criticality for Uniform Water Moderated Lattices," WCAP-3269-25 (1964) NON-PROPRIETARY.

6. Eich, W.J., and Kovacik, W.P., "Reactivity and Neutron Flux Studies in Multiregion Loaded Cores," WCAP-1433 (1961), NON-PROPRIETARY.

7. Barry, R.F., "The Revised Leopard Code - A Spectrum Dependent Non-Spatial Depletion Program," WCAP-2759, March 1965, PROPRIETARY.

8. Sha, W.T., "An Analysis of Reactivity Worth of the Rod Cluster Control (RCC) Elements and Local Water Hole Power Density Peaking," WCAP-3269-47 (1965), NON-PROPRIETARY.

9. Poncelet, C.G., "Effects of Fuel Burnup on Reactivity and Reactivity Coefficients in Yankee Core I," WCAP-6076 (1965) NON-PROPRIETARY.

10. "Yankee Core Elevation Program Quarterly Progress Report for the Period Ending June 30, 1963," WCAP-6055 (1963), NON-PROPRIETARY.

11. Hellstrand, E., and Lundgren, G., "The Resonance Integral for Uranium Metal and Oxide," Nuclear Science and Engineering 12, 435, (1962).

12. Hellstrand, E., J. Applied Physics 28, 1493 (1957).

13. Hellstrand, E., Blomberg, P., and Horner, S., "The Temperature Coefficient of the Resonance Integral for Uranium Metal and Oxide," Nuclear Science and Engineering 8, 497 (1960).

14. Sauer, A., "Approximate Escape Probabilities, "Nuclear Science and Engineering" 16, 329 (1963).

15. Case, K.M., deHoffman, F., and Placzek, G., "Introduction to the Theory of Neutron Diffusion," (1953).

16. Sha, W.T., "An Experimental Evaluation of the Power Coefficient in Slightly Enriched PWR Cores," WCAP-3269-40 (1965), NON-PROPRIETARY.

17. Gordon E. Edison (NRC) to W.F. Conway (FPL), "Turkey Point Units 3 and 4 Issuance of Amendments RE: Refueling Shutdown Margin", dated July 18, 1988.

18. R.W. Miller, et al., "Relaxation of Constant Axial Offset Control, Fq Surveillance Technical Specification," WCAP-10216-P-A, dated June 1983.

19. Nuclear Physics Methodology for Reload Design of Turkey Point and St. Lucie Nuclear Plants, FPL Report No. NF-TR-95-01, January 1995 (NRC Approved).

20. Nguyen, T.O., et al., “Qualification of the Phoenix-P/ANC Nuclear Design System for Pressurized Water Reactor Cores,” WCAP-11596-P-A (Proprietary), June 1988.

NUCLEAR DESIGN DATA
(FIRST CYCLE)

STRUCTURAL CHARACTERISTICS

1.	Fuel Weight (UO_2), lbs.	176,000
2.	Zircaloy Weight, lbs.	34,900
3.	Core Diameter, inches	119.7
4.	Core height, inches	144
	Reflector Thickness and Composition	
5.	Top - Water Plus Steel	≈10 in.
6.	Bottom - Water Plus Steel	≈10 in.
7.	Side - Water Plus Steel	≈15 in.
8.	H_2O/U Volume Ratio (cold)	4.18
9.	Number of Fuel Assemblies	157
10.	UO_2 Rods per Assembly	204

PERFORMANCE CHARACTERISTICS

11.	Core Heat Output, MWt (initial rating)	2200
12.	Heat Output, MWt (maximum calculated turbine rating)	2300
13.	Fuel Burnup, MWD/MTU	
	First Cycle (Average)	13,000
	Enrichments, w/o*	
14.	Region 1	1.85
15.	Region 2	2.55
16.	Region 3	3.10
17.	Equilibrium	3.10
18.	Nuclear Heat Flux Hot Channel Factor F^N_q*	3.13 |
19.	Nuclear Enthalpy Rise Hot Channel Factor, $F^N_{\Delta H}$ *	1.75

* Corresponding values for current cycles are given in Appendices 14A and 14B for Units 3 and 4 respectively. |

CONTROL CHARACTERISTICS FOR FIRST CYCLE		
	Effective Multiplication (Beginning of Life)	
	With Burnable Poison Rods in (First Cycle)	
20.	Cold, No Power, Clean	1.180
21.	Hot, No Power, Clean	1.138
22.	Hot, Full Power, Clean	1.119
23.	Hot, Full Power, Xe and Sm Equilibrium	1.077
	Rod Cluster Control Assemblies	
24.	Material	5% Cd; 15%; 80% Ag
	Number of RCC Assemblies	
25.	Full Length	45
26.	Partial Length*	8
27.	Number of Absorber Rods per RCC Assembly	20
28.	Total Rod Worth, BOL, % (See Table 3.2.1-3)	
Boron Concentrations (ppm) for 1st Core Cycle		
Loading with Burnable Poison Rods		
29.	Refueling Shutdown; Rods Inserted (k = .90)	1950 |
30.	Shutdown (k = .99) with Rods Inserted, Clean, Cold	780
31.	Shutdown (k = .99) with Rods Inserted, Clean, Hot	510
32.	Shutdown (k = .99) with No Rods Inserted, Clean, Cold	1250
33.	Shutdown (k = .99) with No Rods Inserted, Clean, Hot	1210
To Control at Hot Full Power, No Rods Inserted		
k = 1.0		
34.	Poison Free	1000 |
35.	Xenon	720
36.	Xenon and Samarian	670
37.	Shutdown, All but one Rod Inserted, Cold (k = .99)	850
38.	Shutdown, All but one Rod Inserted, Hot (k = .99)	610

* Partial length control rods are not used in the present reloads.

BURNABLE POISON RODS

39.	Number and Material*	816 Borated Pyrex Glass
40.	Worth Hot $\Delta k/k$,%	6.9
41.	Worth Cold $\Delta k/k$,%	5.3

RANGE OF KINETIC CHARACTERISTICS FOR FIRST CYCLE*

42.	Moderator Temperature Coefficient, $(\Delta k/k)/^oF$	$+0.3 \times 10^{-4}$ to 3.5×10^{-4}
43.	Moderator Pressure Coefficient $(\Delta k/k)$/psi	-0.3×10^{-6} to $+3.5 \times 10^{-6}$
44.	Moderator Density Coefficient $(\Delta k/k)/gm/cm^3$	-0.1 to 0.3
45.	Doppler Coefficient, $(\Delta k/k)/^oF$	-1.0×10^{-5} to -1.6×10^{-5}
46.	Delayed Neutron Fraction, %	0.52 to 0.72
47.	Prompt Neutron Lifetime, sec.	1.4×10^{-5} to 1.8×10^{-5}
48.	Moderator Void Coefficient, $(\Delta k/k)$% void	$+0.5 \times 10^{-3}$ to -2.5×10^{-3}

*Corresponding values for current cycles are given in the Appendices 14A and 14B for Units 3 and 4, respectively.

TABLE 3.2.1-3

CALCULATED ROD WORTHS, $\Delta\rho$
FOR FIRST CYCLE WITH BURNABLE POISON RODS*

Core Condition	Rod Configuration	Worth	Worth Less 10%**	Design Reactivity Requirements	Shutdown Margin
BOL, HFP	45 rod in	8.14%			
	44 rods in; Highest Worth Rod Stuck Out	7.03%	6.33%	2.65%	3.68%
EOL, HFP (1st Cycle)	45 rods in	8.68%			
	44 rods in; Highest Worth Rod Stuck Out	7.42%	6.68%	3.58%	3.1%

BOL = Beginning of Life
EOL = End of Life
HFP = Hot Full Power

* Corresponding values for current cycles are given in Appendices 14A and 14B for Units 3 and 4 respectively.

** Calculated rod worth is reduced by 10% to allow for uncertainties. Current Cycles (Appendices 14A and 14B) allow 7% uncertainty.

TABLE 3.2.1-4

RESULTS OF CALCULATIONS AS A FUNCTION OF

LABORATORY PROVIDING EXPERIMENTAL DATA

Laboratory	Type of Experiment	No. of Experiments	Calculated $k + \sigma$
Westinghouse Atomic Power Division (WAPD)	Critical	16	0.9968 ± 0.0036
Bettis Atomic Power Laboratory	Critical	14	0.9940 ± 0.0022
Brookhaven National Laboratory	Exponential	35	0.9964 ± 0.0051
Hanford Atomic Products Operation	Exponential	20	0.9953 ± 0.0105
Babcock and Wilcox	Critical	26	0.9885 ± 0.0094
		111	

TABLE 3.2.1-5

CALCULATED AND MEASURED REACTIVITY EFFECTS OF VOID TUBES

		Reactivity Change %Δk/k	
Type of Core	No. of Tubes	Measured	Calculated
Unborated Core	0		
	4	-0.03	-0.034
	16	-0.11	-0.125
	196	-1.33	-1.416
Borated Core	0		
	4	-0.017	-0.020
	16	-0.076	-0.085
	196	-0.850	-0.942

TABLE 3.2.1-6

CORE STARTUP CRITICAL BORON CONCENTRATION

	INDIAN POINT I (Core B)	SELNI	SENA	SCE
Cold				
Critical Boron (ppm)				
Predicted	1949	1910	2040	2380
Measured	1897	1800	1885	2250
Difference	52	110	155	130
Hot Zero Power				
Critical Boron (ppm)				
Predicted	1967	1910	2110	2570
Measured	1893	1840	1972	2524
Difference	74	70	138	46

PATTERN OF CONTROL ROD BANKS

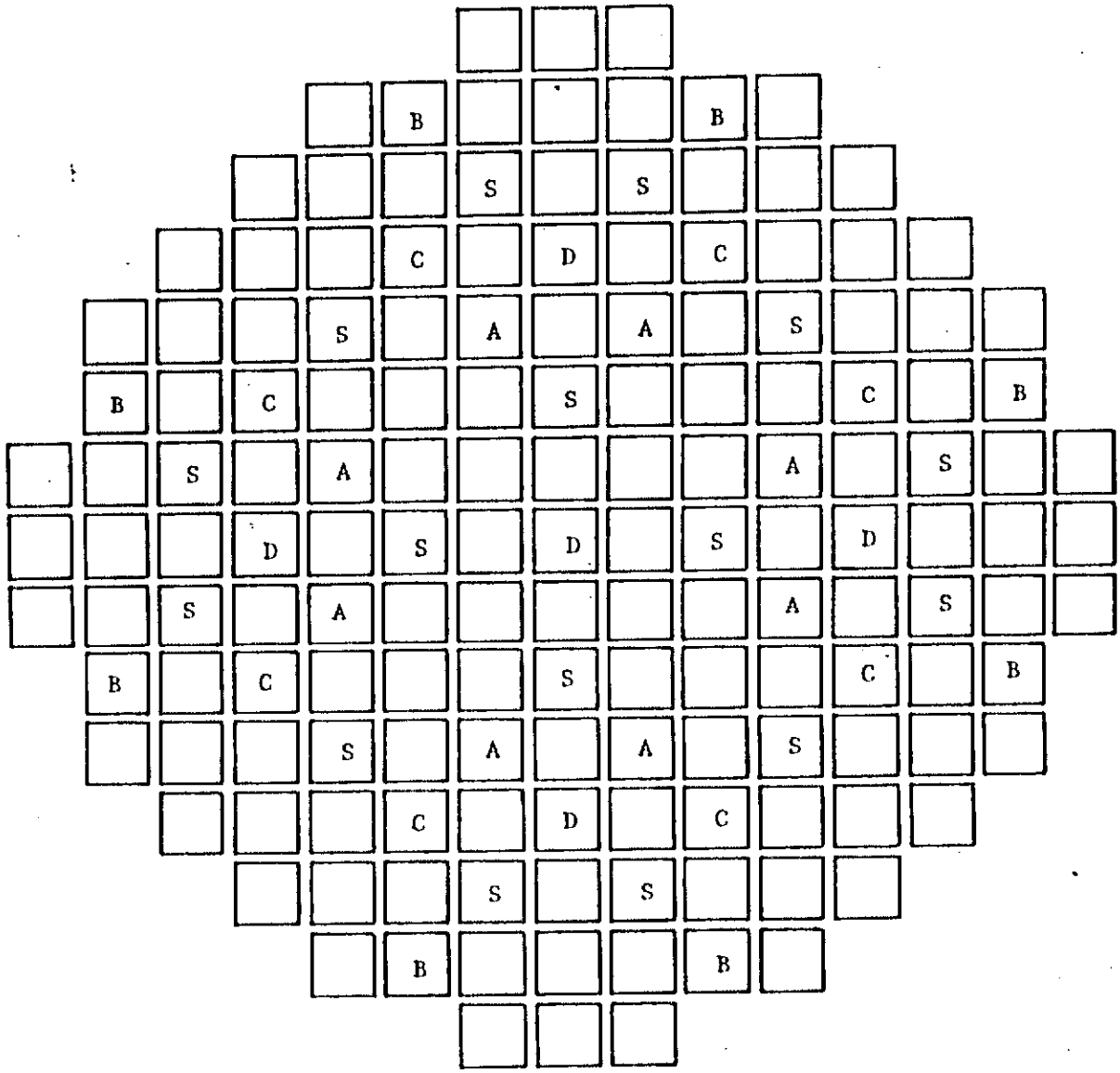

Control Rod Cluster Banks	
Control Bank A	8
Control Bank B	8
Control Bank C	8
Control Bank D	5
Shutdown Bank A&B(S)	16
	45

PATTERN OF CONTROL ROD CLUSTER BANKS

FIG. 3.2.1-1

THE PART LENGTH RODS HAVE BEEN REMOVED FROM THE REACTOR, HENCE THIS FIGURE HAS BEEN DELETED FROM THE UPDATED FSAR

Average Power Density (BOL)
Part Length Rods In
Figure 3.2.1-2

AVERAGE POWER DENSITY (BOL), CONTROL BANK D IN
FIG. 3.2.1-3

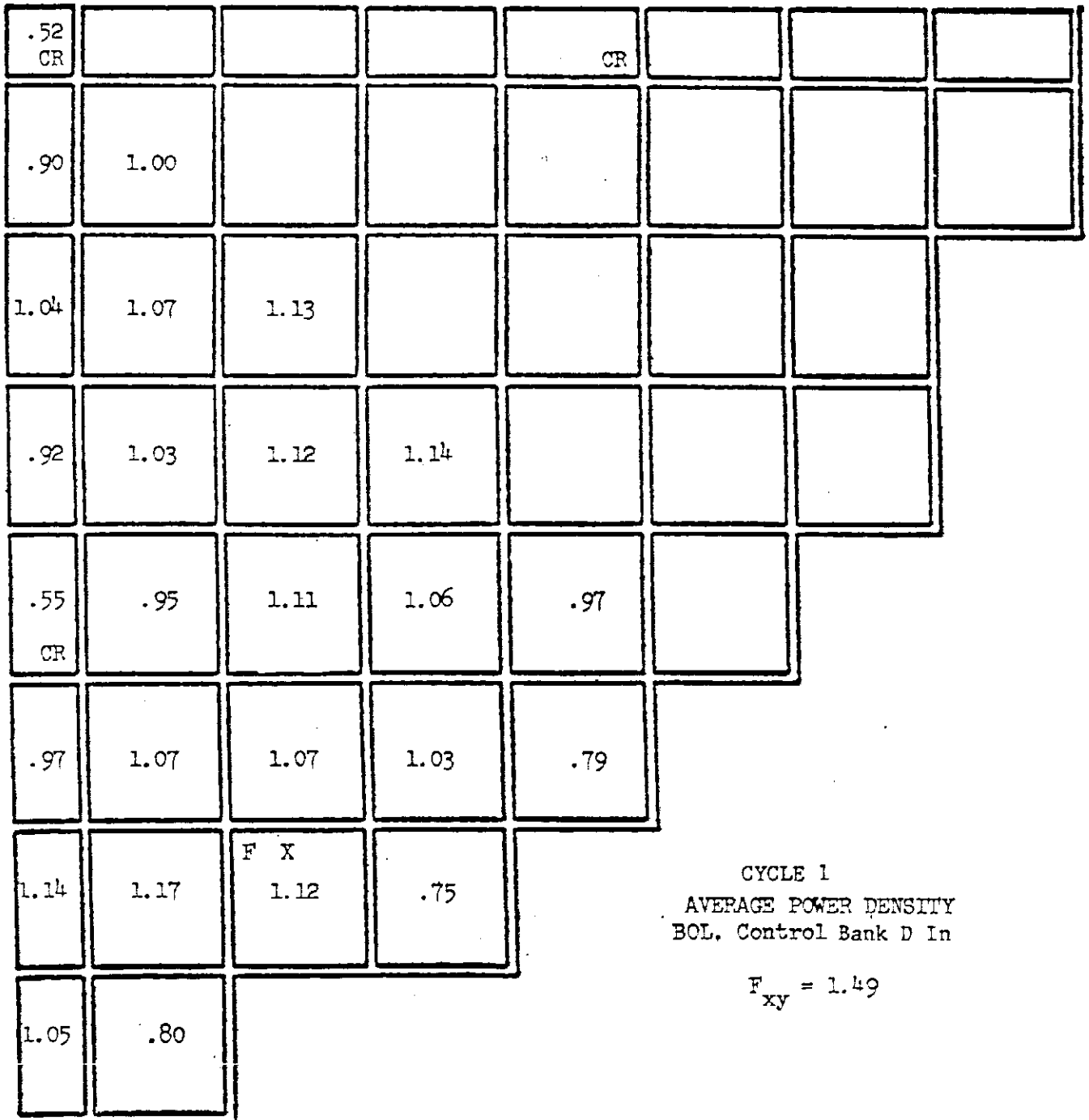

CYCLE 1
AVERAGE POWER DENSITY
BOL. Control Bank D In

$F_{xy} = 1.49$

THE PART LENGTH RODS HAVE BEEN REMOVED
FROM THE REACTOR, HENCE THIS FIGURE HAS
BEEN DELETED FROM THE UPDATED FSAR

Average Power Density (BOL), Control
Bank D In Plus Part Length Rods
Figure 3.2.1-4

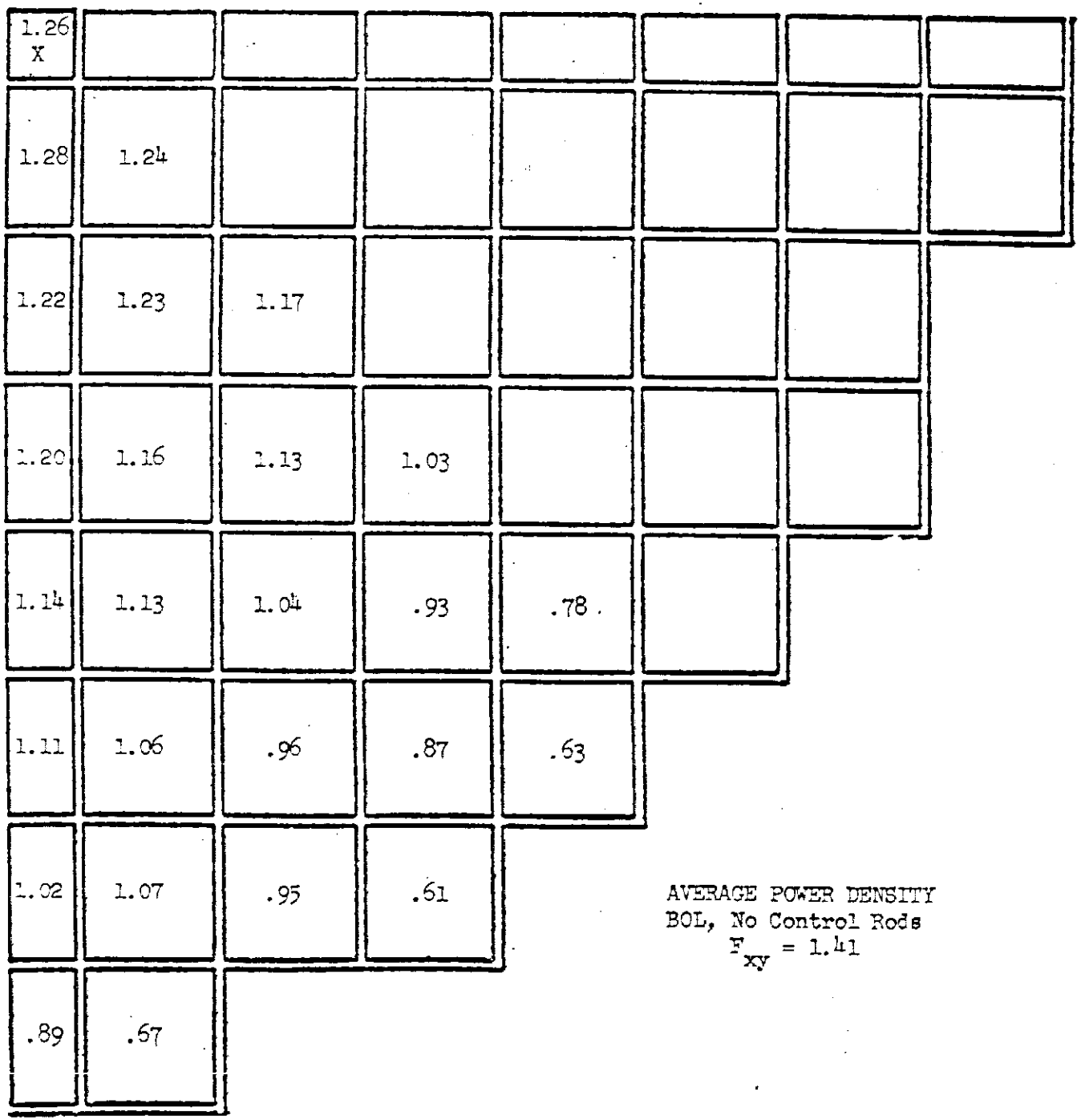

AVERAGE POWER DENSITY
BOL, No Control Rods
F_{xy} = 1.41

AVERAGE POWER DENSITY (BOL),
NO CONTROL RODS IN
FIG. 3.2.1-5

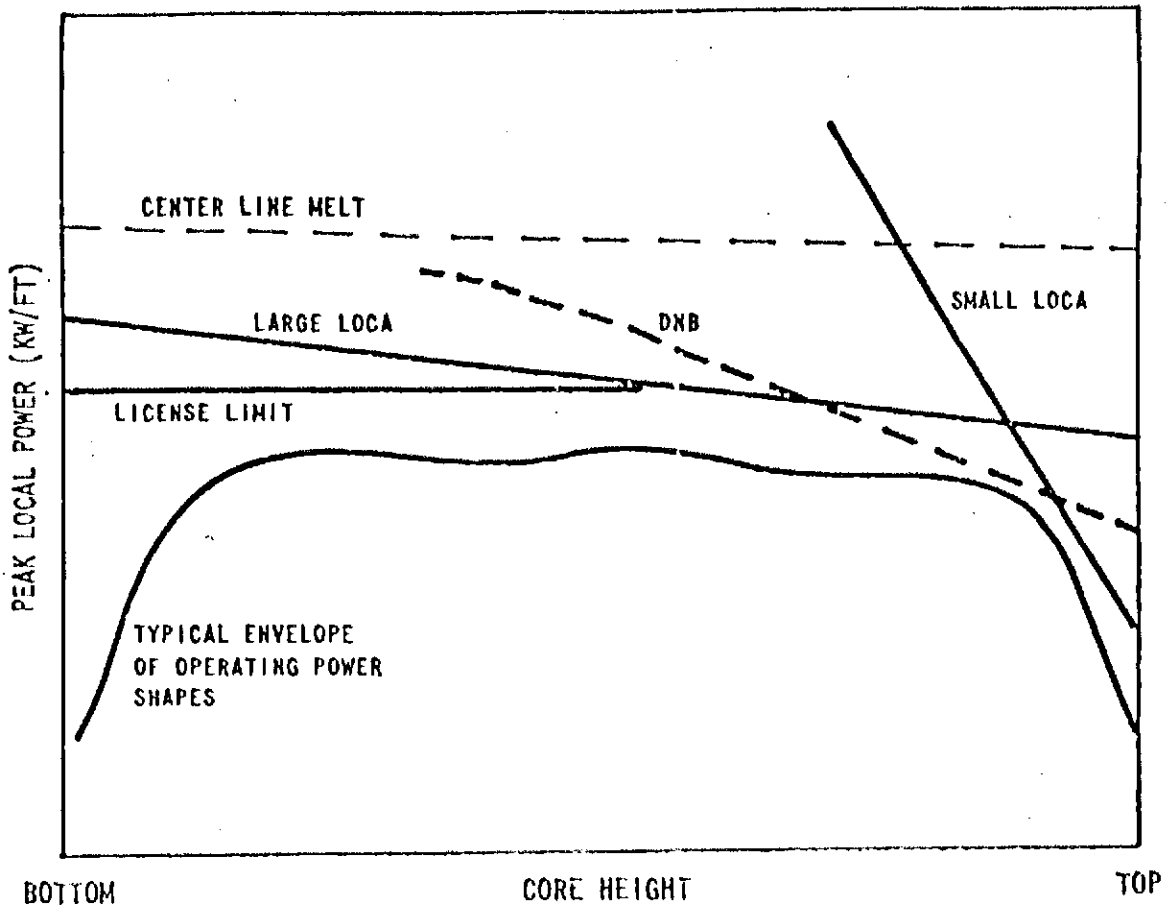

Figure 3.2.1-6 Schematic Demonstration of Typical Kw/ft Limits

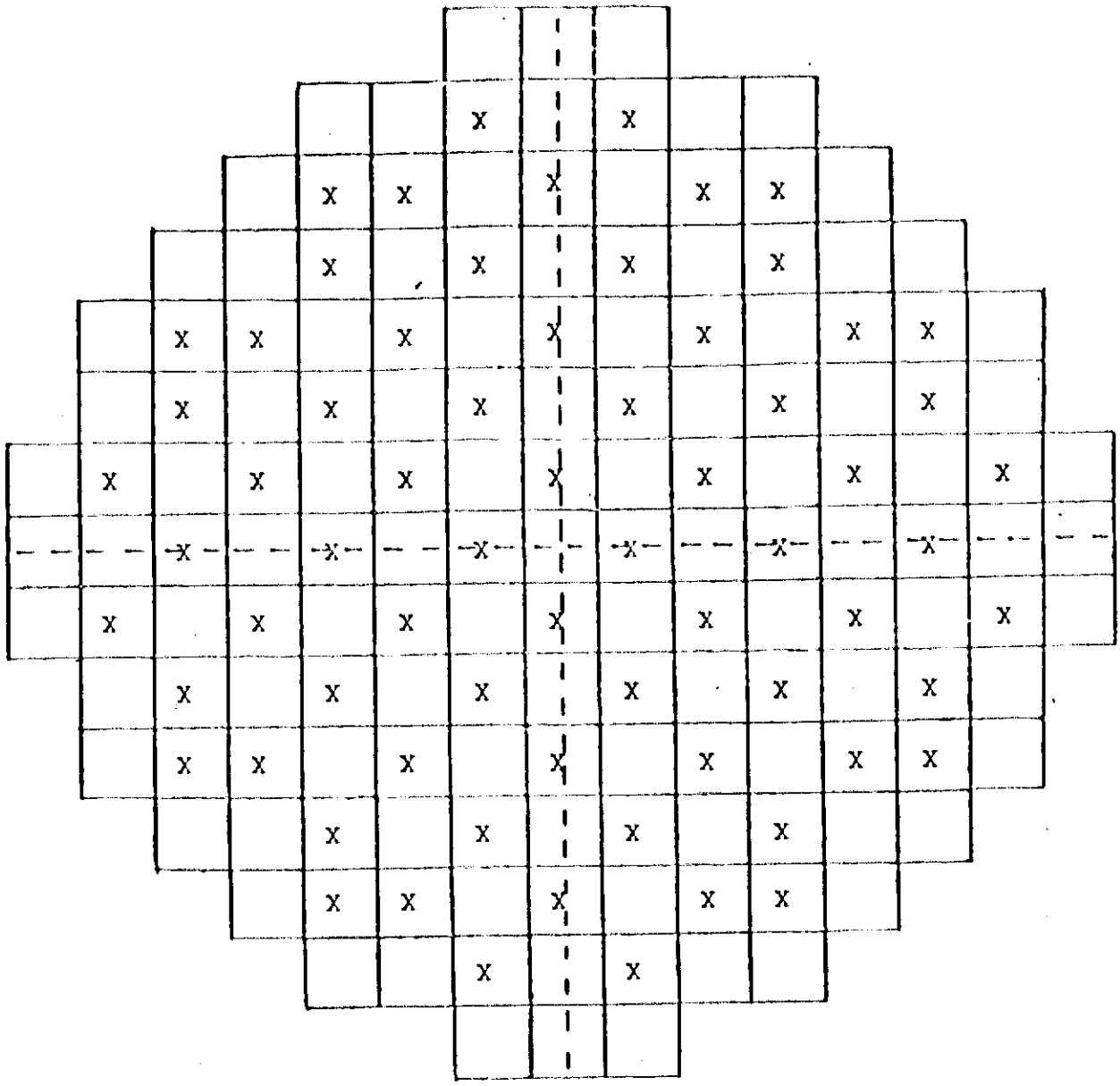

X - Indicates Fuel Assembly Having a Burnable Poison Cluster of 12 Rods

Burnable Poison Cluster Locations*

(Cycle 1)

*Corresponding locations for current cycles are given in the Reload Safety Evaluations, Appendices 14A and 14B.

BURNABLE POISON CLUSTER LOCATIONS

FIG. 3.2.1-7

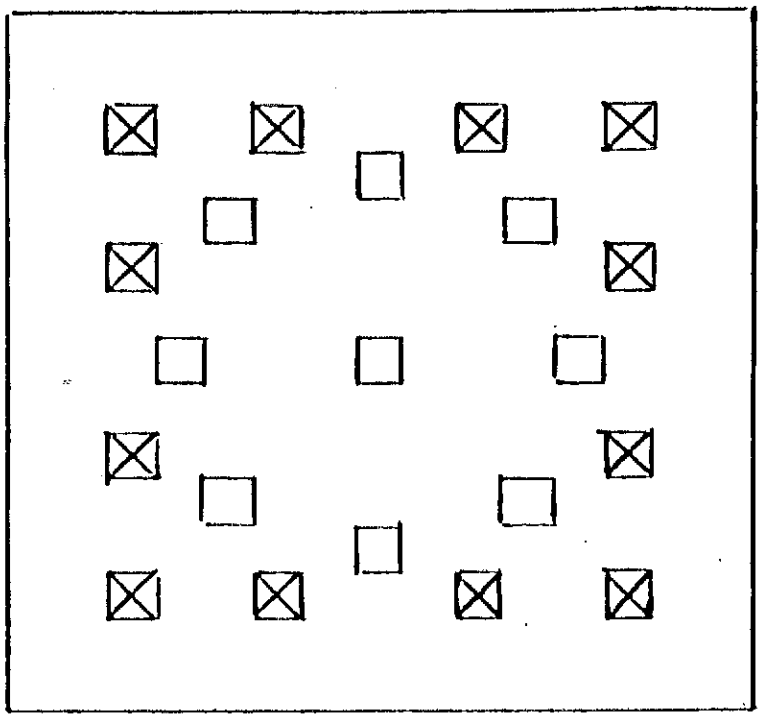

Note: X Denotes Burnable Poison Rods

(Cycle 1)

PATTERN OF POISON ROD LOCATIONS

FIG. 3.2.1-8

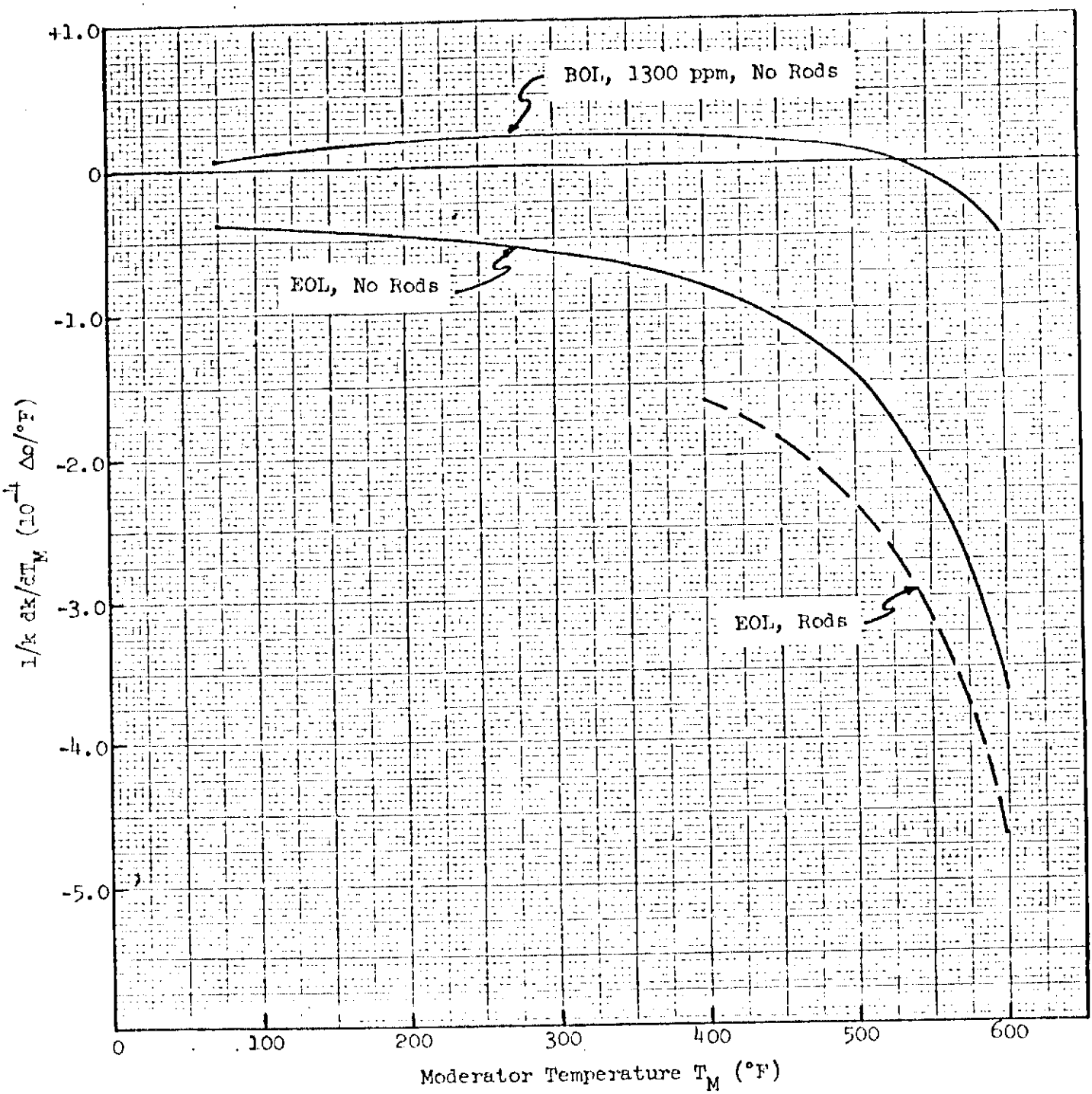

(Cycle 1)

MODERATOR TEMPERATURE COEFFICIEN

VS. MODERATOR TEMPERATURE

FIG. 3.2.1-9

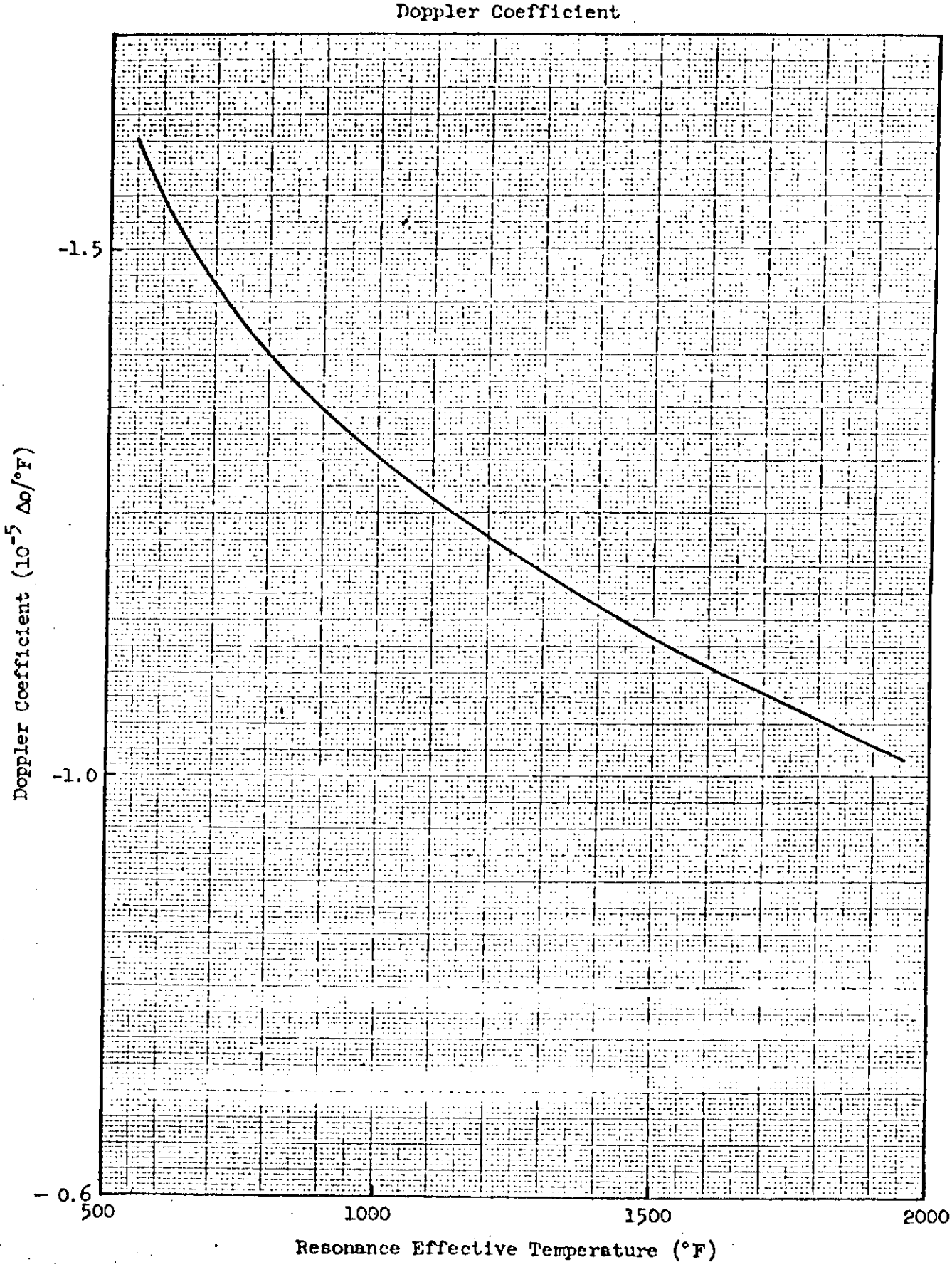

(Cycle 1)

DOPPLER COEFFICIENT VS. EFFECTIVE FUEL TEMPERATURE (BOL) FIG. 3.2.1-10

(DOPPLER CONTRIBUTION ONLY)

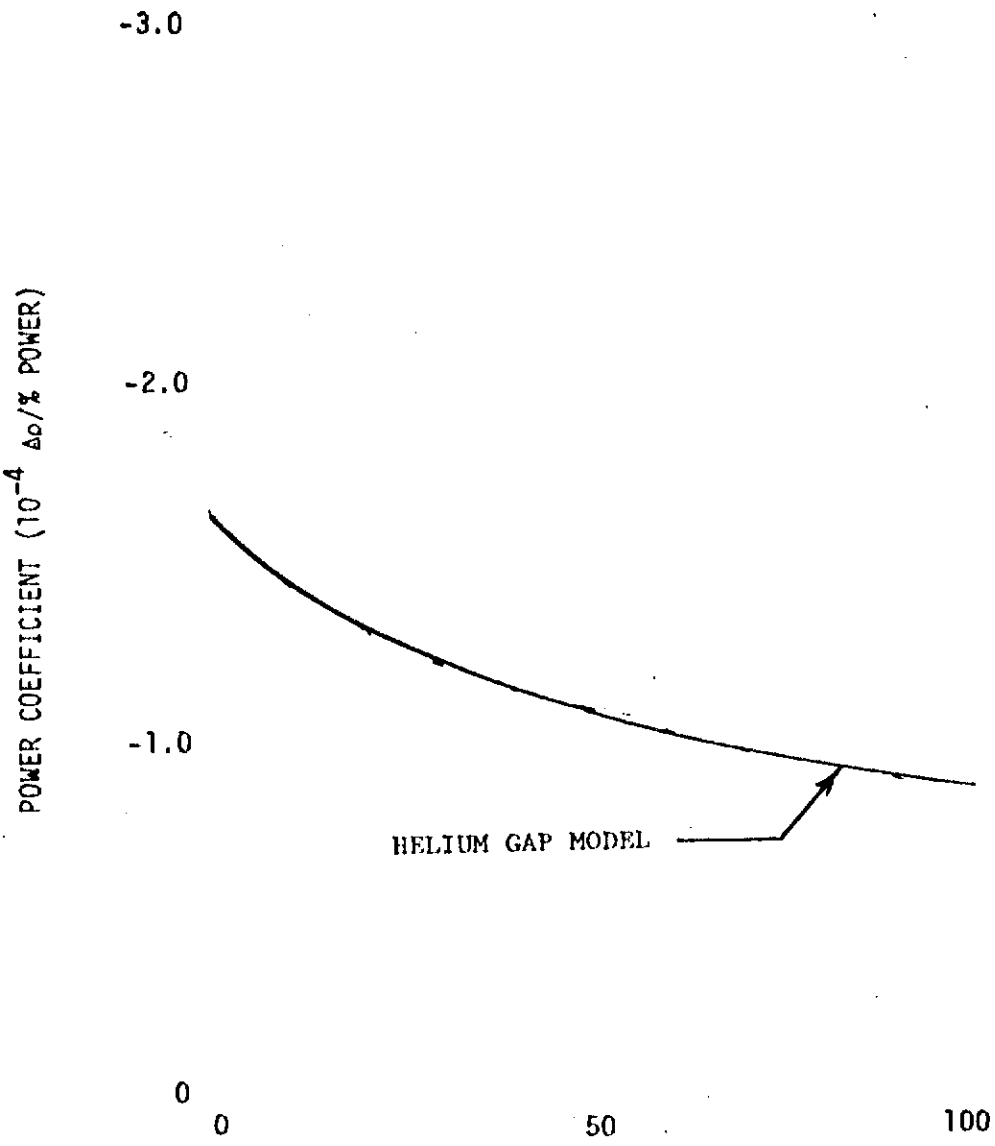

POWER COEFFICIENT
FIGURE 3.2.1-11

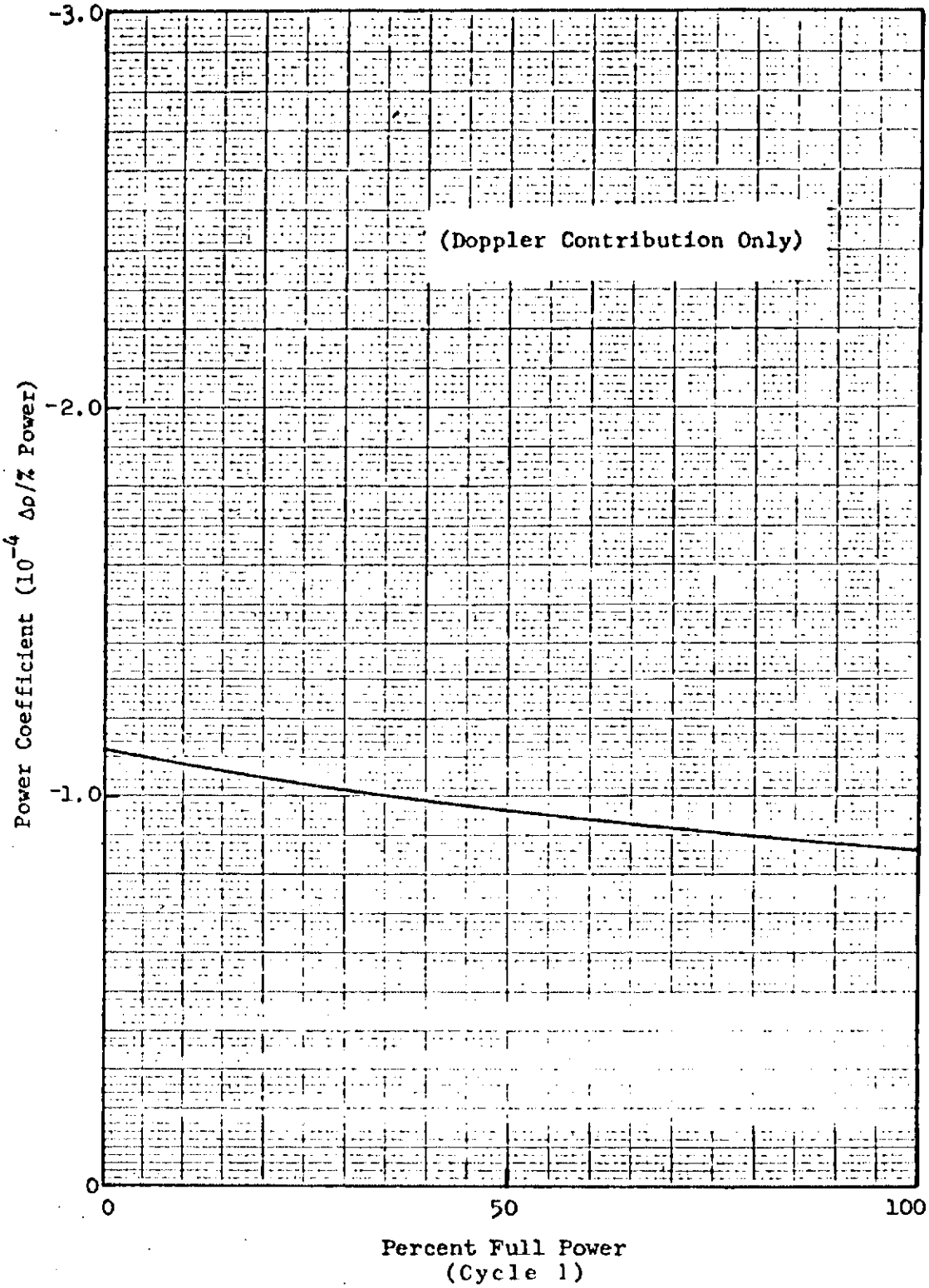

POWER COEFFICIENT (CLOSED GAP MODEL)
FIG. 3.2.1-12

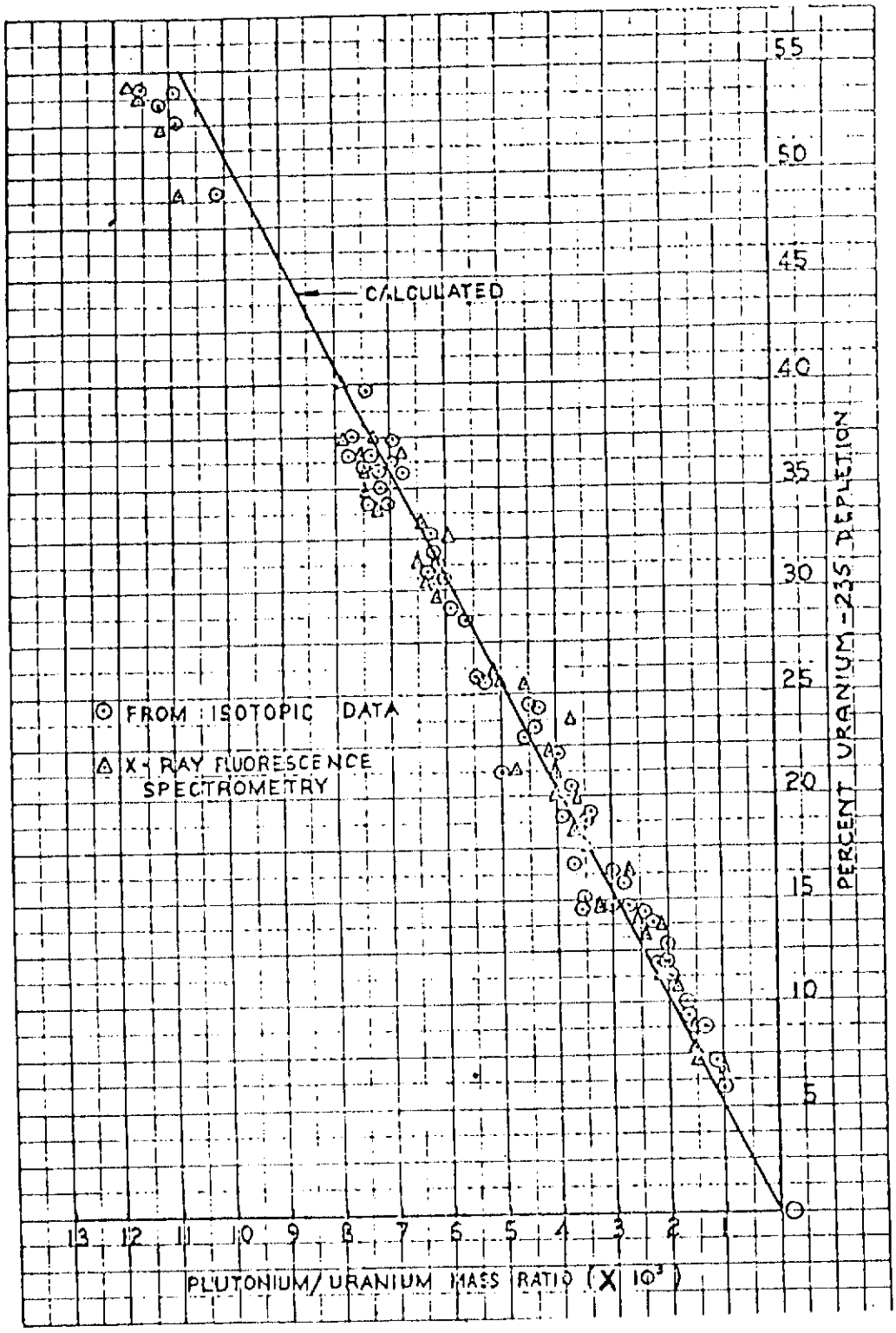

PLUTONIUM/URANIUM MASS RATIO AS A FUNCTION OF URANIUM-235 DEPLETION

FIG. 3.2.1-13

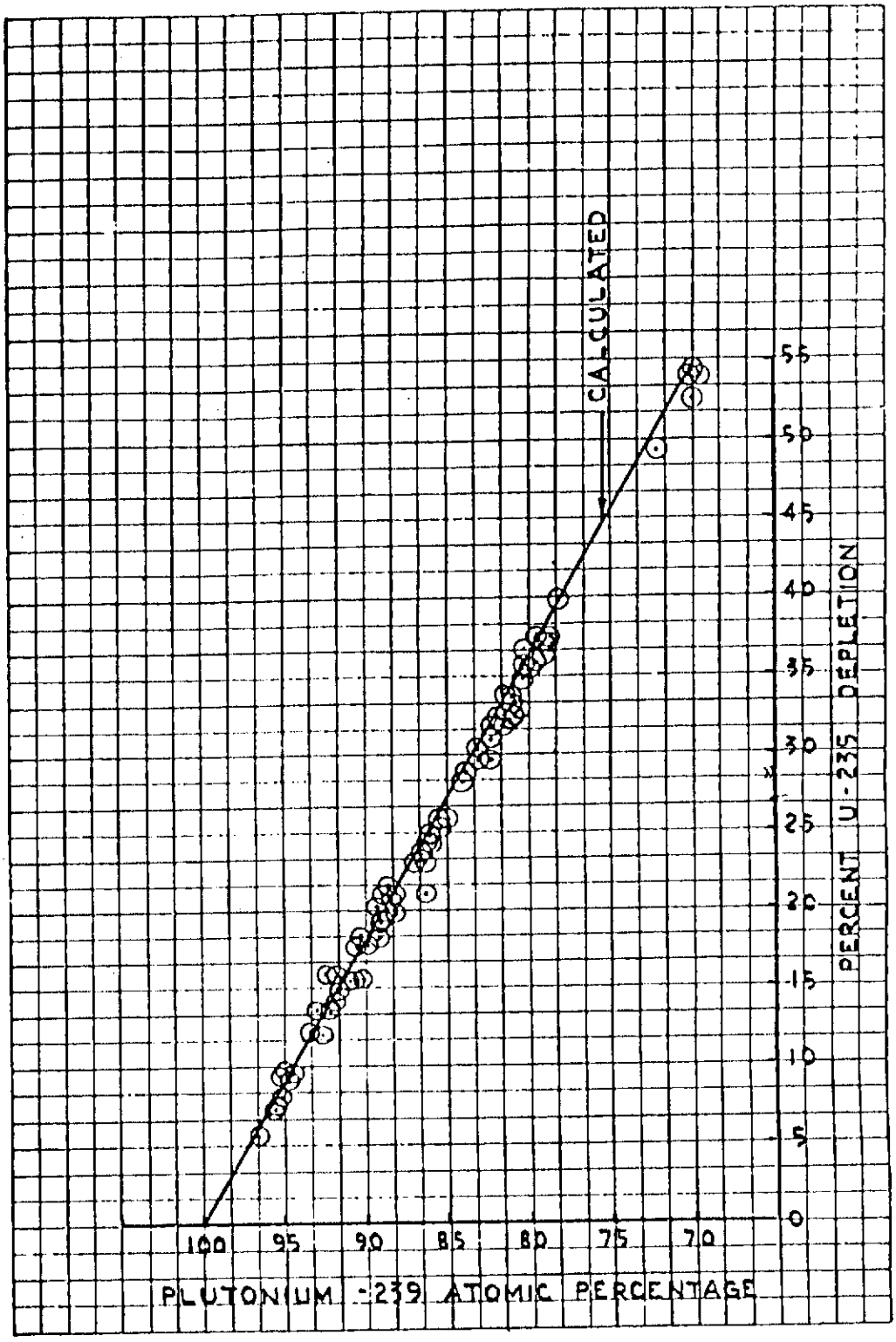

FRACTION OF PLUTONIUM-239 IN PLUTONIUM AS A FUNCTION OF URANIUM-235 DEPLETION

FIG. 3.2.1-14

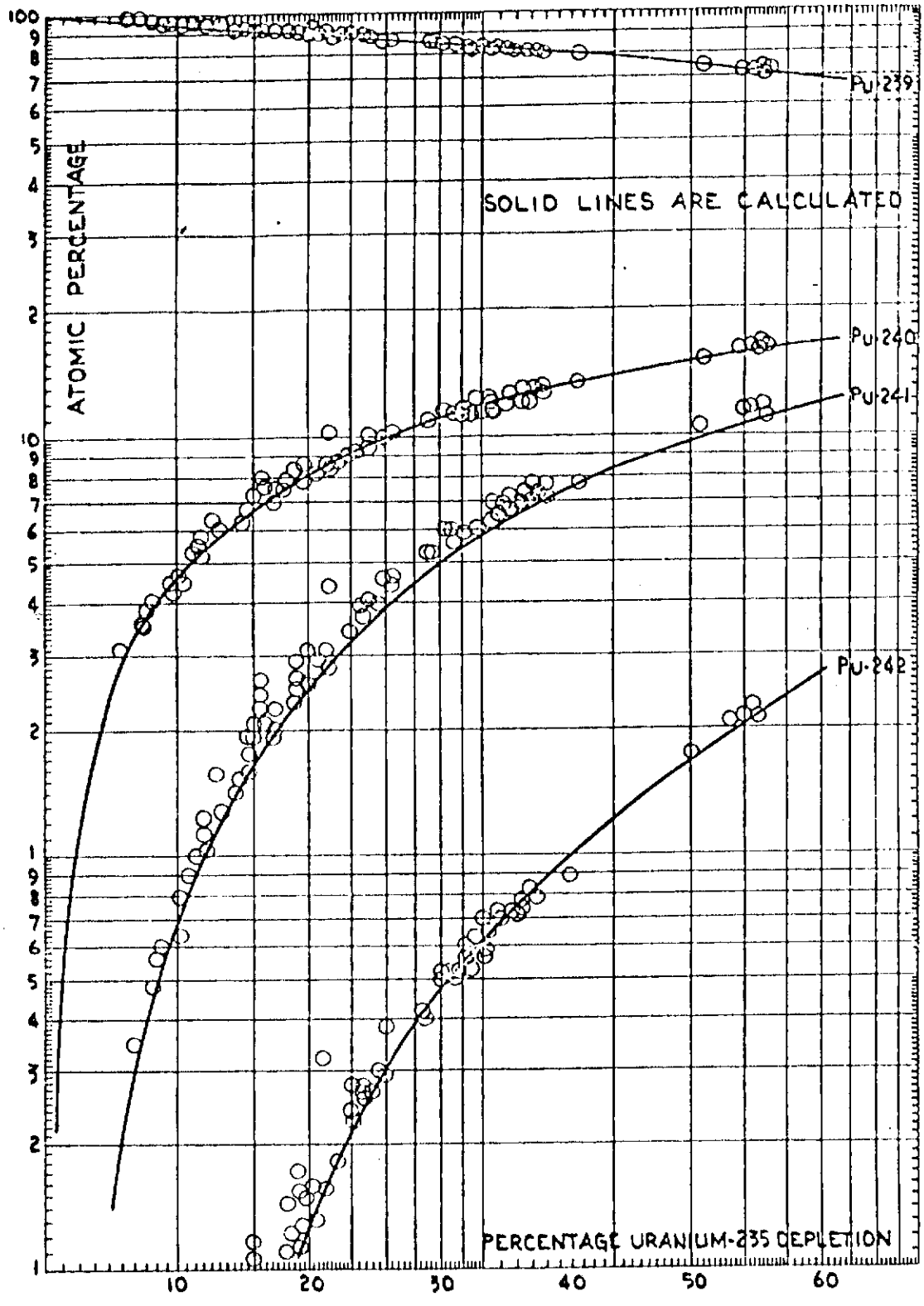

COMPOSITION OF PLUTONIUM AS A FUNCTION OF URANIUM-235 DEPLETION

FIG. 3.2.1-15

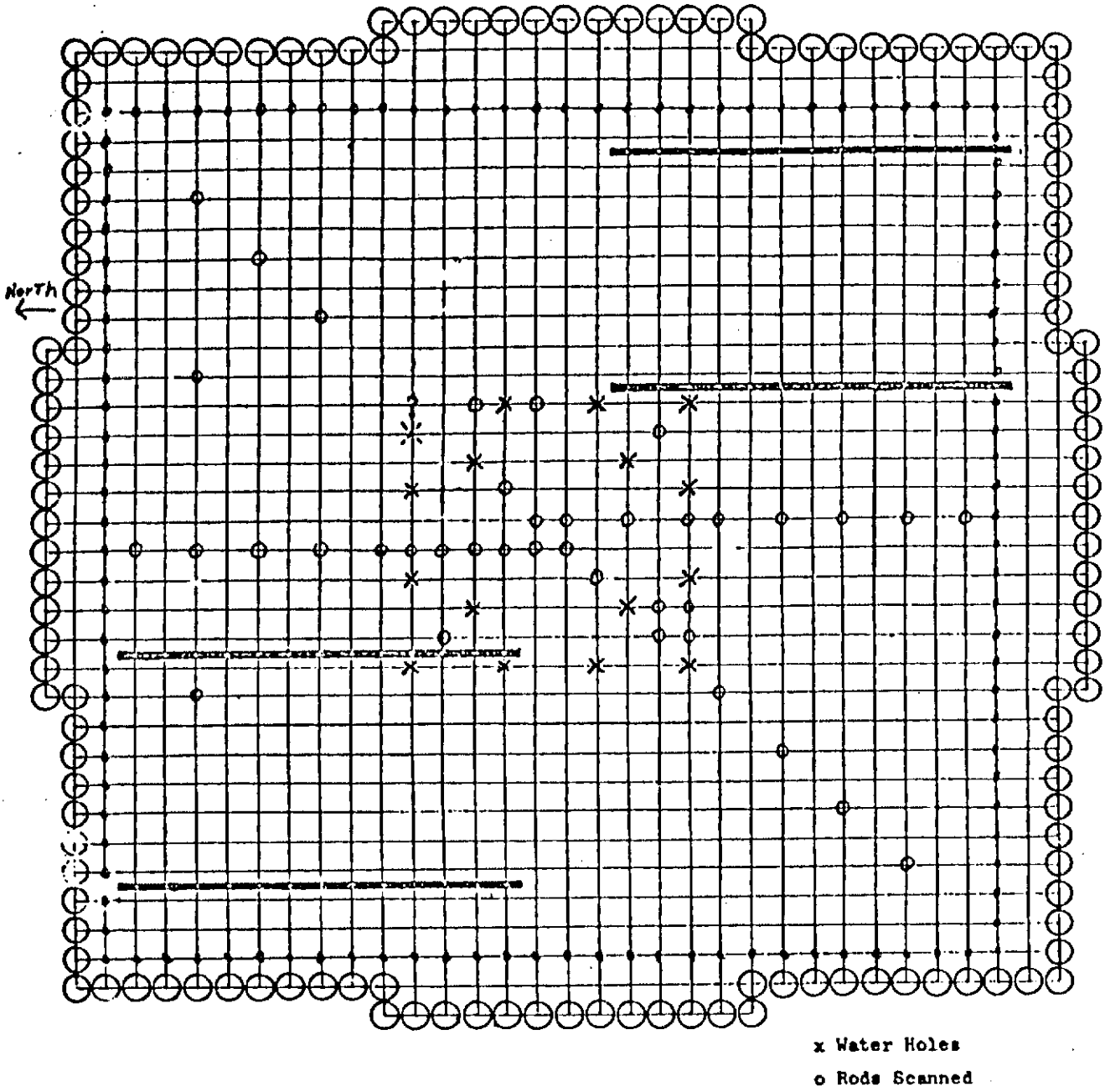

0.484 " Diameter , 0.6 " Pitch

PLAN OF CRITICAL EXPERIMENT (UNBORATED CASE)
FIG. 3.2.1-16

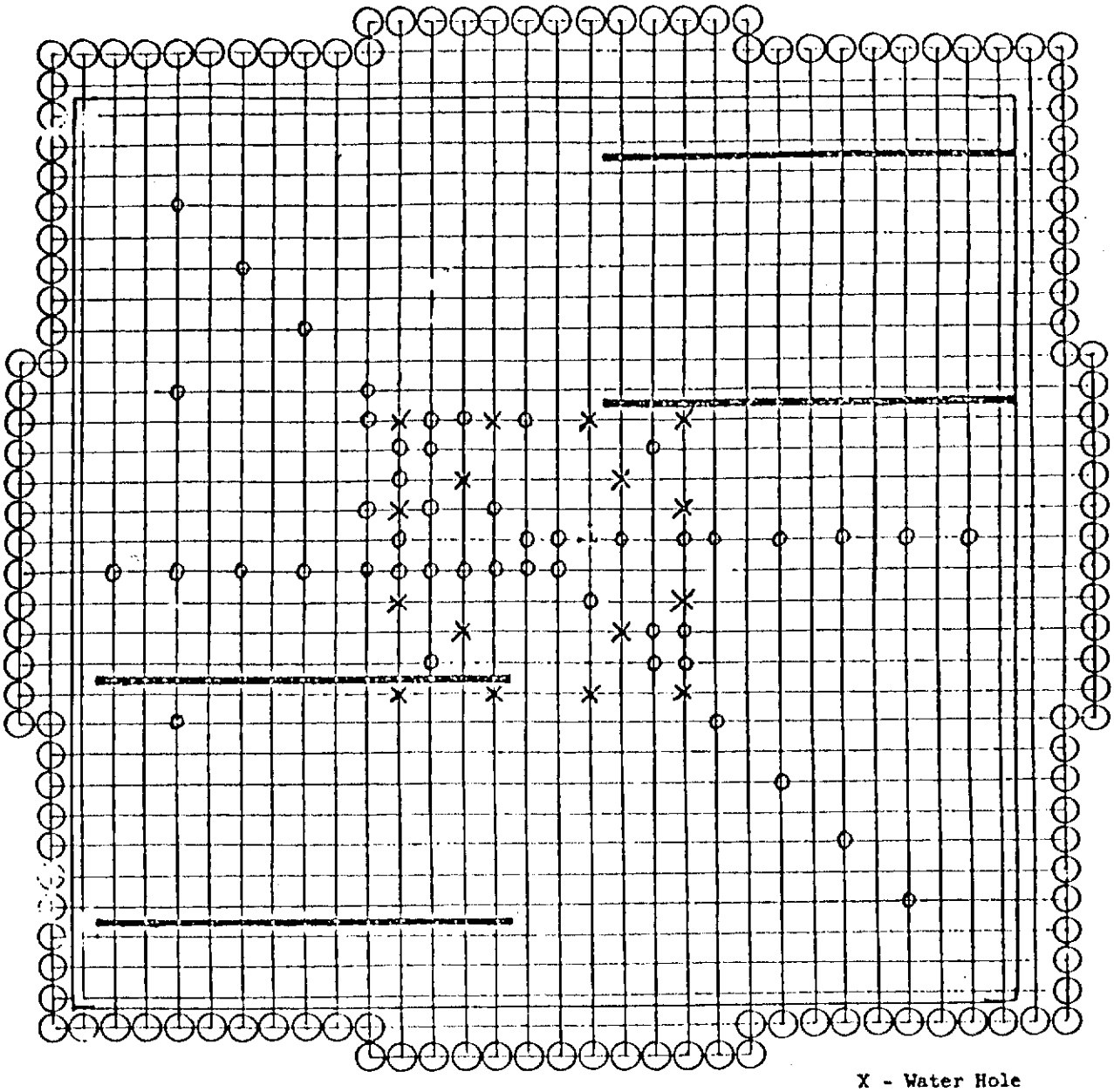

X - Water Hole

O - Rod Scanned

Core: 30 x 30

0.484 " Diameter , 0.6 " Pitch

PLAN OF CRITICAL EXPERIMENT (BORATED CASE)
FIG. 3.2.1-17

Comparison of Experimental and Calculated Power Distribution
30 x 30 Core With 16 Water Holes - 479 ppm Boron in Water
(1/8th Core Symmetry - One Block Represents One Fuel Rod)

(XXXX) PDQ Result
XXXX Experimental Value

BORATED POWER DISTRIBUTION COMPARISON

FIG. 3.2.1-18

Case (2) - Comparison of Experimental and Calculated Power Distribution Using Two Mesh Spacings Per Fuel Rod

(1/8th Core Symmetry - One Block Represents One Fuel Rod)

(xxxx) PDQ Result
xxxx Experimental Value

UNBORATED POWER DISTRIBUTION COMPARISON

FIG. 3.2.1-19

COMPARISON OF EXPERIMENTAL AND CALCULATED POWER DISTRIBUTION
USING ONE MESH SPACING PER FUEL ROD

Case (1) - Comparison of Experimental and Calculated Power Distribution Using One Mesh Spacings Per Fuel Rod

(1/8th Core Symmetry - One Block Represents One Fuel Rod)

(xxxx) PDQ Result
xxxx Experimental Value

FIG. 3.2.1-20

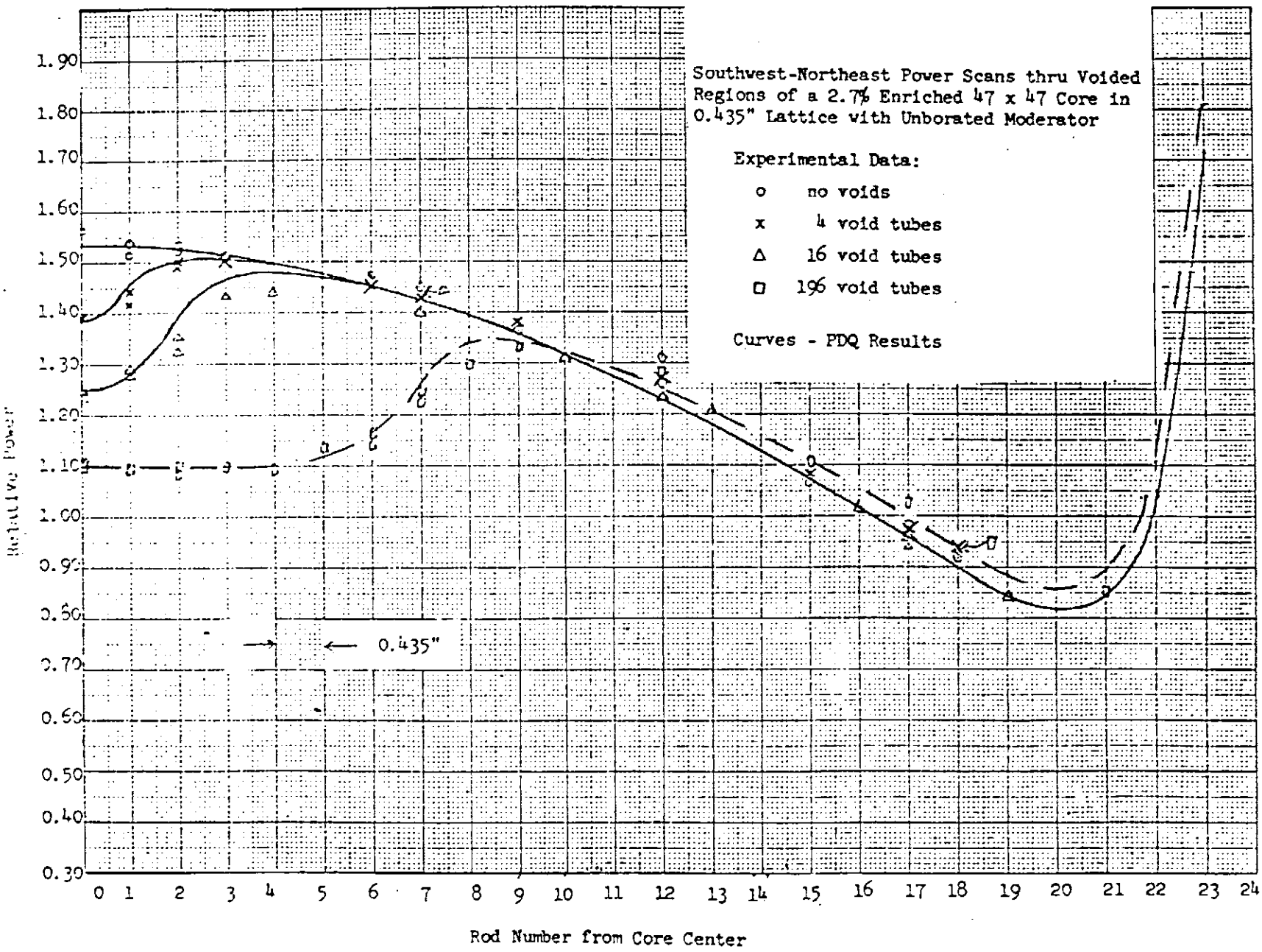

COMPARISON OF CALCULATED POWER DISTRIBUTION WITH EXPERIMENTAL POWER SCANS - UNBORATED CORE

FIG. 3.2.1-21

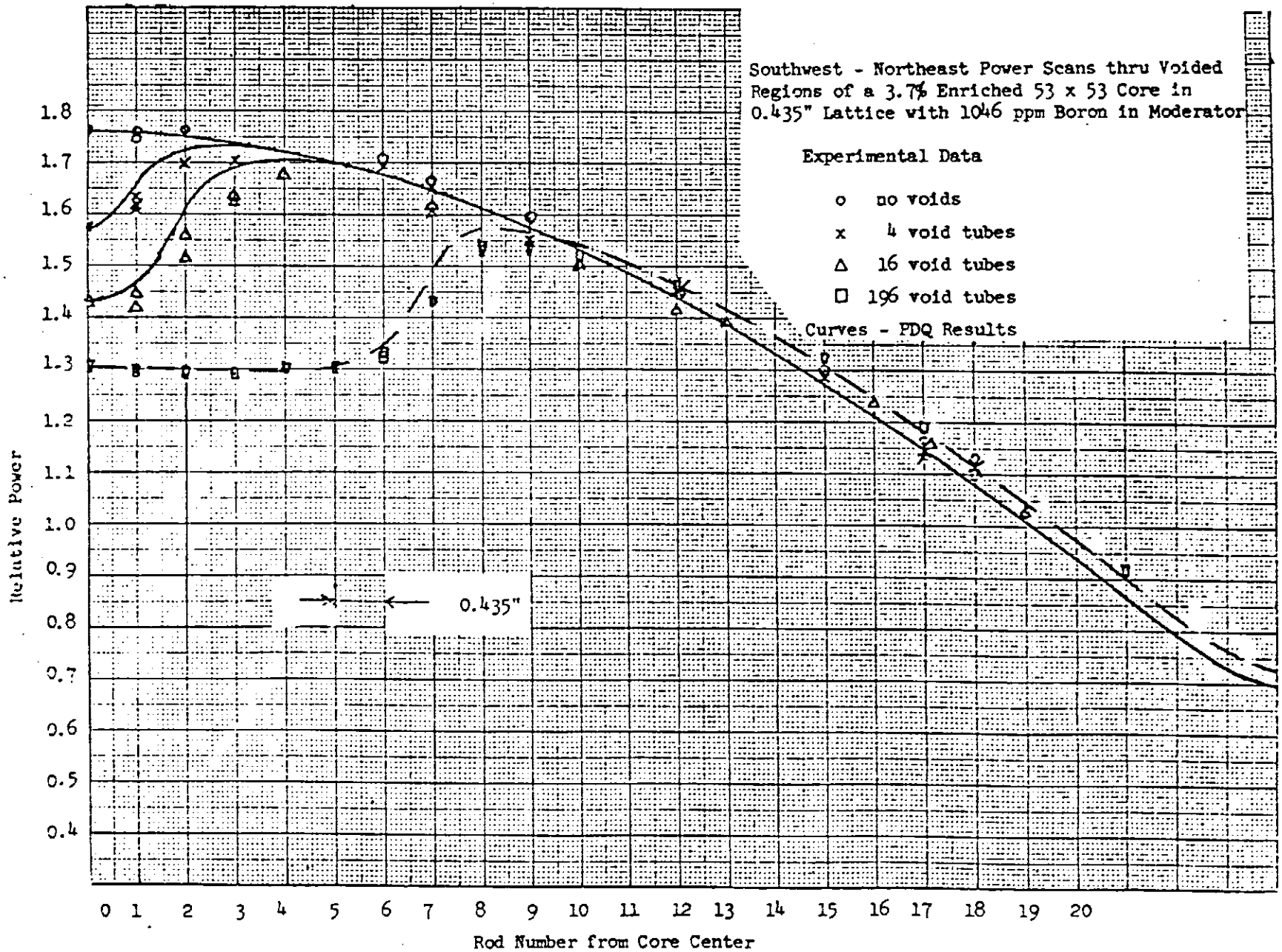

COMPARISON OF CALCULATED POWER DISTRIBUTION WITH EXPERIMENTAL POWER SCANS - BORATED CORE

FIG. 3.2.1-22

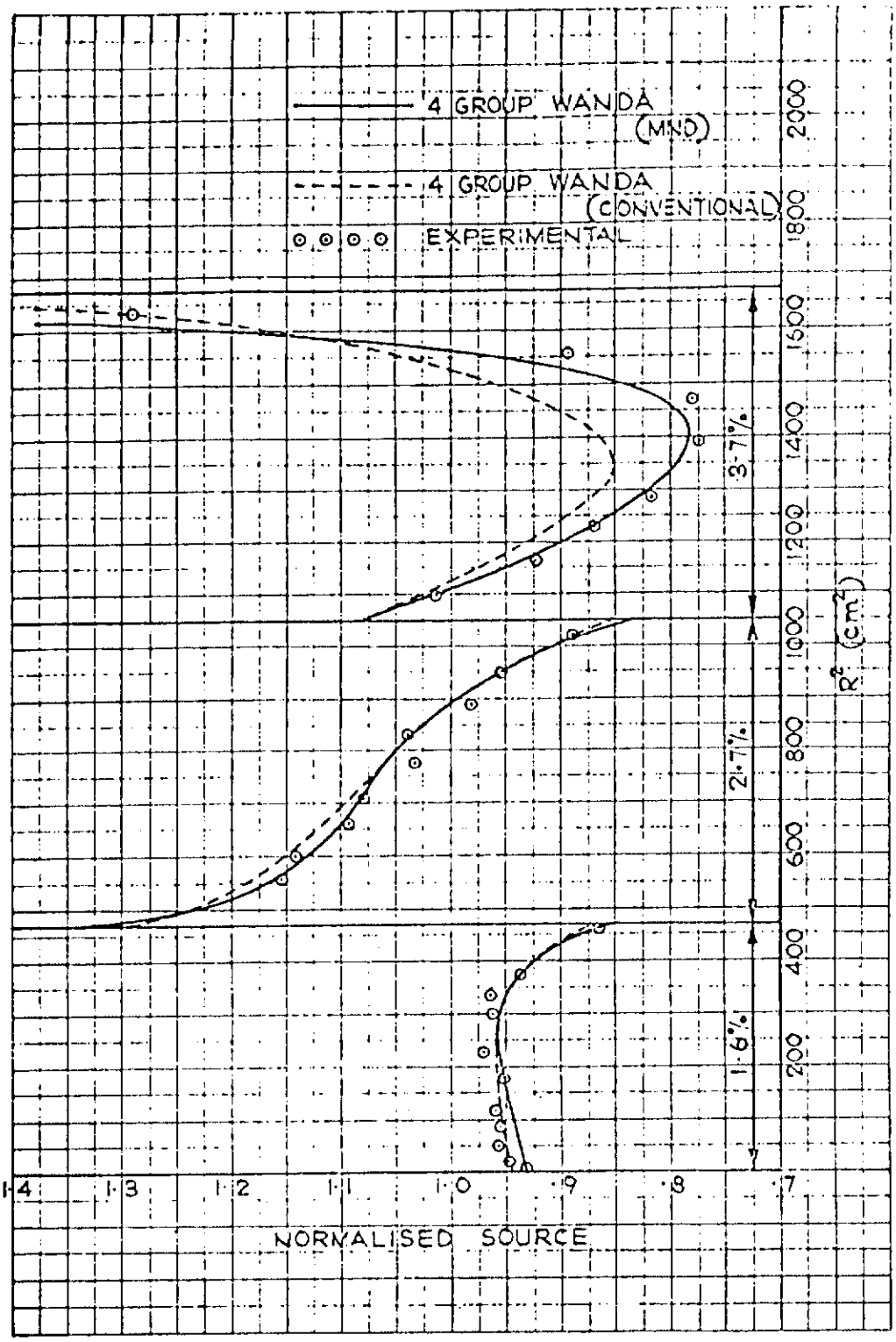

RADIAL FUEL ROD SCAN
FIG. 3.2.1-23

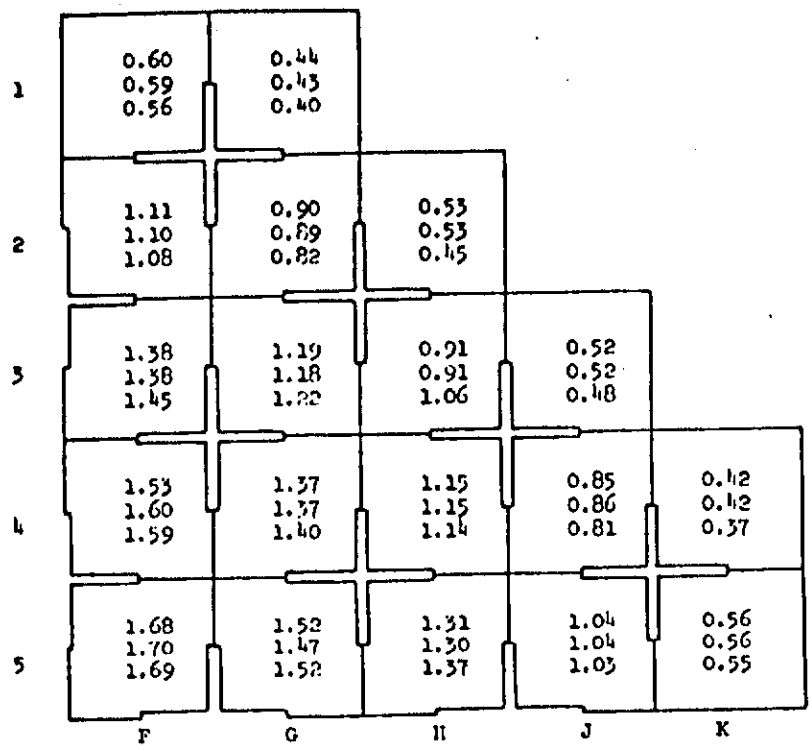

Note: The top value in each assembly is found from the control rod interchange TURBO, the centre value is from the TURBO with no interchange, and the bottom value is experimentally determined.

Analytical and Experimental Power Distribution for YANKEE Core 1. TURBO Time Step 14, 7400 EFPH - $\frac{1}{4}$ core shown.

YANKEE CORE 1 POWER DISTRIBUTION COMPARISON
FIG. 3.2.1-24

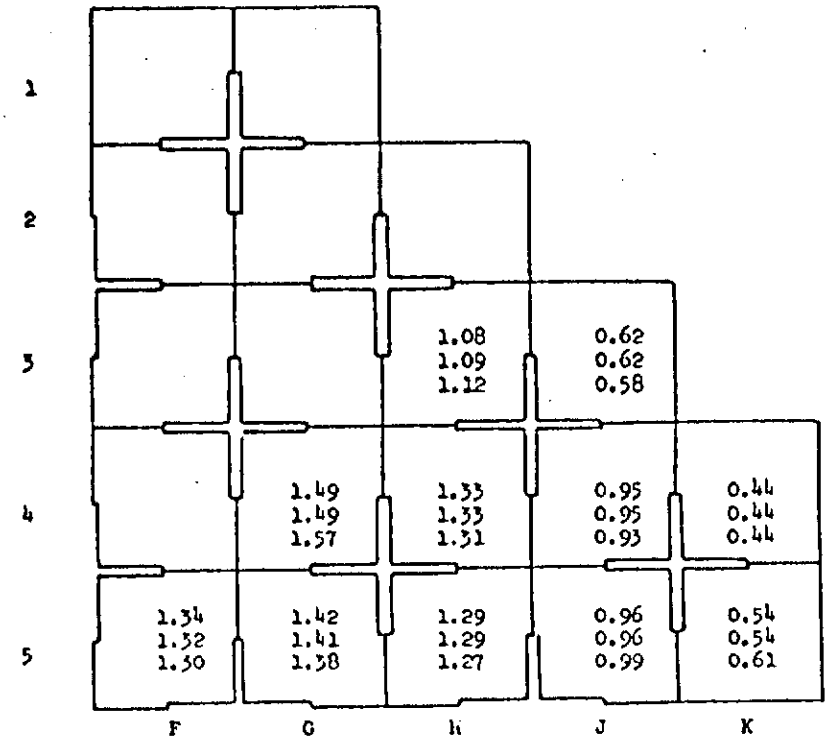

Notes:

1. The top value in each assembly is found from the control rod interchange TURBO, the centre value is from the TURBO with no interchange, and the bottom value is experimentally determined.

2. The burn-up distribution is defined by the ratio of the average burn-up in an assembly to the average in the quadrant. The numbers shown are the average of such values in symmetric assemblies.

Analytical and Experimental Burn-up Distributions for YANKEE Core 1. TURBO Time Step 14, 7400 EFPH - 1/4 core shown, Figures for 1/8 core.

YANKEE CORE 1 BURNUP DISTRIBUTION COMPARISON
FIG. 3.2.1-25

FIG. 3.2.1-26 FAST ABSORPTION OF CLUSTERED ABSORBERS

FAST ABSORPTION OF UNIFORMLY DISTRIBUTED ABSORBERS

FIG. 3.2.1-27

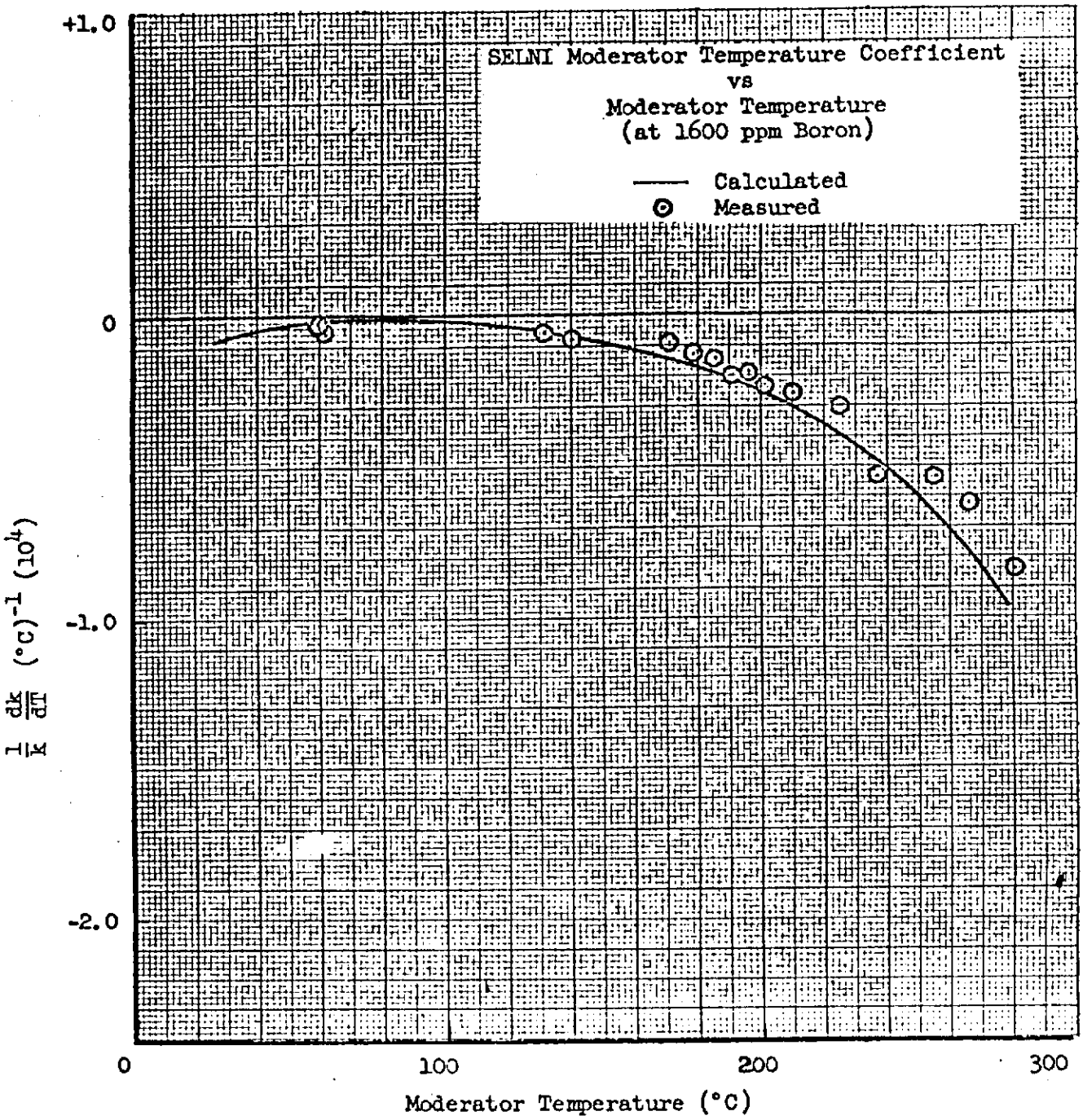

SELNI TEMPERATURE COEFFICIENT Vs. MODERATOR TEMPERATURE
(1600 PPM BORON)
FIG. 3.2.1-28

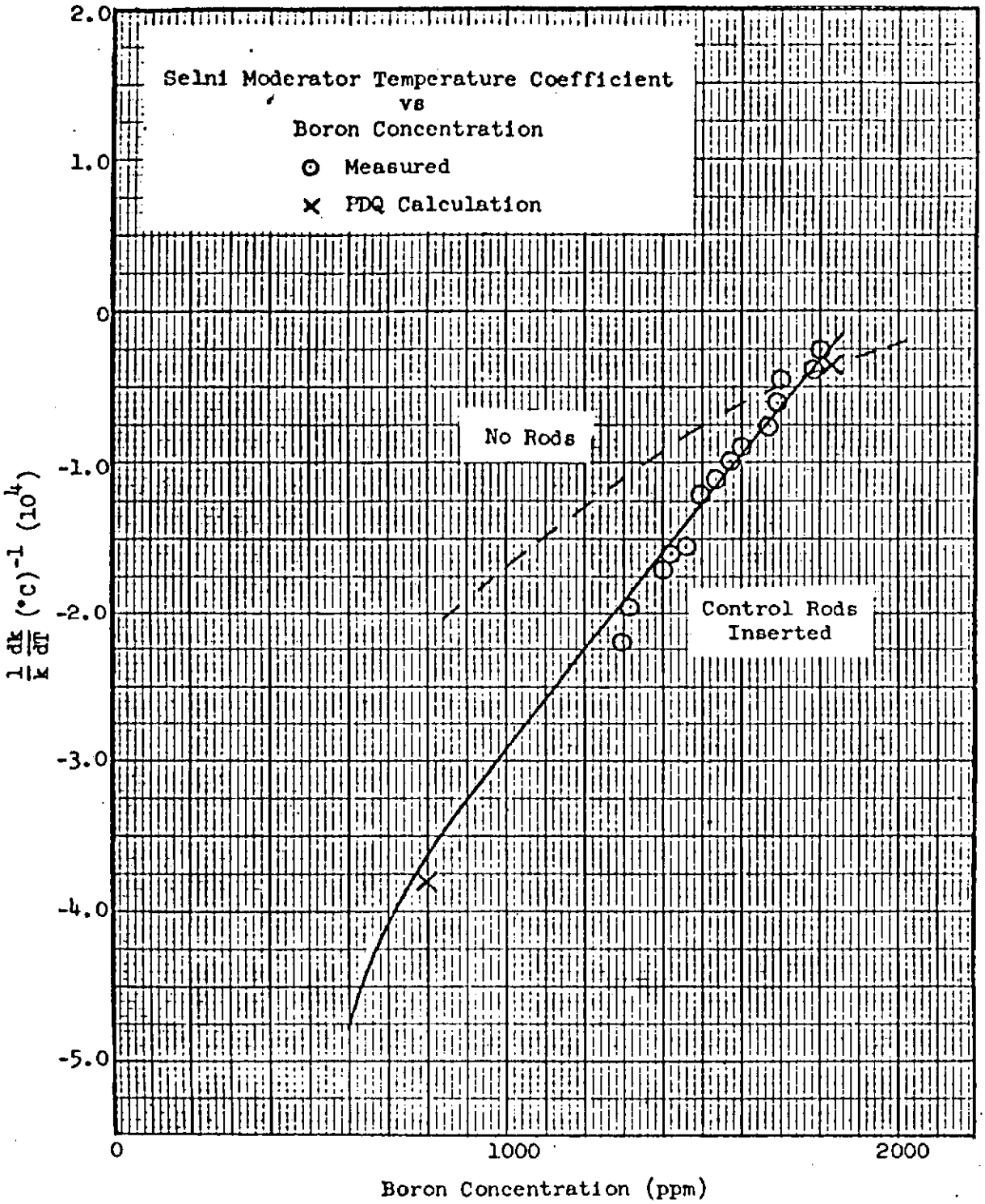

MODERATOR TEMPERATURE COEFFICIENT Vs. BORON CONCENTRATION

FIG. 3.2.1-29

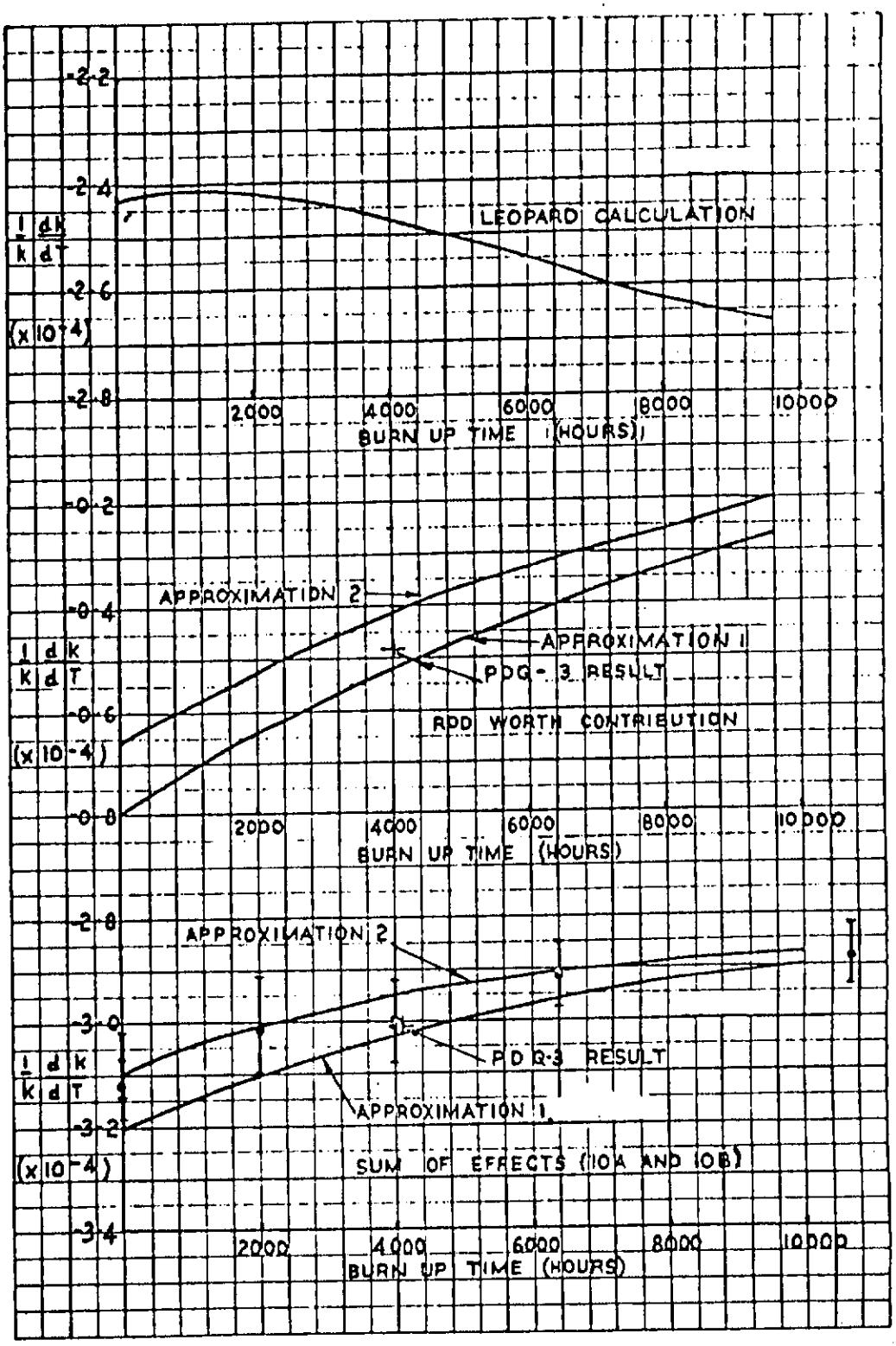

COMPARISON OF CALCULATED AND MEASURED MODERATOR TEMPERATURE COEFFICIENT Vs. BURNUP

FIG. 3.2.1-30

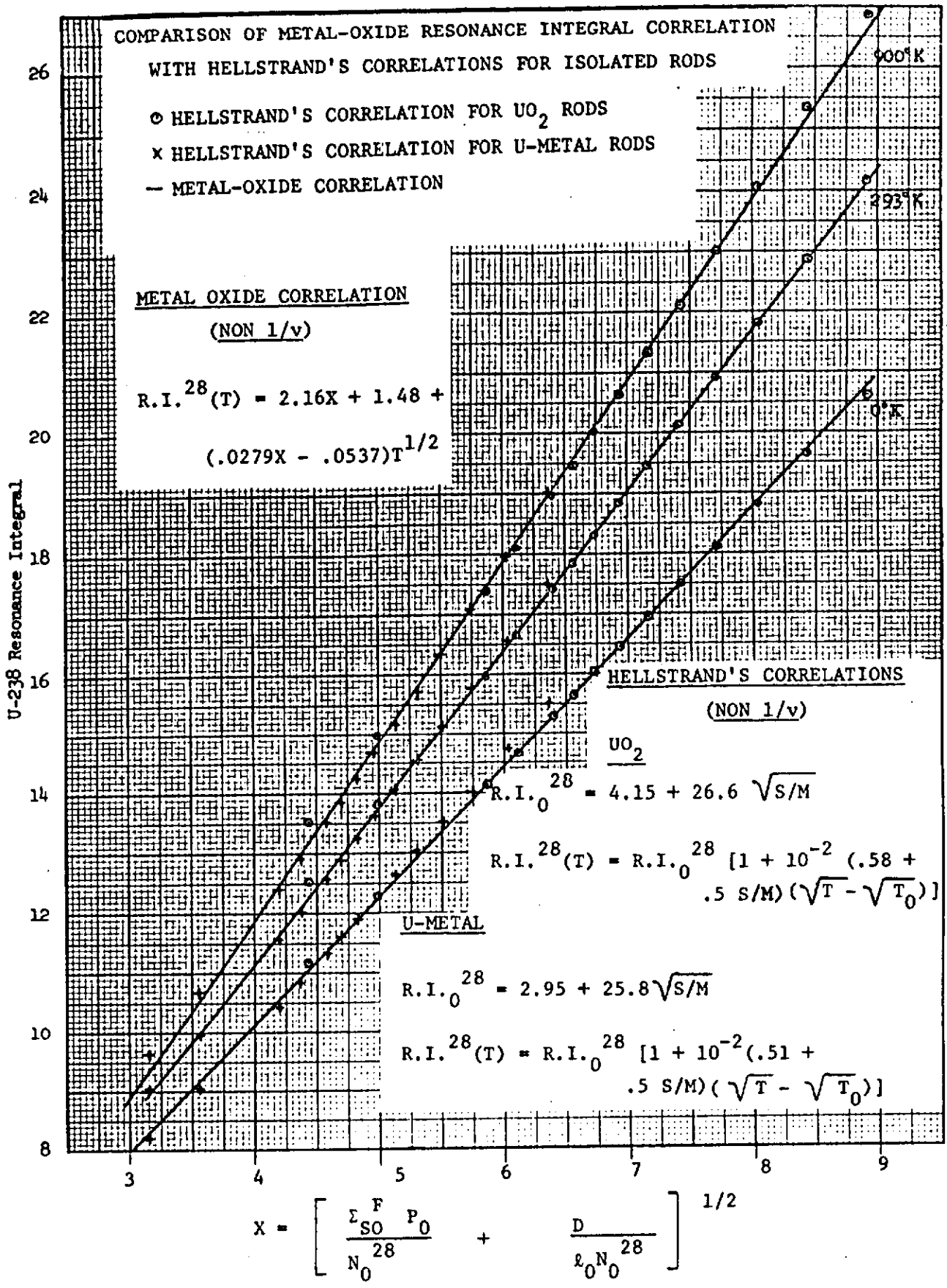

COMPARISON OF RESONANCE INTEGRAL CORRELATIONS
FIG. 3.2.1-31

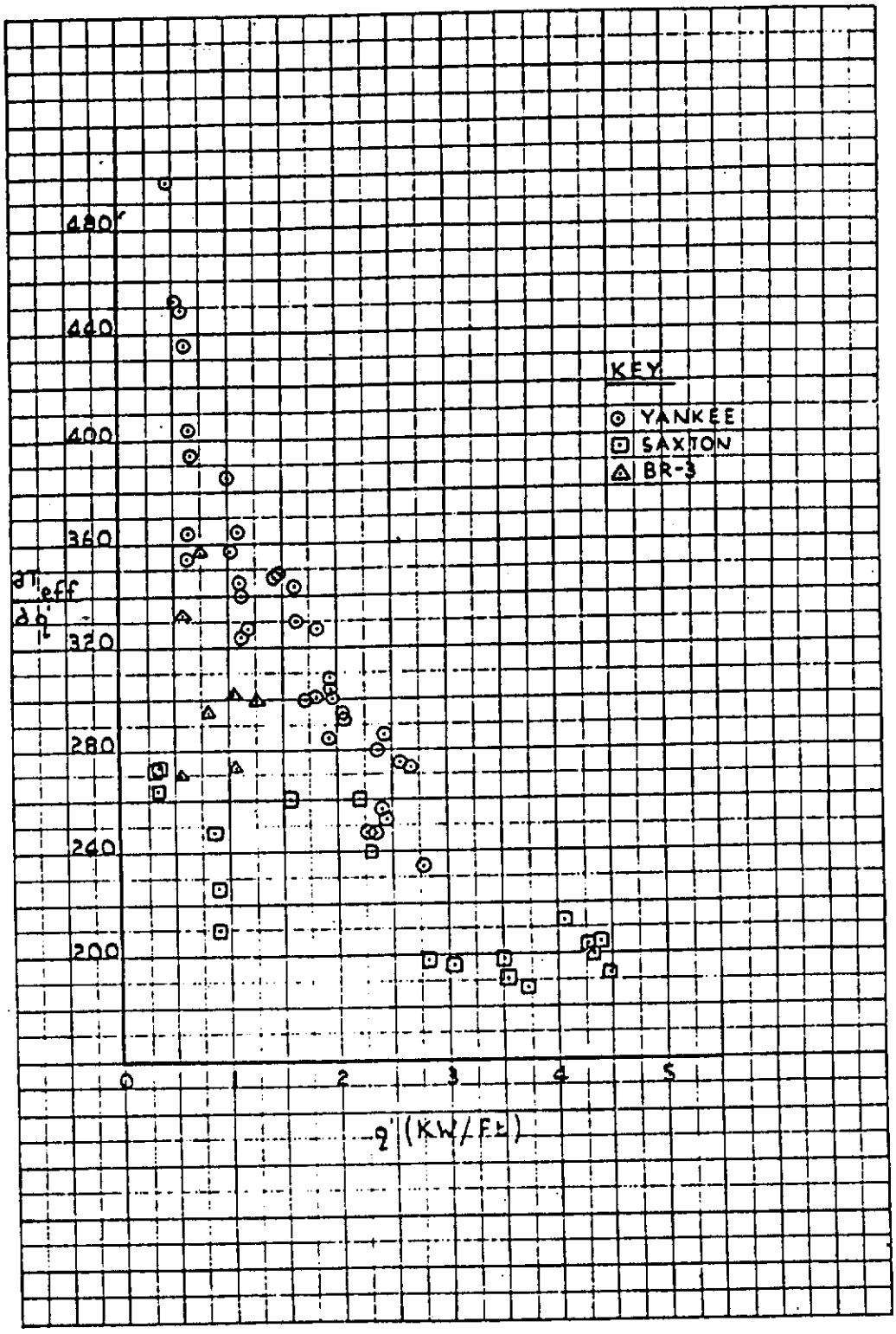

FUEL TEMPERATURE CHANGES Vs. POWER DENSITY
FIG. 3.2.1-32

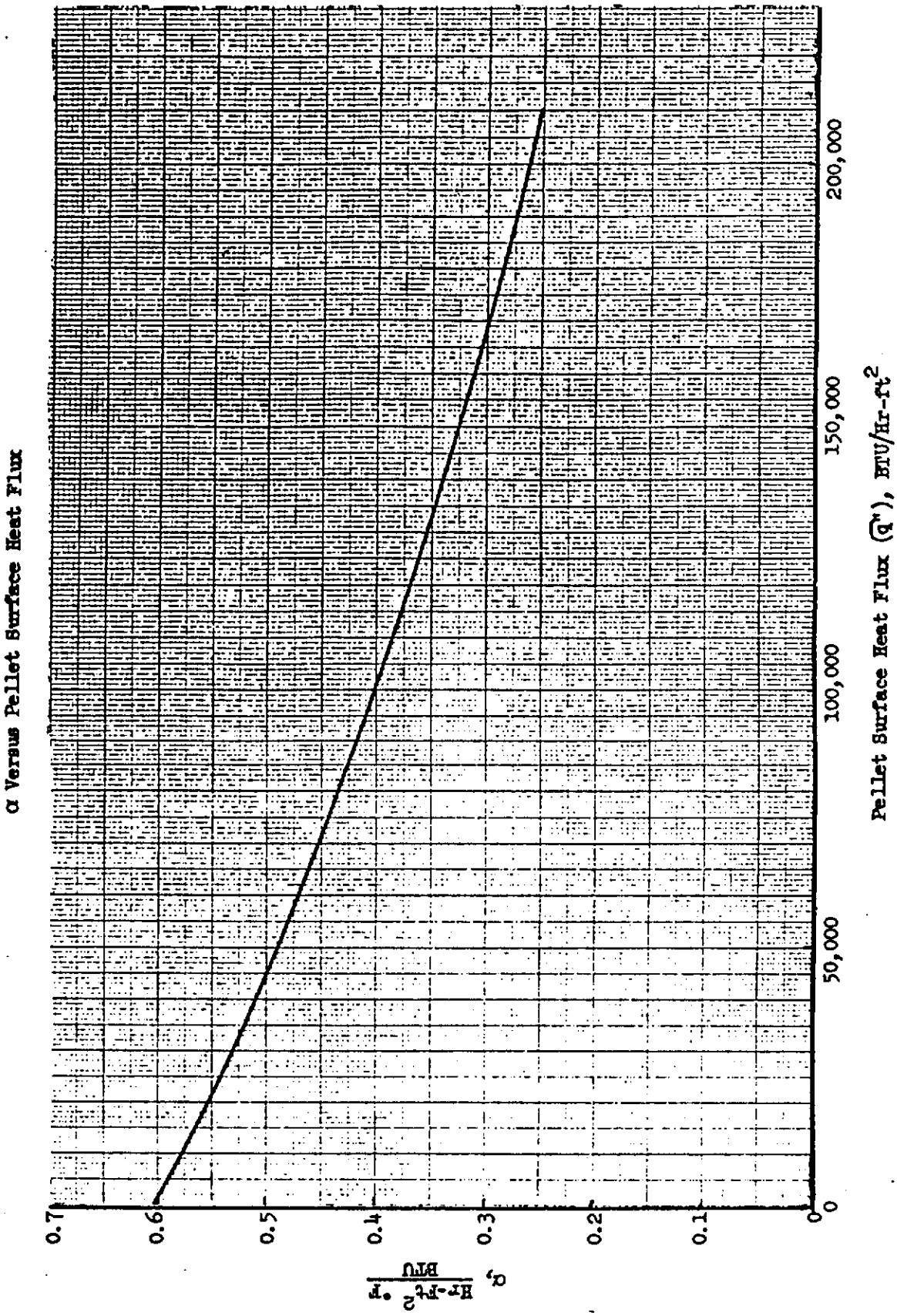

ALPHA Vs. HEAT FLUX
FIG. 3.2.1-33

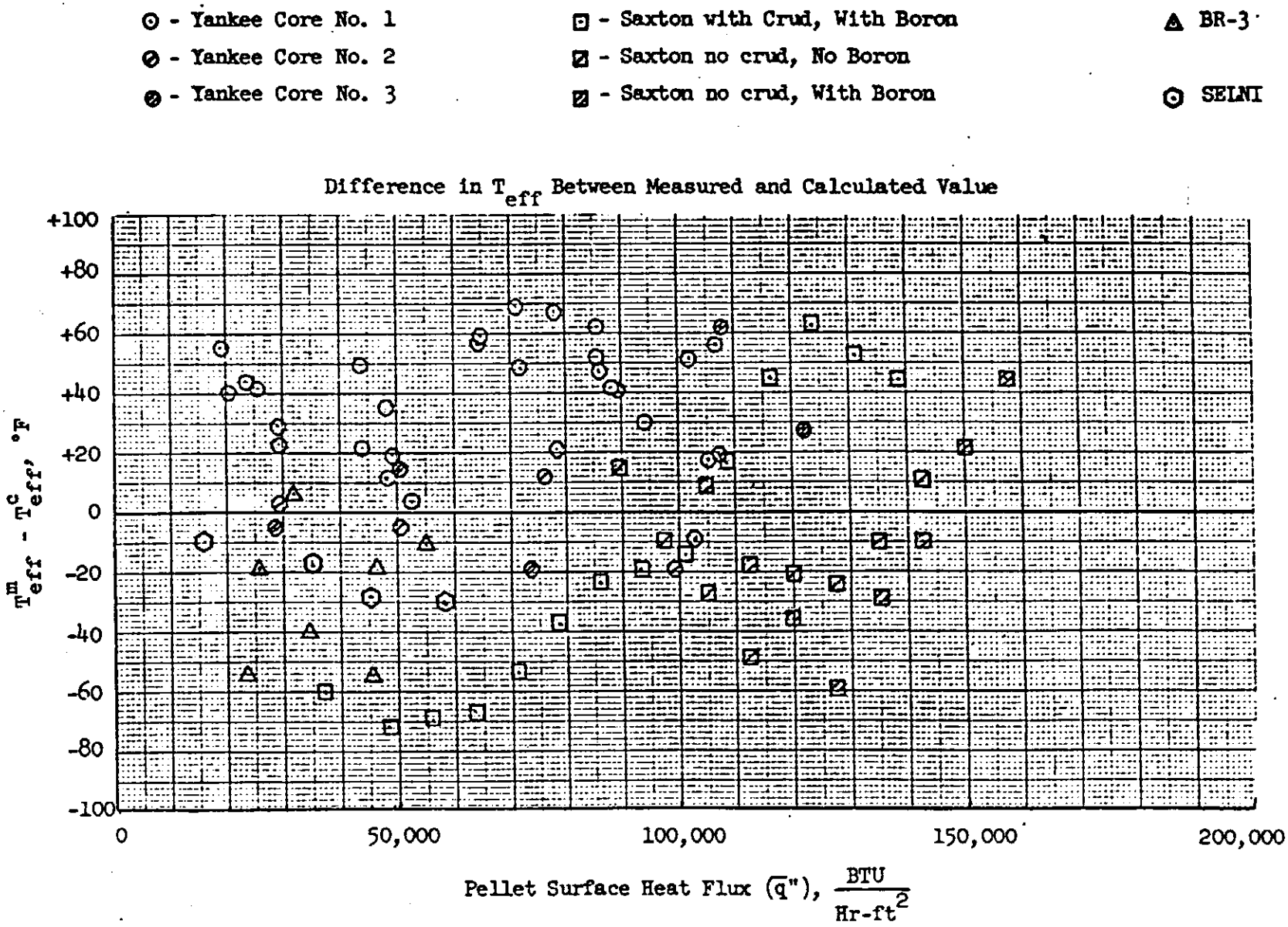

COMPARISONS OF EFFECTIVE FUEL TEMPERATURE WITH CHANGING HEAT FLUX

FIG. 3.2.1-34

Thermal and Hydraulic Characteristics of the Design

Thermal Data

Fuel and Cladding Temperature

The temperature distribution in the pellet is mainly a function of the uranium dioxide thermal conductivity and the local power density. The absolute value of the temperature distribution is affected by the cladding temperature and the thermal conductance of the gap between the pellet and the cladding.

The occurrence of nucleate boiling maintains maximum cladding surface temperature below about 657°F at nominal system pressure. The contact conductance between the fuel pellet and cladding is a function of the contact pressure and the composition of the gas in the gap [1] [2] and may be calculated by the following equation:

$$h = 0.6\ P + \frac{k}{f\,(14.4 \times 10^{-6})}$$

where

h is conductance in Btu/hr ft^2 ◦F

P is contact pressure in psi

k is the thermal conductivity of the gas mixture in the rod in Btu/hr ft^2 ◦F

f is the correction factor for the accommodation coefficient

The thermal-hydraulic design assures that the maximum fuel temperature is below the melting point of UO_2 (melting point of 5080°F (Reference 3) unirradiated and decreasing by 58°F per 10,000 MWD/MTU). To preclude fuel centerline melting and as a basis for overpower protection system setpoints, a calculated centerline fuel temperature of 4700°F has been selected as the overpower limit. This provides sufficient margin for uncertainties in the thermal evaluations. The temperature distribution within the fuel pellet is predominantly a function of the local power density and the UO_2 thermal conductivity. However, the computation of radial fuel temperature distributions combines crud, oxide, cladding gap and pellet conductances. The factors which influence these conductances, such as gap size (or contact pressure), internal gas pressure,

gas composition, pellet density, and radial power distribution within the pellet, etc., have been combined into a semi-empirical thermal model which includes a model for time dependent fuel densification as given in Reference 4. This thermal model enables the determination of these factors and their net effects on temperature profiles. The temperature predictions have been compared to inpile fuel temperature measurements (References 5 through 12), and melt radius data (References 13,14,) with good results.

As described in Reference 15, fuel rod thermal evaluations (fuel centerline, average and surface temperatures) are determined throughout the fuel rod lifetime with consideration of time dependent densification.

The principal factors which are employed in the determination of the fuel temperature are dicussed below.

UO_2 Thermal Conductivity

The thermal conductivity of uranium dioxide was evaluated from data reported by Howard et al. (Reference 16); Lucks et al. (Reference 17); Daniel et al. (Reference 18); Feith (Reference 19); Vogt et al. (Reference 20); Nishijima et al. (Reference 21); Wheeler et al. (Reference 22); Godfrey et al. (Reference 23); Stora et al. (Reference 24); Bush (Reference 25); Asamoto et al. (Reference 26); Kruger (Reference 27); and Gyllander (Reference 28).

At the higher temperatures, thermal conductiviey is best obtained by utilizing the integral conductivity to melt which can be determined with more certainty. From an examination of the data, it has been concluded that the best estimate for the value of $\int^{2800°C} K dt$ is 93 watts/cm. This conclusion is based on the integral values reported by Gyllander (Reference 28), Lyons, et al. (Reference 29), Coplin, et al. (Reference 30), Duncan (Reference 13), Bain (Reference 31), Stora (Reference 32).

The design curve for the thermal conductivity is shown in Figure 3.2.2-1. The section of the curve at temperatures between 0°C and 1300°C is in excellent agreement with the recommendation of the IAEA panel (Reference 33). The section of the curve above 1300°C, is derived for an integral value of 93 watts/cm (References 13,28,32).

Thermal conductivity for UO_2 at 95% theoretical density can be represented best by the following equation:

$$K = \frac{1}{11.8 + 0.0238T} + 8.775 \times 10^{-13} T^3$$

Where:

K= watts/cm-°C
T= °C

Westinghouse Experience With High Power Fuel Rods

The most current summary of Westinghouse cores' operational experience is available in the latest revision of WCAP-8183, "Operational Experience with Westinghouse Cores."[9] This report, revised annually, is a supporting document to safety analysis reports for licensing purposes. The NRC safety analysis report requirements for evaluating fuel and core component failure and burnup experience are met with WCAP-8183.

Heat Flux Ratio and Data Correlation

Departure from Nucleate Boiling, (DNB), is predicated upon a combination of hydrodynamic and heat transfer phenomena and is affected by the local and upstream conditions including the flux distribution.

In reactor design, the heat flux associated with DNB and the location of DNB are both important. The magnitude of the local fuel rod temperature after DNB depends upon the axial location where DNB occurs.

Both the W-3 DNB correlation[10], used for LOPAR fuel analysis, and the WRB-1 DNB correlation[11], used for OFA fuel analysis, incorporate local and system parameters in predicting the local DNB heat flux.

These correlations include the non-uniform flux effect, and the upstream effect which includes inlet enthalpy and a length upstream at which DNB occurs. The local DNB heat flux ratio (defined as the ratio of the DNB heat flux to the local heat flux) is indicative of the contingency available in the local heat flux without reaching DNB.

Definition of Departure from Nucleate Boiling Ratio

The DNB heat flux ratio (DNBR) as applied to typical cells (flow cells with all walls heated) and thimble cells (flow cells with heated and unheated walls) is defined as:

$$DNBR = \frac{q''_{DNB,N}}{q''_{loc}}$$

Where

$$q''_{DNB,N} = \frac{q''_{DBN,prediction}}{F}$$

And $q''_{DNB,prediction}$ is the uniform critical heat flux as predicted by the WRB-1 DNB correlation or W-3 DNB correlation (typical cell only).

F is the flux shape factor to account for nonuniform axial heat flux distributions (Reference 35) with the “C” term modified as in Reference 37.

$$F = \frac{C \int_0^{L_{DNB}} q''(Z)\, e^{-C(L_{DNB}-Z)}\, dz}{q''_{local,\,(at\,L_{DNB})} \times (1-e^{-C(L_{DNB})})}$$

L_{DNB} = distance from the inception of local boiling to the point of DNB.

Z = Distance form the inception of local boiling, measured in the direction of flow.

The empirical constant, C, as presented in Reference (35) has been updated through the use of more recent non-uniform DNB data However, the revised expression does not significantly influence (<1% deviation form that of Reference 35) the value of the F-factor and the DNB-ratio. It Does provide a better prediction of the location of CNB. The new expression is

$$C = 0.15 \frac{(1-X_{DNB})^{4.31}}{(G/10^6)^{0.478}} \quad \text{inch}^{-1}$$

G = Mass Velocity (lb/hr ft^2)

X_{DNB} = Quality of the coolant at the location where DNB flux is calculated

The DNBR as applied to the W-3 DNB correlation when a cold wall is present is:

$$DNBR = \frac{q''_{DNB,N,CW}}{q''_{loc}}$$

Where:

$$q''_{DNB,N,CW} = \frac{q''_{DNB,prediction,Dh} \times CWF}{F}$$

And $q''_{DNB,prediction,Dh}$ is the uniform critical heat flux as predicted by the W-3 cold wall DNB Correlation (Reference 37) when not all flow cell walls are heated (thimble cold wall cell). CWF is the cold wall factor.

W-3 Equivalent Uniform Flux DNB Correlation

In determining the F-factor, the value of q''_{local} at L_{DNB} was measured as $z = L_{DNB}$, the

location where the DNB flux is calculated. For a uniform flux, F becomes unity so that $q''_{DNB,N}$ reduces to $q''_{DNB,prediction}$ as expected. The comparison of predictions by using W-3 correlations and the non-uniform DNB data obtained by B&W[38], Winfrith[39] and Fiat are given in Figure 3.2.2-7 and Figure 3.2.2-8. The criterion for determining the predicted location of DNB is to evaluate the ratio of the predicted DNB flux to the local heat flux along the length of the channel. The location of the minimum DNB ratio is considered to be the location of DNB.

W-3 DNB Correlation

The W-3 correlation, and several modifications of it, have been used in Westinghouse critical heat flux calculations. The W-3 correlation was originally developed from single tube data, (reference 37) but was subsequently modified to apply to the 0.422 inch O.D. rod "L" grid (reference 40) rod bundle data. These modifications to the W-3 correlations have been demonstrated to be adequate for reactor rod bundle design.

The sources of the data used in developing the W-3 correlation are:

WAPD-188	(1958)	CU-TR-No. 1 (NW-208)	(1964)
ASME Paper 62-WA-297	(1962)	CISE-R-90	(1964)
CISE-R-63	(1962)	DP-895	(1964)
ANL-6675	(1962)	AEEW-R-356	(1964)
GEAP-3766	(1962)	BAW-3238-7	(1965)
AEEW-R-213 and 309	(1963)	AE-RTL-778	(1965)
CISE-R-74	(1963)	AEEW-355	(1965)
CU-MPR-XIII	(1963)	EUR-2490.e	(1965)

The comparison of the measured to predicted DNB heat flux of this correlation is given in Figure 3.2.2-2. The local flux DNB ratio versus the probability of not reaching DNB is plotted in Figure 3.2.2-3. This plot indicates that with a DNBR of 1.3 the probability of not reaching DNB is 95% at a 95% confidence level.

Recent rod bundle data without mixing vanes agree very well with the predicted DNB flux as shown in Figure 3.2.2-4, and rod bundle data with mixing vanes (Figure 3.2.2-5) show on the average an 8% higher value of DNB heat flux than predicted by the W-3 DNB correlation.

It should be emphasized that the inlet subcooling effect of the W-3 correlation was obtained from both uniform and non-uniform data. The existence of an inlet subcooling effect has been demonstrated to be real and hence the actual subcooling is used in the calculations. The W-3 correlation was developed from tests with flow in tubes and rectangular channels. Good agreement is obtained when the correlation is applied to test data for rod bundles.

WRB-1 DNB Correlation

The WRB-1 (Reference 36) correlation was developed based exclusively on the large bank of mixing vane grid rod bundle critical heat flux data (in excess of 1100 points) that Westinghouse has collected. The WRB-1 correlation, based on local fluid conditions, represents the rod bundle data with better accuracy over a wide range of variables than the previous correlation used in design (namely the W-3 correlation). This correlation accounts directly for both typical and thimble cold wall cell effects, uniform and nonuniform heat flux profiles, and variations in rod heated length and in grid spacing.

The applicable range of variables is:

Pressure	: $1440 \leq P \leq 2490$ psia
Local Mass Velocity	: $0.9 \times 10^6 \leq G_{loc} \leq 3.7 \times 10^6$ lb/ft^{2}hr
Local Quality	: $-0.2 \leq x_{loc} \leq 0.3$
Heated Length, Inlet to CHF Location	: $L_h \leq 14$ feet
Grid Spacing	: $13 \leq g_{sp} \leq 32$ inch
Equivalent Hydraulic Diameter	: $0.37 \leq d_e \leq 0.60$ inch
Equivalent Heated Hydraulic Diameter	: $0.46 \leq d_h \leq 0.59$ inch

Figure 3.2.2-6 shows measured critical heat flux plotted against predicted critical heat flux using the WRB-1 correlation.

The following subsections are carried over from the original updated FSAR and address only the W-3 DNB correlation. Similar detailed information is available in Reference 36 concerning the WRB-1 DNB correlation.

To calculate the DNBR of a reactor channel, the values of $\frac{q''_{DNB,N}}{q''_{loc}}$ along the channel are evaluated and the minimum value is selected as the minimum DNBR incurred in that channel.

The W-3 correlation depends on both local and inlet enthalpies of the actual system fluid, and the upstream conditions are accommodated by the F-factor. Hence, the correlation provides a realistic evaluation of the safety margin on heat flux.

Surface Heat Transfer Coefficients

Forced convection heat transfer coefficients are obtained from the Dittus-Boelter correlation (Reference 41), with the properties evaluated at bulk fluid conditions:

$$\frac{hD_e}{K} = 0.023\left[\frac{D_e\ G}{\mu}\right]^{0.8}\left[\frac{C_p\ \mu}{K}\right]^{0.4}$$

where:

- h = heat transfer coefficient (Btu/hr.-ft^2-^{o}F)
- D_e = equivalent diameter (ft)
- K = thermal conductivity (Btu/hr.-ft.-^{o}F)
- G = mass velocity (lb_m/hr.-ft.^{2})
- u = dynamic viscosity, (lb_m/ft.-hr)
- C_p = heat capacity, (Btu/lb_m-^{o}F)

This correlation has been shown to be conservative (Reference 42) for rod bundle geometries with pitch to diameter ratios in the range used by pressurized water reactors.

The onset of nucleate boiling occurs when the clad wall temperature reaches the amount of superheat predicted by Thom's (Reference 43) correlation. After this occurrence, the outer clad wall temperature is determined by:

ΔT_{sat} = $[0.072 \exp (-P/1260)] (q")^{0.5}$

Where:

ΔT_{sat} = wall superheat, $T_w - T_{sat}$ °F

q″ = wall heat flux (Btu/hr.-ft.^{2})

P = Pressure (psia)

T_w = outer clad wall temperature, °F

T_{sat} = saturation temperature of coolant at P °F

Hot Channel Factors

The total hot channel factors for heat flux and enthalpy rise are defined as the maximum-to-core average ratios of these quantities. The heat flux factors consider the local maximum linear heat generation rate at a point, and the enthalpy rise factors involve the maximum integrated value along a channel (the "hot channel").

Definition of Engineering Hot Channel Factor

Each of the total hot channel factors considers a nuclear hot channel factor describing the neutron flux distribution and an engineering hot channel factor which allows for variations in flow conditions and fabrication tolerances. The engineering hot channel factors are made up of subfactors accounting for the influence of the variations of fuel pellet diameter, density, enrichment and eccentricity; inlet flow distribution; flow redistribution; and flow mixing.

Heat Flux Engineering Subfactor, F_q^E

The heat flux engineering hot channel factor is used to evaluate the maximum linear heat generation rate in the core. This subfactor is determined by statistically combining the fabrication variations for the fuel pellet diameter, density, enrichment, and has a value of 1.03 at the 95% probability level with 95% confidence. As shown in Reference 44, no DNB penalty need be taken for the short, relatively low intensity heat flux spikes caused by variations in the above parameters, as well as fuel pellet eccentricity and fuel rod diameter variation.

Enthalpy Rise Engineering Subfactor, $F^E_{\Delta H}$

Design values employed in the THINC analysis related to the above fabrication variations are based on applicable limiting tolerances such that these design values are met for 95% of the limiting channels at a 95% confidence level. Measured manufacturing data on Westinghouse fuel show the tolerances used in this evaluation are conservative. The effect of variations in pellet diameter and enrichment is employed in the THINC analysis as a direct multiplier on the hot channel enthalpy rise while the fuel rod diameter, pitch and bowing variation including in-pile effects is considered in the preparation of the THINC input values such as axial flow area, equivalent hydraulic diameter and lateral crossflow area for the hot channel. The items considered contributing to the enthalpy rise engineering hot channel factor are discussed below.

a) Pellet diameter, density and enrichment

Variations in pellet diameter, density, and enrichment are considered statistically in establishing the limit DNBRs for the Revised Thermal Design Procedure (Reference 45) employed in this application. Uncertainties in these variables are determined from sampling of manufacturing data.

b) Inlet Flow Maldistribution

Studies performed on 1/7 scale hydraulic reactor models indicate that a conservative design basis is to consider a 5% reduction in the flow to the hot fuel assembly under isothermal conditions. This inlet flow reduction in the THINC analysis results in an increase of 1% in the hot channel enthalpy rise.

C) Flow Redistribution

The flow redistribution accounts for the reduction in flow in the hot channel resulting from the high flow resistance in the channel due to the local or bulk boiling. The effect of the nonuniform power distribution is inherently considered in the THINC analysis for every operating condition which is evaluated.

d) Flow Mixing

The subchannel mixing model incorporated in the THINC Code and used in reactor design is based on experimental data (Reference 46). The mixing vane incorporated into the spacer grid design induce additional flow mixing between the various flow channels in a fuel assembly and also between adjacent assemblies. This mixing reduces the enthalpy rise in the hot channel resulting from local power peaking or unfavorable mechanical tolerances.

The above subfactors are combined to obtain the total engineering hot channel factor for enthalpy rise of 1.01. Table 3.2.2-2 is a tabulation of the design engineering hot channel factors for the first fuel cycle. For current cycles, the effect of variations in flow conditions and fabrication tolerances on the hot channel enthalpy rise is directly considered in the THINC core thermal subchannel analysis under any reactor operating condition. Therefore, this engineering hot channel factor is no longer applied separately.

Nuclear Enthalpy Rise Hot Channel Factor $F^N_{\Delta H}$

Given the local power density q' (kw/ft) at a point x,y,z in a core with N fuel rods and height H,

$$F^N_{\Delta H} = \frac{\text{hot rod power}}{\text{average rod power}} = \frac{\text{MAX} \int_o^H q'(x_o, y_o, z)\,dz}{\frac{1}{N} \sum_{\text{all rods}} \int_o^H q(x,y,z)\,dz}$$

where x_o, y_o, are the position coordinates of the hot rod.

The way in which $F^N_{\Delta H}$ is used in the DNB calculation is important. The location of minimum DNBR depends on the axial profile and the value of DNBR depends on the enthalpy rise to that point. Basically, the maximum value of the rod

integral is used to identify the most likely rod for minimum DNBR. An axial power profile is obtained which when normalized to the value of $F^N_{\Delta H}$ recreates the axial heat flux along the limiting rod. The surrounding rods are assumed to have the same axial profile with rod average powers which are typical distributions found in hot assemblies. In this manner, worst case axial profiles can be combined with worst case radial distributions for reference DNB calculations.

It should be noted again that $F^N_{\Delta H}$ is an integral and is used as such in DNB calculations. Local heat fluxes are obtained by using hot channel and adjacent channel explicit power shapes which take into account variations in horizontal power shapes throughout the core. The sensitivity of the THINC-IV analysis to radial power shapes is discussed in Reference 47.

For operation at a fraction P of full power, the design $F^N_{\Delta H}$ used is given by:

$$F^N_{\Delta H} = 1.70 (1 + 0.3 (1-P)) \text{ (optimized fuel)}$$

$$F^N_{\Delta H} = 1.55 (1 + 0.3 (1-P)) \text{ (LOPAR fuel)}$$

where P is fraction of full power.

The permitted relaxation of $F^N_{\Delta H}$ is included in the DNB protection setpoints and allows radial power shape changes with rod insertion to the insertion limits (Reference 44), thus allowing greater flexibility in the nuclear design.

Pressure Drop and Hydraulic Forces

For historical purposes the total pressure loss across the reactor vessel, including the inlet and outlet nozzles, and the pressure drop across the core for the first cycle are listed in Table 3.2.2-1. This table also includes the total pressure drop across the core and other data for uprated conditions (Reference 49). These pressure drop values include a 10% uncertainty factor.

DNBR Design Methodology

The design method employed to meet the DNB design basis for the optimized and LOPAR fuel assemblies is the Revised Thermal Design Procedure (RTDP), Reference 45. With the RTDP methodology, uncertainties in plant operating parameters, nuclear and thermal parameters, fuel fabrication parameters, computer codes and DNB correlation predictions are considered statistically to obtain DNB uncertainty factors. Based on the DNB uncertainty factors, RTDP design limit DNBR values are determined such that there is at least a 95 percent probability at a 95 percent confidence level that DNB will not occur on the most limiting fuel rod during normal operation and operational transients and during transient conditions arising from faults of moderate frequency (Condition I and II events). Since the parameter uncertainties are considered in determining the RTDP design limit DNBR values, the plant safety analyses are performed using input parameters at their nominal values.

The RTDP design limit DNBR values are 1.23 and 1.22 for the typical and thimble cells, respectively, for optimized fuel, and 1.44 and 1.42 for the typical and thimble cells, respectively, for LOPAR fuel.

To maintain DNBR margin to offset DNB penalties such as those due to fuel rod bow and transition core, the safety analyses were performed to DNBR limits higher than the design limit DNBR values. These limits are called the DNBR safety analysis limits. The RTDP safety analysis limit DNBR values are 1.43 for typical and 1.42 thimble cells for optimized fuel and 1.58 for both typical and thimble cells for LOPAR fuel. The difference between the design and safety analysis limits results in DNBR margin, M:

$$\text{Safety Analysis Limit DNBR} = \frac{\text{Design Limit DNBR}}{1-M}$$

The design and safety analysis DNBR limits given above give DNBR margins of 14.0% for typical cell and 14.1% for thimble cell for the optimized fuel, and 8.9% for typical cell and 10.1% for thimble cell for the LOPAR fuel. The net DNBR margin, after consideration of all penalties, is available for operating and design flexibility.

The Standard Thermal Design Procedure (STDP) is used for those analyses where RTDP is not applicable. In the STDP method, the parameters used in the analysis are treated in a conservative way from a DNBR standpoint. The parameter uncertainties are applied directly to the plant safety analyses input values to give the lowest minimum DNBR. The DNBR limit for STDP is the appropriate DNB correlation limit increased by sufficient margin to offset the applicable DNBR penalties.

The THINC-IV code is used in the thermal/hydraulic analysis of the core. THINC-IV is a realistic three-dimensional matrix model which has been developed to account for hydraulic and nuclear effects on the enthalpy rise in the core (References 47, 50, 51). The behavior of the hot assembly is determined by superimposing the power distribution among the assemblies upon the inlet flow distribution while allowing for flow mixing and flow distribution between assemblies. The average flow and enthalpy in the hottest assembly is obtained from the core-wide, assembly by assembly analysis. The local variations in power, fuel rod and pellet fabrication, and mixing within the hottest assembly are then superimposed on the average conditions of the hottest assembly in order to determine the conditions in the hot channel.

DNB core safety limits are generated as a function of coolant temperature, pressure, core power, and the axial and radial power distributions. Operation within these DNB safety limits insures that the DNB design basis is met for both steady-state operation and for anticipated operational transients that are slow with respect to fluid transport delays in the primary system. In addition, for fast transients, e.g., uncontrolled rod bank withdrawal at power incident, specific protection functions are provided.

Effects of Rod Bow on DNBR

The phenomenon of fuel rod bowing, as described in Reference 52, is accounted for in the DNBR safety analysis of Condition I and Condition II events for each plant application. Applicable credits for margin resulting from retained conservatism in the evaluation of DNBR are used to offset the effect of rod bow. For the safety analysis of the Turkey Point units, sufficient DNBR margin was maintained to accommodate full flow and low flow DNBR penalties identified in Reference 53. The maximum rod bow penalties accounted for in the design safety analysis are 2.6% for optimized fuel and 2.2% for LOPAR fuel.

Effects of DNB on Neighboring Rods

Westinghouse has never observed DNB to occur in a group of neighboring rods in a rod bundle as a result of DNB in one rod in the bundle. Westinghouse[54] has conducted DNB tests in a 25-rod bundle where physical burnout occurred with one rod. After this occurrence, the 25 rod test section was used for several days to obtain more DNB data from the other rods in the bundle. The burnout and deformation of the rod did not affect the performance of neighboring rods in the test section during the burnout or the validity of the subsequent DNB data points as predicted by the W-3 correlation. No occurrences of flow instability or other abnormal operation were observed.

DNB With Return to Nucleate Boiling

Additional DNB tests have been conducted by Westinghouse[55] in 19 and 21 rod bundles. In these tests, DNB without physical burnout was experienced more than once on single rods in the bundles for short periods of time. Each time, a reduction in power of approximately 10% was sufficient to re-establish nucleate boiling on the surface of the rod. During these and subsequent tests, no adverse effects were observed on this rod or any other rod in the bundle as a consequence of operating in DNB.

Hydrodynamic and Flow Power Coupled Instability

Boiling flows may be susceptible to thermohydrodynamic instabilities (Reference 56). These instabilities are undesirable in reactors since they may cause a change in thermohydraulic conditions that may lead to a reduction in the DNB heat flux relative to that observed during a steady flow condition or to undesired forced vibrations of core components. Therefore a thermohydraulic design criterion was developed with states that modes of operation under Condition I and II events shall not lead to thermohydrodynamic instabilities.

Two specific types of flow instabilities are considered for Westinghouse PWR operation. These are the Ledinegg or flow excursion type of static instability and the density wave type of dynamic instability.

A Ledinegg instability involves a sudden change in flow rate from one steady state to another. This instability occurs (Reference 56) when the slope of the reactor coolant system pressure drop-flow rate curve $(\partial\Delta P/\partial G|_{INTERNAL})$ becomes algebraically smaller than the loop supply (pump head) pressure drop-flow rate curve $(\partial\Delta P/\partial G|_{EXTERNAL})$. The criterion for stability is, thus, $(\partial\Delta P/\partial G|_{INTERNAL}) > (\partial\Delta P/\partial G|_{EXTERNAL})$. The Westinghouse pump head curve has a negative slope $(\partial\Delta P/\partial G|_{EXTERNAL} < 0)$ whereas the reactor coolant system pressure drop-flow curve has a positive slope $(\partial\Delta P/\partial G|_{INTERNAL} > 0)$ over the Condition I and Condition II operational ranges. Thus, the Ledinegg instability will not occur.

The mechanism of density wave oscillations in a heated channel has been described by Lahey and Moody (Reference 57). Briefly, an inlet flow fluctuation produces an enthalpy perturbation. This perturbs the length and the pressure drop of the single phase region and causes quality or void perturbations in the two-phase regions which travel up the channel with the flow. The quality and length perturbations in the two-phase region create two-phase pressure drop perturbations. However, since the total pressure drop across the core is maintained by the characteristics of the fluid system external to the core, then the two-phase pressure drop perturbation feeds back to the single phase region. These resulting perturbations can be either attenuated or self-sustained.

A simple method has been developed by Ishii (Reference 58) for parallel closed channel systems to evaluate whether a given condition is stable with respect to the density wave type of dynamic instability. This method had been used to assess the stability of typical Westinghouse reactor designs (References 59, 52, 53), under Condition I and II operation. The results indicate that a large margin to density wave instability exists, e.g., increases on the order of 150 to 200% of rated reactor power would be required for the predicted inception of this type of instability.

The application of the method of Ishii (Reference 58) to Westinghouse reactor designs is conservative due to the parallel open channel feature of Westinghouse PWR cores. For such cores, there is little resistance to lateral flow leaving the flow channels of high power density channels. This coupling with cooler channels has led to the opinion that an open channel configuration is more stable than the above closed channel analysis under the same boundary

conditions. Flow stability tests (Reference 62) have been conducted where the closed channel systems were shown to be less stable than when the same channels were cross connected several locations. The cross-connections were such that the resistance to channel to channel cross flow and enthalpy perturbations would be greater than that which would exist in a PWR core which has a relatively low resistance to cross flow.

Flow instabilities which have been observed have occurred almost exclusively in closed channel systems operating at low pressure relative to the Westinghouse PWR operating pressures. Kao, Morgan and Parker (Reference 63) analyzed parallel closed channel stability experiments simulating a reactor core flow. These experiments were conducted at pressures up to 2200 psia. The results showed that for flow and power levels typical of power reactor conditions, no flow oscillations could be induced above 1200 psia.

Additional evidence that flow instabilities do not adversely affect thermal margin is provided by the data from the rod bundle DNB tests. Many Westinghouse rod bundles have been tested over wide ranges of operating conditions with no evidence of premature DNB or of inconsistent data which might be indicative of flow instabilities in the rod bundle.

In summary, it is concluded that thermohydrodynamic instabilities will not occur under Condition I and II modes of operation for Westinghouse PWR reactor designs. A large power margin exists to predicted inception of such instabilities. Analysis has been performed which shows that minor plant to plant differences in Westinghouse reactor designs such as fuel assembly arrays, core power to flow ratios, fuel assembly length, etc. will not result in gross deterioration of the above power margins.

Effect of Fuel Densification

Fuel densification is the process where geometric dimensions of fuel pellets under irradiation shrink from their as-built values. The cause of this shrinkage is the elimination of fine porosity from within the pellet grain structure. For modern design fuel, the densification process is essentially

complete after approximately 2000 MWD/MTU burnup. A competing process, fuel swelling is then dominant and lead to increased fuel dimensions with burnup. The basic densification model used by Westinghouse is given in Reference 15.

Radial shrinkage of the pellet causes an increase in the pellet-to-cladding gap and results in a decrease in gap conductance and a corresponding increase in fuel temperature and stored energy for a given heat generation rate. This effect is accounted for in the fuel temperature calculations.

Axial shrinkage of fuel pellets causes an increase in the fuel pellet linear heat generation rate. This increase is quantified by the stack height factor, a multiplier on the undensified linear heat generation rate.

An additional potential consequence of axial shrinkage will occur if the fuel pellets can become hung up in the cladding, which causes a formation of fuel-free interpellet gap. Removing neutron absorber material from a portion of a rod, as has occurred in the gap, causes an increase in the neutron density in the vicinity of the pellets near the gap, both on the rod with the gap and the adjacent rods. Interaction of these extra neutrons with the fuel pellets causes power generation spikes on the adjacent rods and the rod with the gap. The effect of such power spikes is accounted for with the use of a power spike factor, S(Z), where Z is the axial position in the core.

DNB power tests have shown that local power spikes have no effect on DNB[40]. Radial shrinkage of the pellet does not significantly affect the rod average heat flux at the cladding outer surface. Reference 64 indicates that process improvements in fuel pellet manufacturing have lead to the production of fuel pellets which exhibit controlled microstructure with respect to both grain size and pore size distribution. As a result, the current Westinghouse fuel used at Turkey Point is stable with respect to densification, and significant axial pellet column gaps do not occur. Thus, starting with Unit 4 Cycle 16, the elimination of the densification spike factor or the use of a factor of 1.0 in fuel design evaluation is appropriate.

REFERENCES, SECTION 3.2.2

1. Dean, R. A., "Thermal Contact Conductance Between UO_2 and Zircaloy-2," CVNA-127, May 1962.

2. Ross, A. M. and Stoute, R. D., "Heat Transfer Coefficient Between UO_2 and Zircaloy-2," AECL-1552, June 1962.

3. Christensen, J. A., Allio, R. J., and Biancheria, A., "Melting Point of Irradiated Uranium Dioxide," WCAP-6065, February 1965, NON-PROPRIETARY.

4. Weiner, R. A., et al., "Improved Fuel Performance Models for Westinghouse Fuel Rod Design and Safety Evaluations," WCAP-10851-P-A, August 1988.

5. Kjaerheim, G., and Rolstad, E., "In Pile Determination of UO Thermal Conductivity, Density Effects and Gap Conductance," HPR-80, December 1967.

6. Kjaerheim, G., "In-Pile Measurements of Centre Fuel Temperatures and Thermal conductivity Determination of Oxide Fuels," paper 1FA-175 presented at the European Atomic Energy Society Symposium on Performance Experience of Water-Cooled Power Reactor Fuel, Stockholm, Sweden, October 21-22, 1969.

7. Cohen, I., Lustman, G., and Eichenberg, D., "Measurement of the Thermal conductivity of Metal-Clad Uranium Oxide Rods During Irradiation," WAPD-228, 1960.

8. Clough, D.J., and Sayers, J.B., "The Measurement of the Thermal Conductivity of UO_2 under Irradiation in the Temperature Range 150°-1600°C," AERE-R24690, UKAEA. Research Group, Harwell, December 1964.

9. Stora, J.P., et al., "Thermal Conductivity of Sintered Uranium Oxide under In-Pile Conditions," EURAEC-1095, 1964.

10. Devold, I., "A Study of the Temperature Distribution in UO Reactor Fuel Elements," AE-318, Aktiebolaget Atomenergi, Stockholm, Sweden, 1968.

11. Balfour, M. G., Christensen, J. A., and Ferrari, H. M., "In-Pile Measurement of UO_2 Thermal Conductivity," WCAP-2923, 1966.

12. Leech, W. J., et al., "Revised PAD Code Thermal Safety Model," WCAP-8720, Addendum 2, October 1982.

13. Duncan, R. N., "Rabbitt Irradiation of UO_2," CVNA-142, June 1962.

14. Nelson, R. C., et al., "Fission Gas Release from UO_2 Fuel Rods with Gross Central Melting," GEAP-4571, July 1964.

15. Hellman, J. M., (Ed.), "Fuel Densification Experimental Results and Model for Reactor Application," WCAP-8218-P-A (Proprietary) March 1975 and WCAP-8219-A, March 1975.

16. Howard, V. C., and Gulvin, T. G., "Thermal Conductivity Determinations on Uranium Dioxide by a Radial Flow Method," UKAEA IG-Report 51, November 1960.

17. Lucks, C. F., and Deem, H. W., "Thermal Conductivity and Electrical Conductivity of UO_2," in Progress Reports Relating to Civilian Applications, BMI-1448 (Rev.) for June 1960; BMI-1489 (Rev.) for December 1960 and BMI-1518 (Rev.) for May 1961.

18. Daniel, J. L., Matolich, J., Jr., Deem, H. W., "Thermal Conductivity of UO_2," HW-69945, September 1962.

19. Feith, A. D., "Thermal Conductivity of UO_2 by a Radial Heat Flow Method," TID-21668, 1962.

20. Vogt, J., Grandell, L., and Runfors, U., "Determination of the Thermal Conductivity of Unirradiated Uranium Dioxide," AB Atomenergi Report RMB-527, 1964, Quoted by IAEA Technical Report Series No. 59, "Thermal Conductivity of Uranium Dioxide."

21. Nishijima, T., Kawada, T., and Ishihata, A., "Thermal Conductivity of Sintered UO_2 and Al_2O_3 at High Temperature," J. American Ceramic Society, 48, 31, 34, 1965.

22. Ainscough, J. B., and Wheeler, M. J., "Thermal Diffusivity and Thermal Conductivity of Sintered Uranium Dioxide," in Proceedings of the Seventh Conference of Thermal conductivity, P. 467, National Bureau of Standards, Washington, 1968.

23. Godfrey, T. G., et al., "Thermal Conductivity of Uranium Dioxide and Armco Iron by an Improved Radial Heat Flow Technique," ORNL-3556, June 1964.

24. Stora, J. P., et al., "Thermal Conductivity of Sintered Uranium Oxide Under In-Pile Conditions," EURAEC-1095, August 1964.

25. Bush, A. J., "Apparatus of Measuring Thermal Conductivity to 2500◦C," Westinghouse Research Laboratories Report 64-1P6-401-43, (Proprietary) February 1965.

26. Asamoto, R. R., Anselin, F. L., and Conti, A. E., "The Effect of Density on the Thermal Conductivity of Uranium Dioxide," GEAP-5493, April 1968.

27. Kruger, O. L., "Heat Transfer Properties of Uranium and Plutonium Dioxide," Paper 11-N-68F presented at the Fall meeting of Nuclear Division of the American Ceramic Society, Pittsburgh, September 1968.

28. Gyllander, J. A., "In-Pile Determination of the Thermal Conductivity of UO_2 in the Range 500-2500◦C," AE-411, January 1971.

29. Lyons, M. F., et al., "UO_2 Powder and Pellet Thermal Conductivity During Irradiation," GEAP-5100-1, March 1966.

30. Coplin, D. H., et al., "The Thermal Conductivity of UO_2 by Direct In-reactor Measurements," GEAP-5100-6, March 1968.

31. Bain, A. S., "The Heat Rating Required to Produce Center Melting in Various UO_2 Fuels," ASTM Special Technical Publication, No. 306, pp. 30-46, Philadelphia, 1962.

32. Stora, J. P., "In-Reactor Measurements of the Integrated Thermal Conductivity of UO_2 - Effect of Porosity," Trans. ANS, 13, 137-138, 1970.

33. International Atomic Energy Agency, "Thermal Conductivity of Uranium Dioxide," Report of the Panel held in Vienna, April 1965, IAEA Technical Reports Series, No. 59, Vienna, The Agency, 1966.

34. Slagle, W. H., "Operational Experience with Westinghouse Cores," (through December 31, 1993) WCAP-8183, Revision 22, December 1994.

35. Tong, L. S., "Prediction of Departure from Nucleate Boiling for an Axially Non-Uniform Heat Flux Distribution," Journal of Nuclear Energy, Vol. 21, pp. 241-248, (1967).

36. Motley, F. E., Mill, K. W. , et al., "New Westinghouse Correlation WRB-1 for Predicting Critical Heat Flux in Rod Bundles with Mixing Vane Grids," WCAP-8762-P-A, July 1984.

37. Tong, L. S., "Boiling and Critical Heat Flux," TID-25887, 1972.

38. Judd, D. F., et al., "Non-Uniform Heat Generation Experimental Program" BAW-3238-7 (1965).

39. Lee, D. H. "An Experimental Investigation of Forced Convection Burnout in High Pressure Water, Part IV, Large Diameter Tubes at About 1600 psi", AEEW-R-479, Winfrith, England (1966).

40. Motley, F. E., Cadek, F. F., "Applications of Modified Spacer Factor to L. Grid Typical and Cold Wall Cell DNB, "WCAP-7988 (Westinghouse Proprietary), and WCAP-8030-A (Non-Proprietary), and WCAP-8030-A (Non-Proprietary), October, 1972.

41. Dittus, F.W., and Boelter, L.M.K., "Heat Transfer in Automobile Radiators of the Tubular Type," Calif. Univ. Publication in Eng., 2, No. 13, 443461 (1930).

42. Weisman, J., "Heat Transfer to Water Flowing Parallel to Tube Bundles," Nucl. Sci. Eng., 6, 78-79 (1959)

43. Thom, J.R.S., Walker, W.M., Fallon, T.A. and Reising, G.F.S., "Boiling in Sub-cooled Water During Flowup Heated Tubes or Annuli," Prc. Instn. Mech. Engrs., 180, Pt. C, 226-46 (1955-66).

44. Hill, K. W., Motley, F. E. and Cadek, F. F., "Effect of Local Heat Flux Spikes on DNB in Non-Uniform Heated Rod Bundles," WCAP-8174, August, 1973 (Proprietary) and WCAP-8202, August, 1973 (Nonproprietary).

45. Friedland, A. J., Ray, S., "Revised Thermal Design Procedure," WCAP-11397-P-A, April, 1989.

46. Cadek, F. F., "Interchannel Thermal Mixing with Mixing Vane Grids," WCAP-7667-P-A (Proprietary), January 1975 and WCAP-7755-A, January 1975.

47. Hochreiter, L. E., "Application of the THINC IV Program to PWR Design," WCAP-8054 (Proprietary), October 1973, and WCAP-8195, October 1973.

48. McFarlane, A. F., "Power Peaking Factors," WCAP-7912-P-A (Proprietary), January 1975 and WCAP-7912-A, January 1975.

49. Turkey Point Units 3 and 4 Uprating NSSS Engineering Report, Westinghouse, WCAP-14291, December 1995.

50. Hochreiter, L. E., Chelemer, H., and Chu, P. T., "THINC-IV An Improved Program for Thermal-Hydraulic Analysis of Rod Bundle Cores," WCAP-7956, June 1973.

51. Friedland, A. J., and Ray, S., "Improved THINC-IV Modeling for PWR Core Design," CAP-12330-P, August 1989.

52. Skaritka, J., (Ed.), "Fuel Rod Bow Evaluation," WCAP-8691, Rev. 1, July 1979.

53. "Partial Response to Request Number 1 for Additional Information on WCAP-8691, Revision 1" Letter, E. P. Rahe, Jr., (Westinghouse) to J. R. Miller (NRC), NS-EPR-2515, dated October 9, 1981; "Remaining Response to Request Number 1 for Additional Information on WCAP-8691, Revision 1" Letter, E. P. Rahe, Jr., (Westinghouse) to J. R. Miller (NRC), NS-EPR-2572, dated March 16, 1982.

54. Weisman, J., Wenzel, A. H., Tong, L. S., Fitzsimmons, D., Thorne, W., and Batch, J., "Experimental Determination of the Departure from Nucleate Boiling in Large Rod Bundles at High Pressure," AIChE, Preprint 29, 9th National Heat Transfer Conference, 1967, Seattle, Washington.

55. Tong, L.S., Chelemer, H., Casterline, J.E. and Matzner, B. "Critical Heat Flux (DNB) in Square and Triangular Array Rod Bundles", JSME, Semi-International Symposium, Paper #256, 1967, Tokyo, Japan.

56. Boure, J. A., Bergles, A. E., and Tong, L. S., "Review of Two-Phase Flow Instability," Nucl. Engr. Design 25 (1973) pp. 165-192.

57. Lahey, R. T., and Moody, F. J., "The Thermal Hydraulics of a Boiling Water Reactor," American Nuclear Society, 1977.

58. Saha, P., Ishii, M., and Zuber, N., "An Experimental Investigation of the Thermally Induced Flow Oscillations in Two-Phase Systems," J. of Heat Transfer, No. 1976, pp. 616-622.

59. Virgil C. Summer FSAR, Docket #50-395.

60. Byron/Braidwood FSAR, Docket #50-456.

61. South Texas FSAR, Docket #50-498.

62. Kakac, S., Veziroglu, t. N., Akyuzlu, K., Berkol, O., "sustained and Transient Boiling Flow Instabilities in a Cross-Connected Four Parallel-Channel Upflow System," Proc. of 5th International Heat Transfer Conference, Tokyo, Sept. 3-7, 1974.

63. Kao, H. S., Morgan, C. D., and Parker, W. B., "Prediction of Flow Oscillation in Reactor Core Channel," Trans. ANS, Vol. 16, 1973, pp. 212-213.

64. WCAP-13589-A, "Assessment of Clad Flattening and Densification Power Spike Factor Elimination in Westinghouse Nuclear Fuel," Kersting, P.J. et al, March 1995.

TABLE 3.2.2-1

THERMAL AND HYDRAULIC DESIGN PARAMETERS

	Original	Uprated
Total Primary Heat Output, MWt	2208	2308
Total Reactor Coolant Pump Heat Output, MWt	8	8
Total Core Heat Output, MWt	2200	2300
Total Core Heat Output, Btu/hr	7508.6 x 10^6	7847.9 x 10^6
Heat Generated in Fuel, %	97.4	97.4
Maximum Thermal Overpower, %	12	12
Nominal System Pressure, psia	2250	2250
Hot Channel Factors (First cycle) (1)		
Heat Flux		
Nuclear, F^N_q	3.13	
Engineering, F^E	1.03	
Total, F_q	3.23	
Enthalpy Rise		
Nuclear, $F^N_{\Delta H}$	1.75	
Engineering, $F^E_{\Delta H}$	1.01	
Total, $F_{\Delta H}$	1.77	
Coolant Flow		
Total Flow Rate 1b/hr	101.5 x 10^6	96.7 x 10^6
Average Velocity Along Fuel Rods, ft/sec	14.3 (14.0)(2)	
Average Mass Velocity, 1b/hr-ft^2	2.32 x 10^6 (2.28 x 10^6)(2)	
Coolant Temperature, °F		
Nominal Inlet	546.2	543.5
Average Rise in Vessel	55.9	61.4
Average Rise in Core	58.3 (59.3)(2)	64.9
Average in Core	575.4 (575.9)	577.4
Average in Vessel	574.2	574.2 ± 3
Nominal Outlet of Hot Channel	642.0 (643.2)(2)	
Heat Transfer (First Cycle)		
Active Heat Transfer Surface Area, ft^2	42,460	
Average Heat Flux, Btu/hr-ft^2	171,600	
Maximum Heat Flux, Btu/hr-ft^2	554,200	
Maximum Thermal Output, kw/ft	17.9	
Maximum Clad Surface Temperature at Nominal Pressure, °F	657	
Maximum Average Clad Temperature at Rated Power, °F	715	
Fuel Centerline Temperatures, °F (First Cycle)		
Maximum at 100% Power	4150	
Maximum at 112% Power	4400	
DNB Ratio (First Cycle)		
Minimum DNB Ratio at nominal operating Conditions (first cycle)	1.81	
Typical Cell		1.43
Thimble Cell		1.42
Pressure Drop, psi (First Cycle)		
Across Core	26	
Across Vessel, including nozzles	46	
Pressure Across the Core		21.5±2.5

NOTES :

1. Core design values for current cycles are given in Appendices 14A and 14 B.
2. Values for complete thimble plug removal.

TABLE 3.2.2-2

ENGINEERING HOT CHANNEL FACTORS

(FIRST CYCLE)

F_q^E	Pellet Diameter, Density Enrichment, and Eccentricity Rod Diameter,Pitch and Bowing	1.03

$F_{\Delta H}^E$	Pellet Diamter, Density, Enrichment	1.08
	Rod Diameter, Pitch and Bowing	
	Inlet Flow Maldistribution	1.01
	Flow Redistribution	1.03
	Flow Mixing	0.90*
	Resulting $F_{\Delta H}^E$	1.01

*To Point of Minimum DNB ratio

THERMAL CONDUCTIVITY OF URANIUM DIOXIDE

FIG. 3.2.2-1

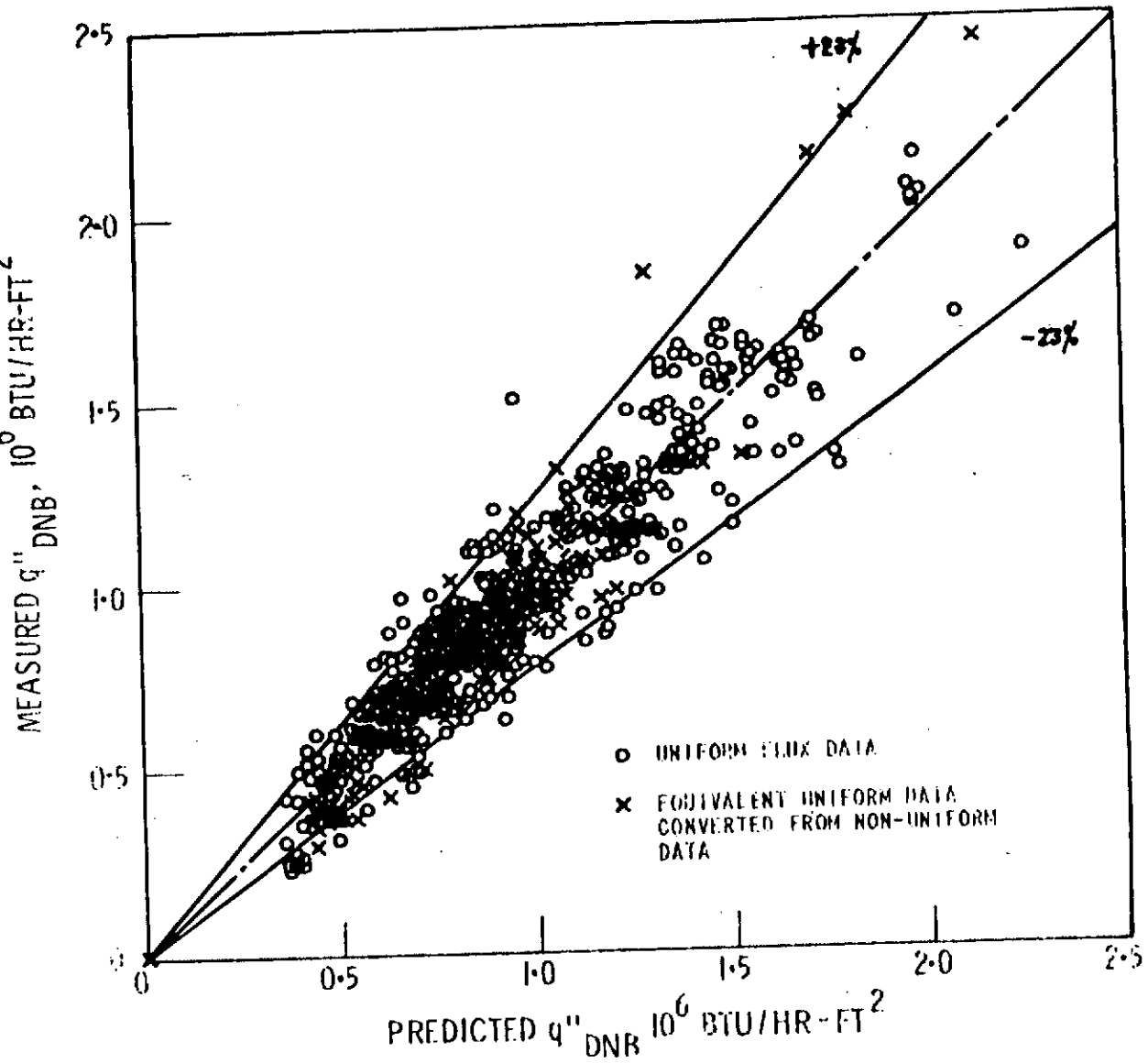

Rev. 4-7/86

COMPARISON OF W-3 PREDICTION AND UNIFORM FLUX DATA

FIG. 3.2.2-2

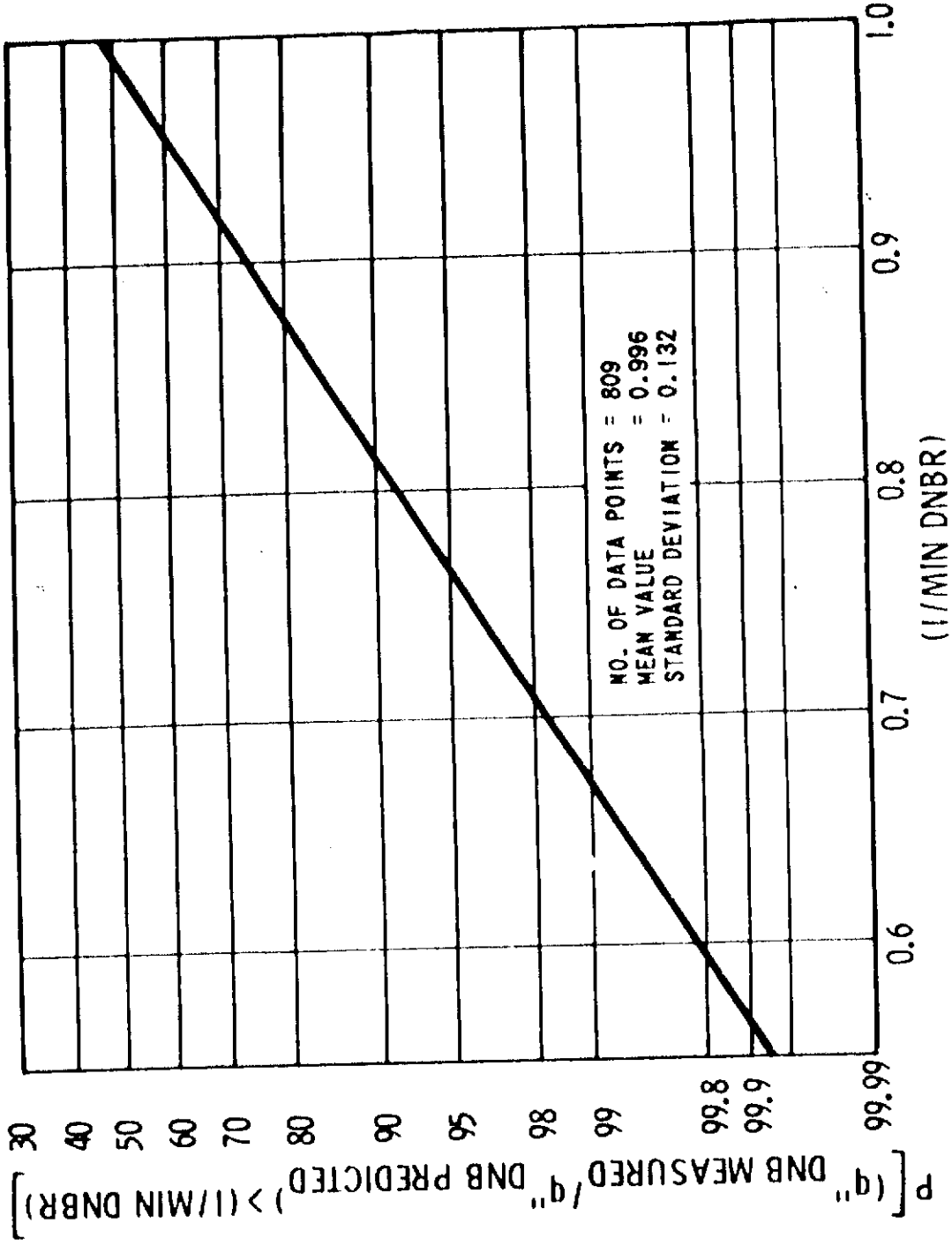

Rev. 4-7/86

W-3 CORRELATION PROBABILITY DISTRIBUTION CURVE

FIG. 3.2.2-3

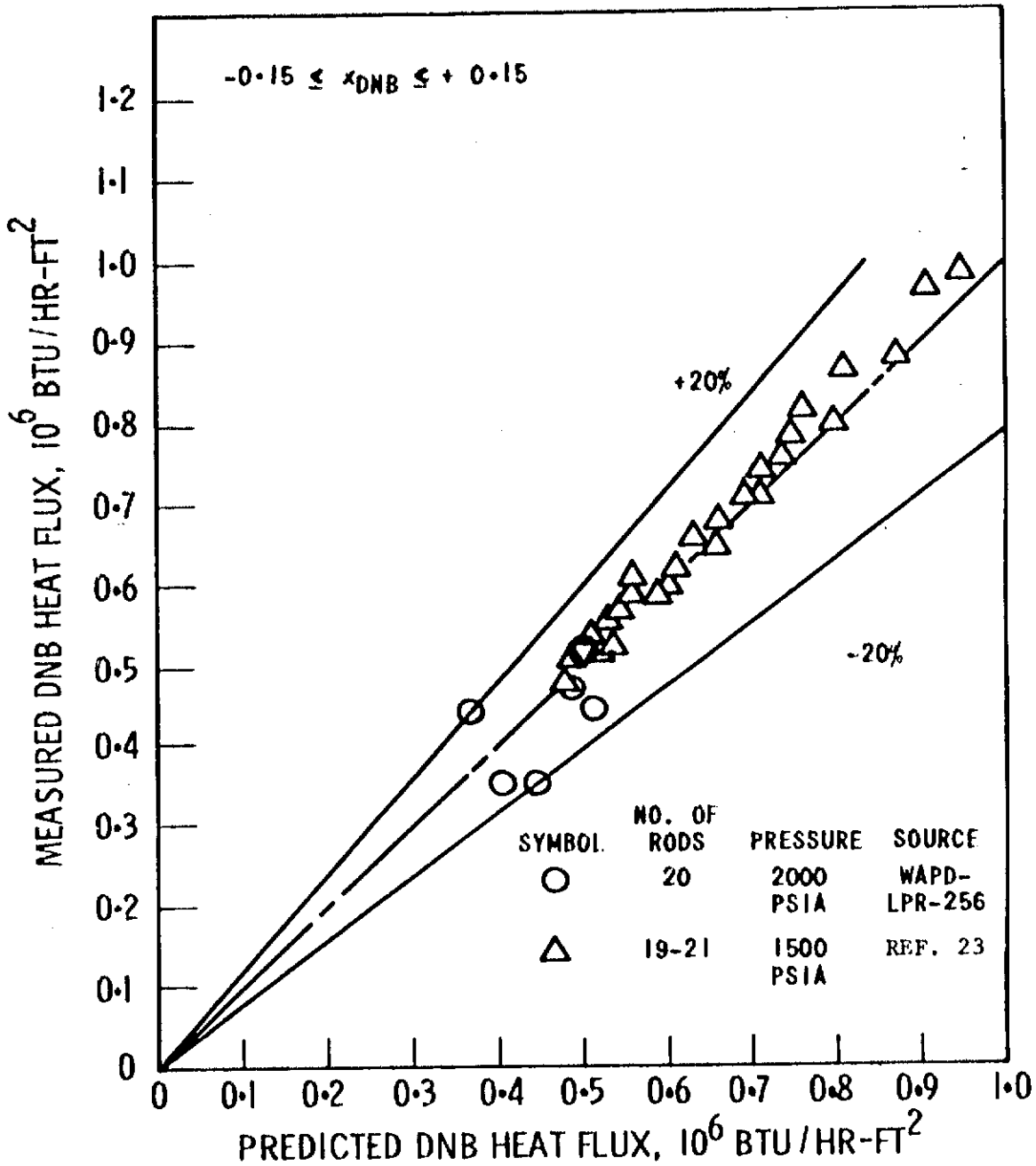

Rev. 4-7/86

COMPARISON OF W-3 CORRELATION WITH ROD BUNDLE DNB DATA (SIMPLE GRID WITHOUT MIXING VANE)

FIG. 3.2.2-4

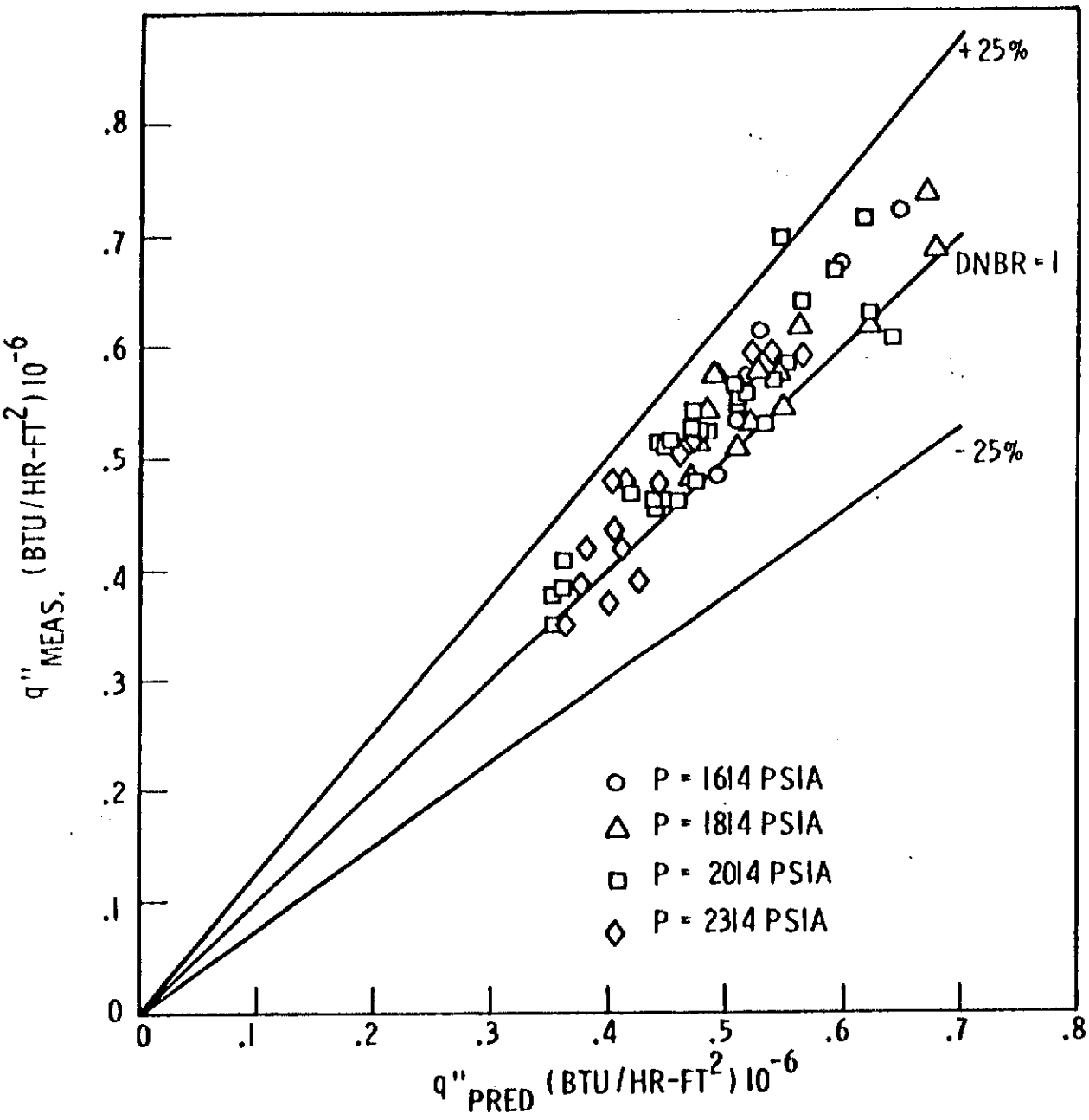

Rev. 4-7/86

COMPARISON OF W-3 CORRELATION WITH ROD BUNDLE DNB DATA (SIMPLE GRID WITH MIXING VANE)

FIG. 3.2.2-5

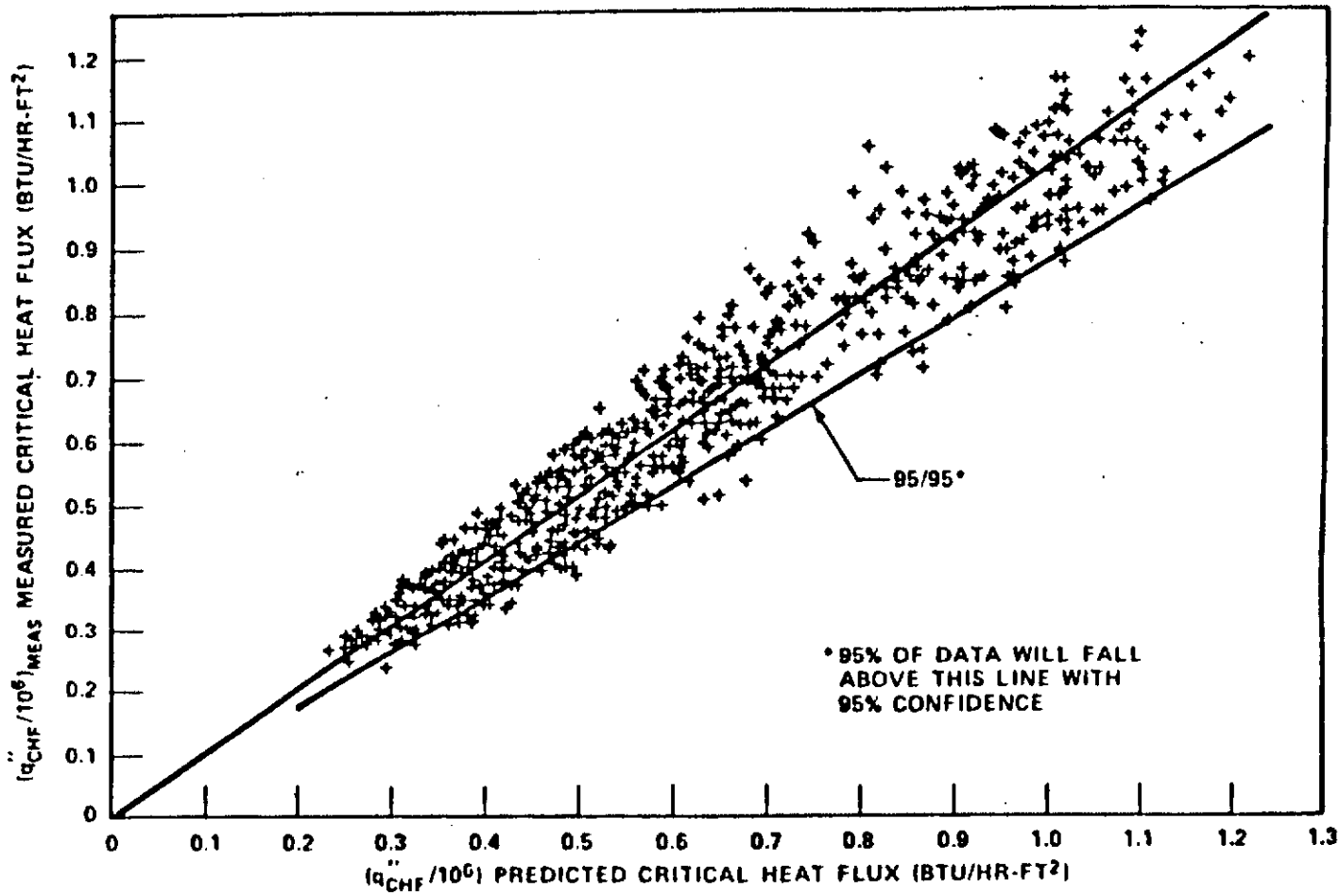

Rev. 4-7/86

MEASURED VERSUS PREDICTED
CRITICAL HEAT FLUX-WRB-1 CORRELATION

FIG. 3.2.2-6

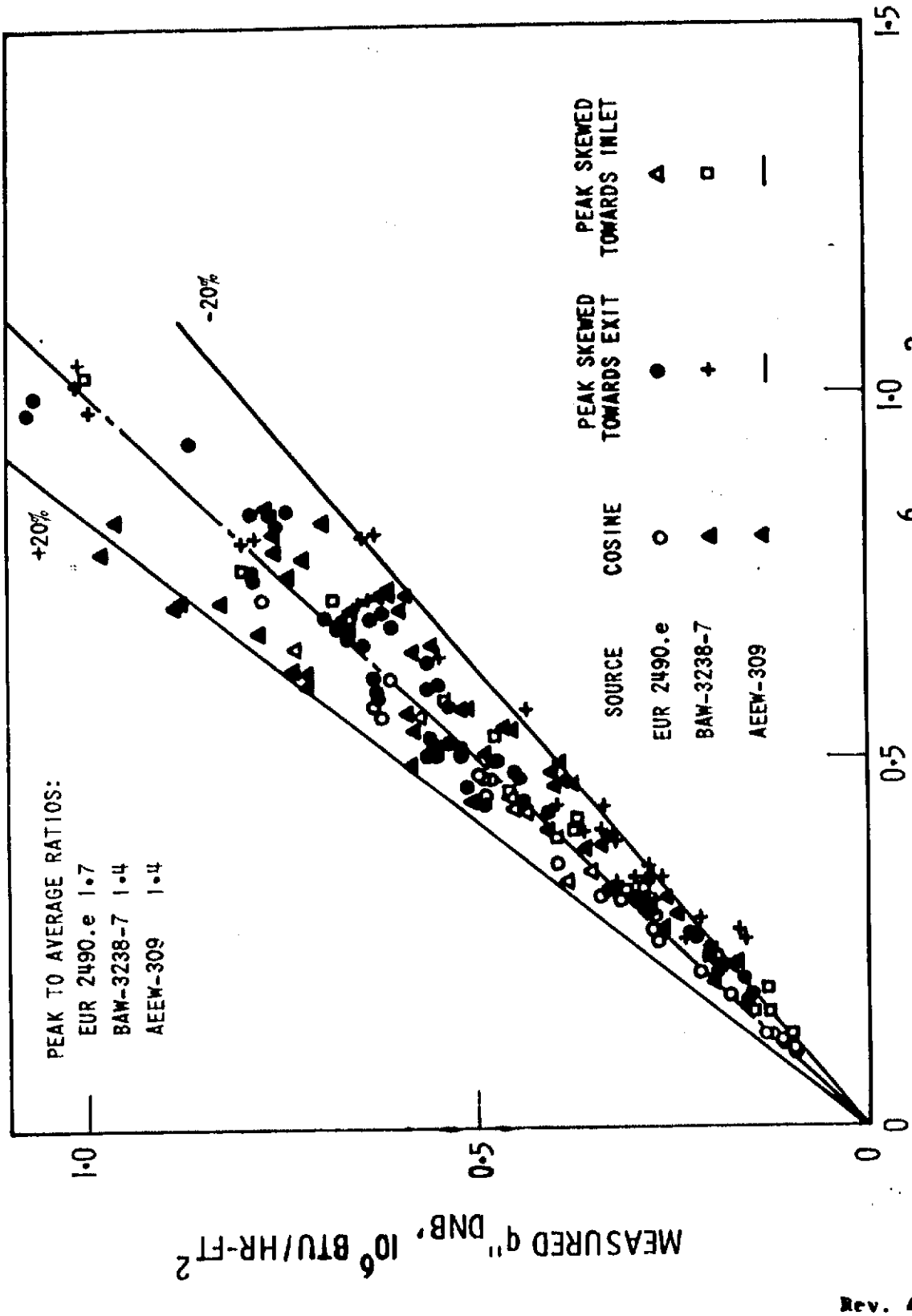

Rev. 4-7/86

COMPARISON OF W-3 PREDICTION AND NON-UNIFORM FLUX DATA

FIG. 3.2.2-7

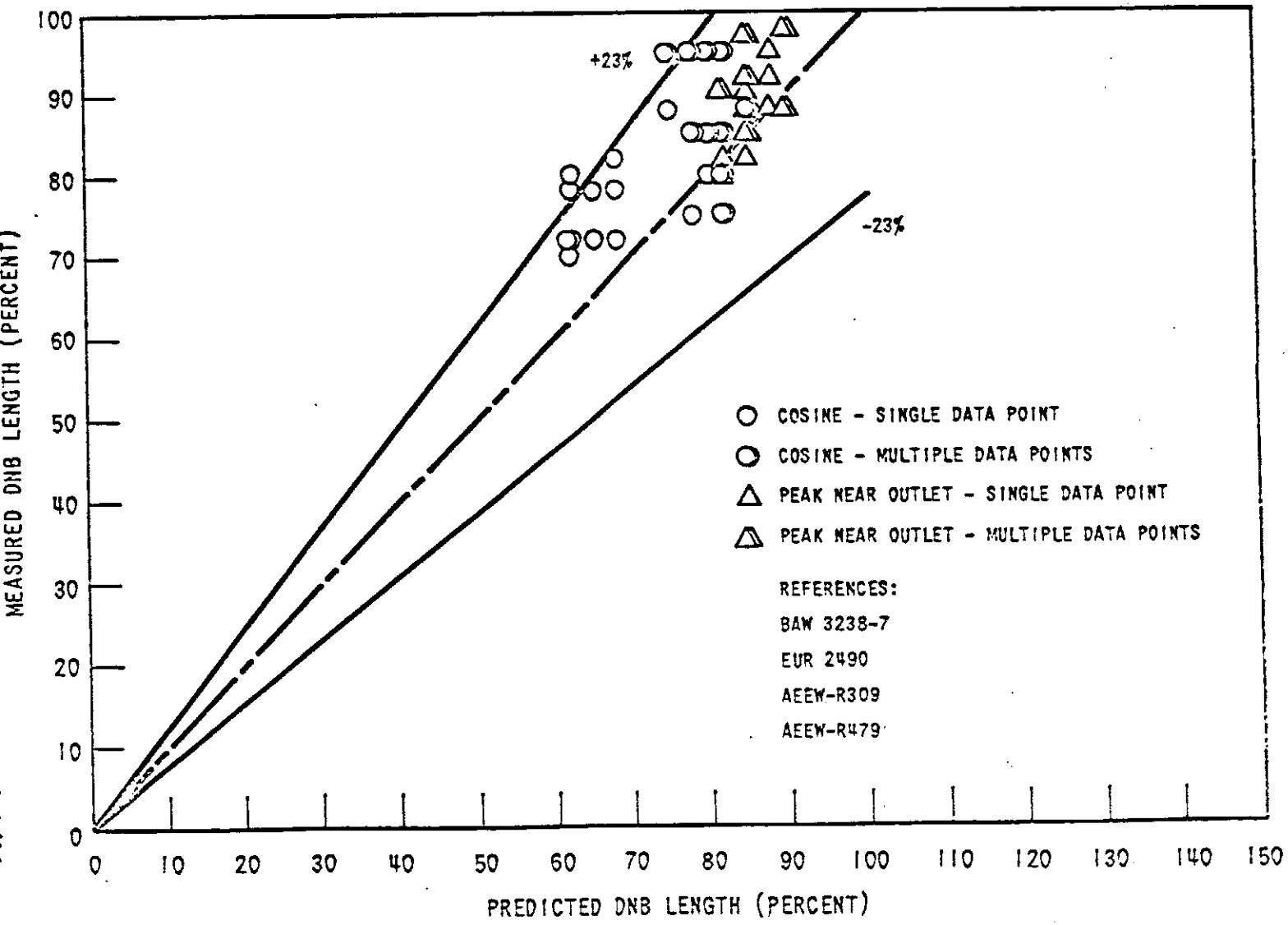

COMPARISON OF W-3 PREDICTION WITH MEASURED DNB LOCATION

FIG. 3.2.2-8

Rev. 4-7/86

3.2.3 MECHANICAL DESIGN AND EVALUATION

The reactor core and reactor vessel internals are shown in cross-section in Figure 3.2.3-1 and in elevation in Figure 3.2.3-2. The core, consisting of the fuel assemblies, control rods, source rods and burnable poison rods provides and controls the heat source for the reactor operation. The internals, consisting of the upper and lower core support structure, are designed to support, align, and guide the core components, direct the coolant flow to and from the core components, and to support and guide the in-core instrumentation. A listing of the core mechanical design parameters is given in Table 3.2.3-1.

The Optimized Fuel Assemblies (OFA) including the Debris Resistant Fuel Assemblies (DRFA) are arranged in a roughly circular cross-sectional pattern in the core. The LOPAR and OFA (including DRFA) assemblies are nearly identical in their geometric configuration (number of fuel rods and thimble tubes, fuel rod dimensions, assembly pitch, etc.) with the following exceptions: 1) the diameter of the upper portion of the OFA guide thimble tubes has been reduced, relative to the LOPAR assembly, to accommodate the increased Zircaloy-4 grid strap thickness and results in reduced diameter thimble plugs, and; 2) the five intermediate support grids are of different materials. Note that evaluations documented in Section 3.1.1 support the complete or partial removal of thimble plugs from Turkey Point Units 3 & 4. Beginning with Unit 3 Cycle 12 and Unit 4 Cycle 13, Debris Resistant Fuel Assemblies (DRFA) have been loaded. DRFA’s are essentially the same as OFA’s, except for a long end plug on the bottom of each fuel rod. This longer end plug prevents debris from fretting through the fuel rod below the bottom spacer grid. The enrichment of each region of fuel will vary slightly depending on the energy requirements for a given cycle of operation.

The fuel is in the form of slightly enriched uranium dioxide ceramic pellets. The pellets are stacked to an active height of 144 inches within Zircaloy-4 or ZIRLO tubular cladding, which is plugged and seal welded at the ends to encapsulate the fuel. The enrichments of the fuel for the various regions in the first core are given in Table 3.2.3-1. Enrichments for subsequent cycles are given in the cycle specific Reload Characteristics and Parameters report included in Appendices 14A and 14B for Units 3 and 4, respectively. All fuel rods are internally pressurized with helium during fabrication. Heat generated by the fuel is removed by demineralized borated light water which flows upward through the fuel assemblies and acts as both moderator and coolant.

The stress criteria of Article 4 Section III of the ASME code is employed in the design of the fuel assembly with the exception of the fuel clad which is specifically excluded by the code. The criteria for the design of fuel rods

are listed in Section 3.1.3. Zircaloy-4 or ZIRLO which is used for fabricating the guide thimbles of the fuel assembly and Inconel 718 which is used for fabricating grids and assembly hold down springs are not yet considered as code materials. In LOPAR fuel, all grids are made of Inconel-718. In OFA fuel, intermediate grids are made of Zircaloy-4 or ZIRLO and the top and bottom grids of Inconel-718. The method for establishing design stress intensity values for the materials is consistent with that outlined in the code.

For historical purposes, the initial core was divided into regions of three different enrichments. The loading arrangement for the initial cycle is indicated on Figure 3.2.3-3. Refueling generally follows an inward loading schedule. However to increase neutron economy and as part of a vessel flux reduction program to resolve pressurized thermal shack concerns, the Turkey Point Units now employ a low leakage loading pattern aimed at reducing the neutron flux at the periphery of the core. This consists of using once-burned and twice-burned assemblies in peripheral core locations and loading a maximum number of fresh assemblies in-board while meeting energy requirements and ensuring the safe operation of the core. The typical reload core is divided into three different regions: feed, once burned and twice burned fuel assemblies of varied enrichments. The loading patterns for current cycles are given in the Reload Characteristics and Parameters report included in Appendices 14A and 14B for Units 3 and 4, respectively.

The control rods, designated as Rod Cluster Control Assemblies (RCCA's), consist of groups of individual absorber rods which are held together with a spider at the top end and actuated as a group. The absorber rods fit within hollow guide thimbles in the fuel assemblies. The guide thimbles are an integral part of the fuel assemblies and occupy locations within the regular fuel rod pattern. In the withdrawn position, the absorber rods are guided and supported laterally by guide tubes which form an integral part of the upper core support structure. Figure 3.2.3-4 shows a typical RCCA.

As shown in Figure 3.2.3-2, the fuel assemblies are positioned and supported vertically in the core between the upper and lower core plates. The core plates are provided with pins which index into closely fitting mating holes in the fuel assembly top and bottom nozzles. The pins maintain the fuel assembly alignment which permits free movement of the control rods from the fuel assembly into the guide tubes in the upper support structure without binding or restriction between the rods and their guide surfaces.

Operational or seismic loads imposed on the fuel assemblies are transmitted through the core plates to the upper and low support structures and ultimately to the internals support ledge at the pressure vessel flange in the case of vertical loads or to the lower radial support and internals support

ledge in the case of horizontal loads. The internals also provide a form fitting baffle surrounding the fuel assemblies which confines the upward flow of coolant in the core area to the fuel bearing region.

Reactor Internals

Design Description

The reactor internals are designed to support and orient the reactor core fuel assemblies and RCCA's, absorb the RCCA dynamic loads and transmit these and other loads to the reactor vessel flange, provide a passageway for the reactor coolant, and support incore instrumentation. The reactor internals are shown in Figure 3.2.3-2.

Stresses in reactor internals are computed following the rule established by Section III of the ASME Code, Article 4.

Materials used for boltings, 316 SS, cold work, and Inconel X750 do not have allowable and yield stresses in the Code. These bolts are not used as pressure containing members where leakage and gasketing considerations are paramount; they are instead used as mechanical attachments. The membrane stress is kept within the yield stress of the material, including preload. The basic philosophy is to obtain maximum clamping force and maintain joint integrity during service.

Fabrication techniques regarding these materials are not different than the materials considered by the Code except for the cold work of the 316 SS, and the heat treatment of Inconel X750. The following summarizes these two materials.

The materials used for bolting of the internals meet non-destructive testing requirements comparable to requirements of Section III. In addition, all bolting materials (of diameters less than two inches) have been ultrasonically tested. Special mechanical property tests are applied to these bolting materials where their properties were enhanced by strain hardening of solution treated bars and by precipitation hardening respectively. Specific written specifications are used for procurement of these bolts.

The Type 316 strain hardened bolting conforms to the following properties at room temperature. (The bolting material is strain hardened following a carbide solution treatment):

	Internals Bolting	Bolting ASTM SA193 Type B8M Strain Hardened to Surface Brinell of 320 Max			
		to-3/4"	3/4 to 1"	1 to 1-1/4"	1-1/4" to 1-1/2"
Tensile Strength Psi Min.	Exceed the actual yield strength by 15,000 psi for yield strengths of 75,000 psi and less, and by 10,000 psi for yield strength greater than 75,000 psi.	125,000	115,000	105,000	100,000
Yield Strength Psi Min.	60-85,000	100,000	80,000	65,000	50,000
Elongation in % Min.	30	12	15	20	28
Reduction in Area % Min.	60	35	35	35	45

The strain hardened bolting materials require special processing which results in higher properties than annealed material similar to the approach used for special processing for SA453 Grades 651A, 651B, and 660. The base material chemistry is equivalent to SA193 B8M. The strain hardening concept is included in SA193, however, more restrictive mechanical property limits as noted above are applied.

The use of cold drawn material to enhance mechanical properties is similarly used for Nickel-Copper SB164.

Successful experience with strain hardened austenitic stainless steel (Type 304SS) of yield strength levels of 75,000 Psi Min. YS has been obtained on fuel element cladding used in SAXTON Nuclear Power Plant.

Nickel-Chromium age-hardenable alloys A461 Grade 688 is used for core internal bolting per Code Case 1390. The heat treatment used was optimized for the diameters used and differs from the established ASTM specification.

The internals are designed to withstand the forces due to weight, preload of fuel assemblies, control rod dynamic loading, vibration, and LOCA blowdown coincident with earthquake acceleration. The internals are analyzed in a manner similar to Connecticut Yankee, San Onofre, Zorita, Saxton and Yankee. Under the loading conditions, including conservative effects of design earthquake loading, the structure satisfies stress values prescribed in Section III, ASME Nuclear Vessel Code.

The reactor internals are equipped with bottom-mounted in-core instrumentation supports. These supports are designed to sustain the applicable loads outlined above.

The components of the reactor internals are divided into three parts consisting of the lower core support structure (including the entire core barrel and thermal shield), the upper core support structure and the in-core instrumentation support structure.

Lower Core Support Structure

The major containment and support member of the reactor internals is the lower core support structure, shown in Figure 3.2.3-5. This support structure assembly consists of the core barrel, the core baffle, the lower core plate and support columns, the thermal shield, the intermediate diffuser plate and the bottom support plate which is welded to the core barrel. All the major material for this structure is Type 304 Stainless Steel. The core support structure is supported at its upper flange from a ledge in the reactor vessel head flange and its lower end is restrained in its transverse movement by a radial support system attached to the vessel wall. Within the core barrel are axial baffle and former plates which are attached to the core barrel wall and form the enclosure periphery of the assembled core. The lower core plate is positioned at the bottom level of the core below the baffle plates and provides support and orientation for the fuel assemblies.

The lower core plate provides the necessary flow distributor holes for each fuel assembly. Fuel assembly locating pins (two for each assembly) are also inserted into this plate. Columns are placed between this plate and the bottom support plate of the core barrel in order to provide stiffness to this plate and transmit the core load to the bottom support plate. Intermediate between the support plate and lower core support plate is positioned a perforated plate to diffuse uniformly the coolant flowing into the core.

The one piece thermal shield is fixed to the core barrel at the top with rigid bolted connections. The bottom of the thermal shield is connected to the core barrel by means of axial flexures. This bottom support allows for differential axial growth of the thermal shield with respect to the core barrel but restricts radial or horizontal movement of the bottom of the shield. Irradiation baskets in which materials samples can be inserted and irradiated during reactor operation are attached to the thermal shield. The irradiation capsule basket supports are welded to the thermal shield so that they do not extend above the thermal shield. Thus, the basket is not in the high flow disturbance zone.

The welded attachment to the shield extends the full length of the support except for small interruptions about one inch long. This type of attachment has an extremely high natural frequency. The specimens are held in position within the baskets by a stop on the bottom and a slotted cylindrical spring at the top which fits against a relief in the basket. The specimen does not extend through the top of the basket and thus is protected by the basket from the flow.

The lower core support structure and principally the core barrel serve to provide passageways and control for the coolant flow. Inlet coolant flow from the vessel inlet nozzles proceeds down the annulus between the core barrel and the vessel wall, flows on both sides of the thermal shield, and then into a plenum at the bottom of the vessel. It then turns and flows through the lower support plate, passes through the intermediate diffuser plate and then through the lower core plate. The flow holes in the diffuser plate and the lower core plate are arranged to give a very uniform entrance flow distribution to the core. After passing through the core the coolant enters the area of the upper support structure then flows generally radially to the core barrel outlet nozzles and directly through the vessel outlet nozzles.

A small amount of water also flows between the baffle plates and core barrel to provide additional cooling of the barrel. Similarly, a small amount of the entering flow is directed into the vessel head plenum and exits through the vessel outlet nozzles.

Vertically downward loads from weight, fuel assembly preload, control rod dynamic loading and earthquake acceleration are carried by the lower core plate partially into the lower core plate support flange on the core barrel shell and partially through the lower support columns to the bottom support plate and thence through the core barrel shell to the core barrel flange supported by the vessel head flange. Transverse loads from earthquake acceleration, coolant crossflow, and vibration are carried by the core barrel shell to be distributed to the lower radial support to the vessel wall and to the vessel head flange. Transverse acceleration of the fuel assemblies is transmitted to the core barrel shell by direct connection of the lower core support plate to the barrel wall and by a radial support type connections of the upper core plate to slab sided pins pressed into the core barrel.

The main radial support system of the core barrel is accomplished by "key" and "keyway" joints to the reactor vessel wall. At equally spaced points around the circumference, an Inconel block is welded to the vessel I.D. Another Inconel block is bolted to each of these blocks, and has a "keyway" geometry. Opposite each of these is a "key" which is attached to the internals. At assembly, as the internals are lowered into the vessel, the keys engage the keyways in the axial direction. With this design, the internals are provided with a support at the farthest extremity, and may be viewed as a beam fixed at the top and simply supported at the bottom.

Radial and axial expansions of the core barrel are accommodated, but transverse movement of the core barrel is restricted by this design. With this system, cycle stresses in the internal structures are within the ASME Section III limits.

In the event of downward vertical displacement of the internals, energy absorbing devices limit the displacement by contacting the vessel bottom head. The load is transferred through the energy devices to the vessel. The energy absorbers, cylindrical in shape, are contoured on their bottom surface to the reactor vessel bottom head geometry. Their number and design are determined so as to limit the forces imposed to a safe fraction of yield strength. Assuming a downward vertical displacement, the potential energy of the system is absorbed mostly by the strain energy of the energy absorbing devices.

The free fall in the hot condition is on the order of 1/2 inch, and there is an additional strain displacement in the energy absorbing devices of approximately 3/4 inch. Alignment features in the internals prevent cocking of the internals structure during this postulated drop. The RCCA's are designed to provide assurance of control rod insertion capabilities under these assumed drop of internals conditions. The drop distance of about 1-1/4 inch is not enough to cause the tips of the shutdown group of RCCA's in the full withdrawn position to come out of the guide tubes in the fuel assemblies.

Upper Core Support Assembly

The upper core support assembly, shown in Figure 3.2.3-6, consists of the top support plate, deep beam sections, and upper core plate between which are contained support columns and guide tube assemblies. The support columns establish the spacing between the top support plate, deep beam sections, and the upper core plate and are fastened at top and bottom

to these plates and beams. The support columns transmit the mechanical loadings between the two plates and serve the supplementary function of supporting thermocouple guide tubes. The guide tube assemblies, shown on Figure 3.2.3-7, sheath and guide the control rod drive shafts and control rods and provide no other mechanical functions. They are fastened to the top support plate and are guided by pins in the upper core plate for proper orientation and support. Additional guidance for the control rod drive shafts is provided by the control rod shroud tube which is attached to the upper support plate and guide tube.

The upper core support assembly, which is removed as a unit during refueling operation, is positioned in its proper orientation with respect to the lower support structure by flat-sided pins pressed into the core barrel which in turn engage in slots in the upper core plate. At an elevation in the core barrel where the upper core plate is positioned, the flat-sided pins are located at equal angular positions. Slots are milled into the core plate at the same positions. As the upper support structure is lowered into the main internals, the slots in the plate engage the flat-sided pins in the axial direction. Lateral displacement of the plate and of the upper support assembly is restricted by this design. Fuel assembly locating pins protrude from the bottom of the upper core plate and engage the fuel assemblies as the upper assembly is lowered into place. Proper alignment of the lower core support structure, the upper core support assembly, the fuel assemblies and control rods is thereby assured by this system of locating pins and guidance arrangement. The upper core support assembly is restrained from any axial movements by a large circumferential spring which rests between the upper barrel flange and the upper core support assembly and is compressed by the reactor vessel head flange.

Vertical loads from weight, earthquake acceleration, hydraulic loads and fuel assembly preload are transmitted through the upper core plate via the support columns to the deep beams and top support plate and then to the reactor vessel head. Transverse loads from coolant crossflow, earthquake acceleration, and possible vibrations are distributed by the support columns to the top support plate and upper core plate. The top support plate is particularly stiff to minimize deflection.

In-Core Instrumentation Support Structures

The in-core instrumentation support structures consist of an upper system to convey and support thermocouples penetrating the vessel through the head and a lower system to convey and support flux thimbles penetrating the vessel through the bottom.

The upper system utilizes the reactor vessel head penetrations. Instrumentation port columns are slip-connected to in-line columns that are in turn fastened to the upper support plate. These port columns protrude through the head penetrations. The thermocouples are routed through these port columns and across the upper support plate to positions above their readout locations. The thermocouple conduits are supported from the columns of the upper core support system. The thermocouple conduits are sealed stainless steel tubes.

During the Unit 4 Cycle 17 refueling, the northeast core exit thermocouple column, containing 13 core exit thermocouples, was damaged while removing the reactor vessel closure head. During the outage the upper portion of the column was removed. The loss of this column's 13 thermocouples will not impede the ability to provide core exit temperature monitoring during mid-loop operations, and monitoring of post-accident conditions.

In addition to the upper in-core instrumentation, there are reactor vessel bottom port columns which carry the retractable, cold worked stainless steel flux thimbles that are pushed upward into the reactor core. Conduits extend from the bottom of the reactor vessel down through the concrete shield area and up to a thimble seal line. The minimum bend radii are about 90 inches and the trailing ends of the thimbles (at the seal line) are extracted approximately 13 feet during refueling of the reactor in order to avoid interference within the core. The thimbles are closed at the leading ends and serve as the pressure barrier between the reactor pressurized water and the containment atmosphere.

Mechanical seals between the retractable thimbles and the surrounding conduits are provided at the seal table. During normal operation, the retractable thimbles are stationary in the core and move only during refueling or for maintenance, at which time a space of approximately 13 feet above the seal table is cleared for the retraction operation. Section 7.4 contains more information on the layout of the in-core instrumentation system.

The incore instrumentation support structure is designed for adequate support of instrumentation during reactor operation and is rugged enough to resist damage or distortion under the conditions imposed by handling during the refueling sequence.

Evaluation of Core Barrel and Thermal Shield

The internals design is based on analysis, test and operational information. Experience in previous Westinghouse PWR's has been evaluated and information derived has been considered in this design. For example, Westinghouse uses a one-piece thermal shield which is attached rigidly to the core barrel at one end and flexured at the other.

The Connecticut Yankee reactor and the Zorita reactor core barrels are of the same construction as the Turkey Point reactor core barrel. Deflection measuring devices employed in the Connecticut Yankee reactor during the hot-functional test, and deflection and strain gages employed in the Zorita reactor during the hot-functional test have provided important information that has been used in the design of the present day internals, including that for Turkey Point. When the Connecticut Yankee thermal shield was modified to the same design as for Southern California Edison, it, too, operated satisfactorily as was evidenced by the examination

after the hot-functional test. After these hot-functional tests on all of these reactors, a careful inspection of the internals was provided. All the main structural welds were examined, nozzle interfaces were examined for any differential movement, upper core plate inside supports were examined, the thermal shield attachments to the core barrel including all lockwelds on the devices used to lock the bolt were checked, no malfunctions were found.

Substantial scale model testing was performed by the Westinghouse Atomic Power Division (APD). This included tests which involved a complete full scale fuel assembly which was operated at reactor flow, temperature and pressure conditions. Tests were run on a 1/7th scale model of the Indian Point reactor. Measurements taken from these tests indicate very little shield movement, on the order of a few mils when scaled up to Turkey Point. Strain gage measurements taken on the core barrel also indicate very low stresses. Testing to determine thermal shield excitation due to inlet flow disturbances has been included. Information gathered from these tests was used in the design of the thermal shield and core barrel. It can be concluded from the testing program and the analyses with the experience gained that the design as employed for Turkey Point is adequate.

Core Components

Design Description

Fuel Assembly

A modified OFA design which incorporates several debris resistant features was introduced beginning in Cycle 12 of Unit 3 and Cycle 13 of Unit 4. The main features of this Debris Resistant Fuel Assembly (DRFA) include: a) a longer fuel rod bottom end plug, b) the fuel pellet stack height increased by 1.4 inches, and c) lowering of grids 1 through 6 by one inch. A detailed description of the DRFA is found in Reference 9. The overall configuration of the fuel assemblies is shown in Figures 3.2.3-8 through 3.2.3-9A. A comparison between the standard OFA and the DRFA designs is shown in Figure 3.2.3-9C. The assemblies are square in cross-section, nominally 8.426 inches on a side, and have an overall height of approximately 161.5 inches. The height of the active fuel column is 144 inches.

Beginning with Unit 3 Cycle 17, the DRFA fuel assembly fuel rod cladding, guide tubes, instrument thimble, and mid-span grids are fabricated from ZIRLO to provide added corrosion resistance and fuel reliability. The ZIRLO mid-span grid design is similar to the previous Zircaloy-4 Design except the ZIRLO sleeves are shorter in length and larger in diameter to distinguish them from the Zircaloy-4 design and improve skeleton fabrication. The use of ZIRLO material was submitted to the NRC for review in Reference 16 and received NRC approval. In addition, the fuel rod length was increased slightly.

The fuel rods in a fuel assembly are arranged in a square array with 15 rod locations per side and a nominal centerline-to-centerline pitch of 0.563 inch between rods. Of the total possible 225 rod locations per assembly, 21 are occupied by guide thimble tubes; 20 for the RCCA's or burnable absorbers and one for in-core instrumentation. The remaining 204 locations contain fuel rods. In addition to fuel rods, a fuel assembly is composed of a top nozzle, a bottom nozzle, 7 grid assemblies, 20 absorber rod guide thimble tubes, and one instrumentation thimble tube.

The guide thimble tubes in conjunction with the grid assemblies and the top and bottom nozzles comprise the basic structural fuel assembly skeleton. The top and bottom ends of the guide thimble tubes are fastened to the top and bottom nozzles respectively. The grid assemblies, in turn, are fastened to the guide thimble tubes at each location along the height of the fuel assembly at which lateral support for the fuel rods is required. Within this skeletal framework the fuel rods are contained and supported and the rod-to-rod centerline spacing is maintained along the assembly.

Bottom Nozzle

The bottom nozzle is a square box-like structure which controls the coolant flow distribution to the fuel assembly and functions as the bottom structural element of the fuel assembly. The nozzle, which is square in cross-section, is fabricated from 304 stainless steel parts consisting of a perforated plate, 4 angle legs, and four pads or feet. The legs are welded to the plate to form a plenum and for the inlet coolant to the fuel assembly. The perforated plate serves as the bottom end support for the fuel rods. The bottom support surface for the fuel assembly is formed by the four pads which are welded to the corner angles. Starting in Turkey Point Unit 4 Cycle 13, the bottom nozzle was stiffened with 1/4-inch x 1-inch bars extending between the legs. Beginning with the Turkey Point Unit 3 Cycle 14 reload (Region 16), the fuel assemblies contain a cast composite bottom nozzle. The composite bottom nozzle is functionally interchangeable with the old design.

Coolant flow to the fuel assembly is directed from the plenum in the bottom nozzle upward to the interior of the fuel assembly through the holes in the nozzle plate and to the channel between assemblies through the spaces between

the corner legs. The ligaments between the holes of the nozzle plate are positioned laterally beneath the fuel rods to prevent passage of the rods beyond this surface.

The guide thimble tubes, which carry axial loads imposed on the assembly, are fastened to the bottom nozzle end plate. These loads as well as the weight of the assembly are distributed through the nozzle to the lower core support plate. Indexing and positioning of the fuel assembly in the core is controlled through two holes in diagonally opposite pads which mate with locating pins in the lower core plate. Lateral loads imposed on the fuel assembly are also transferred to the core support structures through the locating pins.

The OFA bottom nozzle assembly is essentially the same design as the LOPAR bottom nozzle, except for the instrumentation tube counterbore diameter being reduced. This reduction accommodates a reduced outside diameter on the OFA guide tube and provides the same radial clearance with the OFA instrumentation tube as the LOPAR assembly nozzle. This assures retention of the instrumentation tube lower end.

The OFA bottom nozzle design has a feature which allows it to be easily removed. As shown in Figure 3.2.3-9B, a locking cup is used to lock the thimble screw of a guide thimble tube in place, instead of the lockwire used for the standard LOPAR nozzle design. The reconstitutable nozzle design facilitates removal of the bottom nozzle and relocking of thimble screws as the bottom nozzle is reattached.

Top Nozzle

The top nozzle is a box-like structure, which functions as the fuel assembly upper structural element and forms a plenum space where the heated fuel assembly discharge coolant is directed toward the flow holes in the upper core plate. The nozzle is comprised of an adapter plate, enclosure, top plate, two clamps, four leaf-spring sets, and assorted hardware. All parts with the exception of the springs and their hold down bolts are constructed of Type 304 stainless steel. The springs and bolts are made from Inconel 718 and Inconel 600, respectively.

The adaptor plate is square in cross-section, and is perforated by machined slots to provide for coolant flow through the plate. At assembly, the top ends of the control guide thimble tubes are fastened to the adaptor. Thus, the adaptor plate acts as the fuel assembly top end plate, and provides a means of distributing evenly among the guide thimble tubes any axial loads imposed on the fuel assemblies.

The OFA top nozzle is the same as the LOPAR assembly top nozzle with the exception of a small increase in the adaptor plate thickness. This increase results in a slightly longer OFA length of .055 inches as shown in Figure 3.2.3-9A. The increased adapter plate thickness is a result of a standardization of the OFA nozzle design. This minor change has no adverse effect on the OFA/LOPAR assemblies fuel handling operation or mixed-core operations.

The nozzle enclosure is actually a square thin walled tubular shell which forms the plenum section of the top nozzle. The bottom end of the enclosure is pinned and welded to the periphery of the adaptor plate, and the top end is welded to the periphery of the top plate.

The top plate is square in cross-section with a central hole. The hole allows clearance for the RCCA absorber rods to pass through the nozzle into the guide thimbles in the fuel assembly and for coolant exiting from the fuel assembly to

the upper internals area. Two pads containing axial through-holes which are located on diametrically opposite corners of the top plate provide a means of positioning and aligning the top of the fuel assembly. As with the bottom nozzle, alignment pins in the upper core plate mate with the holes in the top nozzle plate.

Hold down forces of sufficient magnitude to oppose the hydraulic lifting forces on the fuel assembly are obtained by means of the leaf springs which are mounted on the top plate. The OFA has a slight increase in hydraulic resistance to flow compared to a LOPAR assembly, primarily due to the thicker and wider OFA Zircaloy Or ZIRLO grid straps. This results in an increased OFA lift force and requires the use of 3-leaf holddown springs instead of the LOPAR assembly 2-leaf springs (Figure 3.2.3-9A). The 3-leaf spring has the same height and provides additional holddown force margin when compared to the LOPAR 2-leaf spring. The 3-leaf spring design has been successfully used in the 17x17 OFA demonstration program and other 15x15 LOPAR assemblies. The change to the 3-leaf spring is compatible with the LOPAR assembly and the handling tools at the Turkey Point plants. The springs are fastened to the top plate at the two corners where alignment holes are not used and radiate out from the corners parallel to the sides of the plate. Fastening of the springs is accomplished with a clamp which fits over the ends of the springs and two bolts (one per spring) which pass through the clamp and spring, and thread into the top plate. At assembly, the spring mounting bolts are torqued sufficiently to preload against the maximum spring load and then lockwelded to the clamp which is counter-bored to receive the bolt head.

The spring load is obtained through deflection of the spring set by the upper core plate. The spring form is such that it projects above the fuel assembly and is depressed by the core plate when the internals are loaded into the reactor. The free end of the spring is bent downward into a key slot in the top plate. The free end of the lower spring is captured by the leg of the upper spring. This is done to guard against loose parts in the reactor in the event of spring fracture. In addition, the fit between the upper spring and key slot and between the spring set and the mating slot in the clamp are sized to prevent rotation of either end of the spring set into the control rod path in the event of spring fracture.

In addition to its plenum and structural functions, the nozzle provides a protective housing for components which mate with the fuel assembly. In handling a fuel assembly with a control rod inserted, the control rod spider is contained within the nozzle. During operation in the reactor, the nozzle protects the absorber rods from coolant cross flows in the

unsupported span between the fuel assembly adaptor plate and the end of the guide tube in the upper internals package. The spiders which support the source rods and burnable poison rods are all contained within the fuel top nozzle. Beginning with the Unit 3 Cycle 12 reload, a reconstitutable top nozzle (RTN) was incorporated into the Turkey Point fuel assembly design. The RTN can be removed and reattached repeatedly, if necessary, throughout the assembly's operation. Guide thimble inserts are placed into the circumferentially grooved holes in the adapter plate to connect the RTN with the fuel assembly. A lock tube, inserted into the inner diameter of the insert, holds the insert in place until removal of the RTN is required. The RTN design has the same flow area and loss coefficients as the previous design, therefore, none of the core/fuel inputs to the safety analysis were affected by the introduction of this design. Beginning with Turkey Point Unit 3 Cycle 16, the Composite(CAST) Top Nozzle was implemented and is functionally interchangeable with the old design. The keyless/cuspless nozzle features implemented during Unit 3 Cycle 14 were retained in the modified CAST design.

Guide Thimbles

The control rod guide thimbles in the fuel assembly provide guided channels for the absorber rods during insertion and withdrawal of the control rods. They are fabricated from a single piece of Zircaloy 4 or ZIRLO tubing, which is drawn to two different diameters. The larger inside diameter at the top provides a relatively large annular area for rapid insertion during a reactor trip and to accommodate a small amount of upward cooling flow during normal operations. The bottom portion of the guide thimble is of reduced diameter to produce a dashpot action when the absorber rods near the end of travel in the guide thimbles during a reactor trip. The transition zone at the dashpot section is conical in shape so that there are no rapid changes in diameter in the tube.

Flow holes are provided just above the transition of the two diameters to permit the entrance of cooling water during normal operation, and to accommodate the outflow of water from the dashpot during reactor trip.

The dashpot is closed at the bottom by means of a welded end plug. The end plug is fastened to the bottom nozzle during fuel assembly fabrication.

Grids

The grid assemblies consist of individual slotted straps which are assembled and interlocked in an "egg-crate" type arrangement and then furnace brazed to permanently join the straps at their points of intersection. Details such as spring fingers, support dimples, mixing vanes, and tabs are punched and formed in the individual straps prior to assembly.

Two types of grid assemblies are used in the fuel assembly. One type of these grids having mixing vanes which project from the edges of the straps into the coolant stream is used in the high heat region of the fuel assemblies to promote mixing of the coolant. A grid of this type is shown in Figure 3.2.3-10. The other type of grids, located at the bottom and top ends of the assembly, are of the nonmixing type. They are similar to the mixing type with the exception that they contain no mixing vanes on the internal straps.

There are three materials used to construct support grids for the LOPAR and OFA assemblies. Inconel-718 is used for all seven LOPAR grids, and the top and bottom non-mixing, support grids in the OFA assembly. Zircaloy or ZIRLO is used for the five intermediate mixing-vane grids in the OFA assembly. A more detailed description can be found in the Reload Transition Safety Report (RTSR) for Turkey Point Units (Reference 2).

The outside straps on all grids contain mixing vanes which, in addition to their mixing function, aid in guiding the grids and fuel assemblies past projecting surfaces during handling or loading and unloading the core. Additional small tabs on the outside straps and the irregular contour of the straps are also for this purpose.

Inconel-718, Zircaloy. and ZIRLO are used for the grid material because of their corrosion resistance and high strength properties. The Inconel grids are furnace brazed to permanently join the straps at their intersections. After the combined brazing and solution annealing temperature cycle, the grid material is age hardened to obtain the material strength necessary to develop the required grid spring forces. The Zircaloy-4 and ZIRLO grid interlocking strap joints and grid-to-sleeve joints are fabricated by laser welding.

Impact tests have been performed at 600◦F to obtain the dynamic strength data and verify that the Zircaloy and ZIRLO grid strength data at reactor operating conditions is structurally acceptable. The OFA Zircaloy, ZIRLO, and Inconel grid designs maintain their integrity during the most severe load conditions of a combined seismic/LOCA event.

Beginning with the Unit 3 Cycle 13 reload, snag-resistant top, middle and bottom grids were introduced. In this design, the outer grid straps are modified to help prevent fuel assembly hangup due to grid strap interference during fuel assembly removal and insertion. This was accomplished by changing the grid strap corner geometry and adding guide tabs on the outer grid strap.

Fuel Rods

The fuel rods consist of uranium dioxide ceramic pellets contained in a slightly cold worked and stress relieved Zircaloy-4 or ZIRLO tubing which is plugged and seal welded at the ends to encapsulate the fuel. Sufficient void volume and clearances are provided within the rod to accommodate fission gases released from the fuel, differential thermal expansion between the cladding and the fuel, and fuel swelling due to accumulated fission products without over-stressing of the cladding or seal welds. Shifting of the fuel within the cladding is prevented during handling or shipping prior to core loading by a stainless steel helical compression spring which bears on the top of the fuel.

The fuel rods employed in LOPAR and OFA assemblies are geometrically identical with only slight variations in some design parameters. The Debris Resistant Fuel Assembly (DRFA), a modified OFA with debris resistant features, utilizes a lower end plug which is approximately 1.4 inches longer than in the standard OFA design. On a cycle-to-cycle and region-to-region basis, fuel enrichment, plenum void volume and initial helium backfill pressure will vary somewhat to accommodate specific cycle design requirements. This fact was also applicable prior to the introduction of OFA assemblies. For Unit 3 beginning with cycle-12, the DRFA incorporates axial blankets which consist of low enriched or natural uranium oxide pellets extending 6 inches at the top and bottom of the fuel stack within the fuel rod. Unit 4 has axial blankets starting with Cycle 14 and DRFA starting with Cycle 13.

During fuel rod assembly, the pellets are stacked in the cladding to the required fuel height. The compression spring is then inserted into the top end of the fuel and the end plugs pressed into the ends of the tube and welded. All fuel rods are internally pressurized with helium during the welding process. A hold-down force in excess of the weight of the fuel is obtained by compression of the spring between the top end plug and the top of the fuel pellet stack.

The fuel pellets are right circular cylinders consisting of slightly enriched uranium-dioxide powder which is compacted by cold pressing and sintering to the required density. The ends of each pellet are dished slightly to allow the greater axial expansion at the center of the pellets to be taken up within the pellets themselves and not in the overall fuel length. The ends of each OFA fuel pellet have a small chamfer at the outer cylinder surface.

For historical purposes, the pellet densities in the initial core were adjusted as shown in Table 3.2.3-1 to compensate for the effects of the higher burnup of fuel in regions remaining longest in the core. A different fuel enrichment as listed in Table 3.2.3-1 is used for each of the three regions in the first core loading. Reload region, as-built fuel enrichments and pellet densities are provided in the Reload Characteristics and Parameters report included in Appendices 14A and 14B for Units 3 and 4, respectively.

To prevent the possibility of mixing enrichments during fuel manufacture and assembly, meticulous process control is exercised.

Process Control

Powder withdrawal from storage can be made by one authorized group only who direct the powder to correct pellet production line. All pellet production lines are physically separated from each other and pellets of only a single enrichment and density are produced in a given production line.

Finished pellets are placed on trays having the same color code as the powder containers and transferred to segregated storage racks within the confines of the pelleting area. Physical barriers prevent mixing of pellets of different densities and enrichments in this storage area. Unused powder and substandard pellets are returned to storage in the original color coded containers.

Each fuel assembly will be identified by means of a serial number engraved on the upper nozzle. The fuel pellets will be fabricated by a batch process so that only one enrichment region is processed at any given time. The serial numbers of the assemblies and corresponding enrichment will be documented by the manufacturer and verified prior to shipment.

Each assembly will be assigned a core loading position. A record will then be made of the core loading position, serial number and enrichment. Prior to core loading, independent checks will be made to ensure that this assignment is correct.

During initial core loading and subsequent refueling operations, detailed handling and checkoff procedures will be utilized throughout the sequence. The initial core will be loaded in accordance with the core loading diagram similar to Figure 3.2.3-3 which shows the location for each of the three enrichment types of fuel assemblies in the region. Reload cycle core loading pattern diagrams are provided in the cycle specific Reload Characteristics and Parameters report included in Appendices 14A and 14B for Units 3 and 4 respectively.

Rod Cluster Control Assemblies

The rod cluster control assemblies (RCCA) each consist of a group of individual absorber rods fastened at the top end to a common hub or spider assembly. These assemblies one of which is shown in Figure 3.2.3-4 are provided to control the reactivity of the core under operating conditions. These assemblies consist of rods containing full length absorber material. The number of RCCA’s is specified in Table 3.2.3-1.

The absorber material used in the control rods is silver-indium-cadmium alloy which is essentially "black" to thermal neutrons and has sufficient additional resonance absorption to significantly increase its worth. The alloy is in the form of extruded single length rods which are sealed in stainless steel tubes to prevent the rods from coming in direct contact with the coolant.

The overall control rod length is such that when the assembly has been withdrawn through its full travel, the tip of the absorber rods remain engaged in the guide thimbles so that alignment between rods and thimbles is always maintained. Since the rods are long and slender, they are relatively free to conform to any small misalignments with the guide thimble. Prototype tests have shown that the RCCA's are very easily inserted and not subject to binding even under conditions of severe misalignment.

The spider assembly is in the form of a center hub with radial vanes containing cylindrical fingers from which the absorber rods are suspended. Handling detents, and detents for connection to the drive shaft, are machined into the upper end of the hub. A spring pack is assembled into a skirt integral to the bottom of the hub to stop the RCCA's and absorb the impact energy at the end of a trip insertion. A centerpost which holds the spring pack and its retainer is threaded into the hub within the skirt and welded to prevent loosening in the service. All components of the spider assembly are made from Type 304 stainless steel except for the springs which are Inconel X-750 alloy and the retainer which is of 17-4 Ph material.

The absorber rods are secured to the spider so as to assure trouble free service. The rods are first threaded into the spider fingers and then pinned to prevent rotation, after which the pins are welded in place. The end plug below the pin position is designed with a reduced section to permit flexing of the rods to correct for small assembly misalignments.

In construction, the silver-indium-cadmium rods are inserted into cold-worked stainless steel tubing which is then sealed at the bottom and the top by welded end plugs. Sufficient diametral and end clearance is provided to accommodate relative thermal expansions and to limit the internal pressure to acceptable levels.

The bottom plugs are made bullet-nosed to reduce the hydraulic drag during a reactor trip and to guide smoothly into the dashpot section of the fuel assembly guide thimbles. The upper plug is threaded for assembly to the spider and has a reduced end section to make the joint more flexible.

Stainless steel clad silver-indium-cadmium alloy absorber rods are resistant to radiation and thermal damage ensuring their effectiveness under all operating conditions.

Neutron Source Assemblies

Four neutron source assemblies were utilized in the initial core. They consisted of two secondary source assemblies each, and two primary source assemblies each. The rods in the source assembly are fastened to a spider at the top end similar to the RCCA spiders.

For historical purposes, in the core, the neutron source assemblies were inserted into the RCCA guide thimbles in fuel assemblies at unrodded locations. The location of these assemblies in the core is shown in Figure 3.2.3-3. Based on the evaluations documented in References 6 and 7 of Section 3.1.1, it has been determined that it is acceptable to remove these sources from Turkey Point Units 3 & 4. Consequently, no startup sources have been used beginning with Cycle 13 in both units.

The primary and secondary source rods both utilized the same type of cladding material as the absorber rods (cold-worked type 304 stainless steel tubing, 0.432 in O.D. with 0.019 inch thick walls). The secondary source rods contain Sb-Be pellets stacked to a height of 121.75 inches. Design criteria similar to those for the fuel rods are used for the design of the source rods; ie, the cladding is free standing, internal pressures are always less than reactor operating pressure, and internal gaps and clearances are provided to allow for differential expansions between the source material and cladding.

Thimble Plug Assemblies

Evaluations have been performed to support the complete or partial removal of thimble plugs from Turkey Point Units 3 & 4. These evaluations have addressed the effect of thimble plug removal on Core Design, Core Thermal Hydraulics, Reactor Pressure Vessel System thermal hydraulics and the non-LOCA and LOCA safety analyses. Based on these evaluations, it has been determined that it is acceptable to remove all or any combination of thimble plugs from Turkey Point Units 3 & 4.

The thimble plug assemblies as shown in Figure 3.2.3-10A consist of a flat base plate with short rods suspended from the bottom surface and a spring pack assembly. The twenty short rods, called thimble plugs, project into the upper ends of the guide thimbles to reduce the bypass flow area. Similar short rods are also used on the source assemblies and burnable poison assemblies to plug the ends of all vacant fuel assembly guide thimbles. At installation in the core, the thimble plug assemblies interface with both the upper core plate and with the fuel assembly top nozzles by resting on the adaptor plate. The spring pack is compressed by the upper core plate when the upper internals assembly is lowered into place. Each thimble plug is permanently attached to the base plate by a nut which is locked to the threaded end of the plug by a small lock-pin welded to the nut.

The OFA thimble plug has a smaller diameter (0.485 inch) than the LOPAR thimble plug diameter (0.498 inch) in order to maintain the same thimble plug to thimble tube diametral clearance, and to limit bypass flow through the OFA guide thimbles while providing sufficient coolant flow to cool the core components.

All components in the thimble plug assembly, except for the springs, are constructed from type 304 stainless steel. The springs are wound from an age hardened nickel base alloy for corrosion resistance and high strength.

Burnable Poison Rod

The burnable poison rods are statically suspended and positioned in vacant RCC thimble tubes within the fuel assemblies at nonrodded core locations. The poison rods in each fuel assembly are grouped and attached together at the top end of the rods by a flat base plate which fits within the fuel assembly top nozzle and rests on the top adaptor plate.

The base plate and the poison rods are held down and restrained against vertical motion through a spring pack which is attached to the plate and is compressed by the upper core plate when the reactor upper internals package is lowered into the reactor. This ensures that the poison rods cannot be lifted out of the core by flow forces.

Several types of burnable absorbers have been utilized in Turkey Point Units 3 and 4. Typically, both full-length and part-length borosilicate burnable poison rods which consist of borosilicate glass tubes contained within type 304 stainless steel cladding were used in LOPAR assemblies. These are plugged and sealed at both ends to encapsulate the glass. The glass is also supported along the length of its inside diameter by a thin wall type 304 stainless steel, tubular inner liner (Figure 3.2.3-11).

The second major type is the Wet Annular Burnable Absorber[3] (WABA) (Figure 3.2.3-11A) which will, as necessary, be used with OFA assemblies. The WABA consists of an annular aluminum oxide-boron carbide ($A1_2O_3$-B_4C) absorber pellets in two concentric Zircaloy tubes. Coolant flows through the center holes as well as through the outer annulus between the WABA and the guide thimble tube. The WABA design provides significantly enhanced nuclear characteristics compared with the borosilicate absorber rod design. Fuel cycle benefits result from the reduced parasitic nature of Zircaloy compared to stainless steel tubes, increased water fraction in the burnable absorber cell, and a reduced reaactivity penalty at the end of each cycle.

The third major type of neutron absorber being used is the Hafnium Vessel Flux Depression (HVFD) absorber (Figure 3.2.3-14). The HVFD consists of a reduced length annular hafnium absorber axially positioned within Zircaloy cladding. The primary function of the HVFD is to provide for reactor vessel flux reduction to satisfy pressurized thermal shock considerations[1].

The fourth major type of burnable absorber currently utilized is the Integral Fuel Burnable Absorber (IFBA). The IFBA rods have a thin boride coating on the cylindrical surface of the fuel pellets along the central portion of the fuel stack length. In order to offset the effects of the Helium gas release from the IFBA coating during irradiation, a lower initial Helium backfill pressure is used in the IFBA rods compared to the non-IFBA fuel rods.

The initial implementation of IFBA underwent a detailed quualification at the manufacturer and demonstration program to demonstrate integrity during extended duty. This program included demonstration assemblies which were loaded in the Unit 4 Cycle 10 core (Reference 13). The mechanical design of these assemblies was identical to that of the assemblies in that reload region, except that the demonstration assemblies were of the removable rod type, discussed below. A detailed description of the IFBA fuel rods is found in References 14 and 15.

For historical purposes, the following discussion of the borosilicate glass BP rod design is retained for completeness. This burnable poison design has not been used at Turkey Point since Unit 3 Cycle 9 and Unit 4 Cycle 10. The rods are designed in accordance with the standard fuel rod design criteria; i.e., the cladding is free standing at reactor operating pressures and temperatures and sufficient cold void volume is provided within the rods to limit internal pressures to less than the reactor operating pressure assuming total release of all helium generated in the glass as a result of the B_{10} (n,a) reaction. The large void volume required for the helium is obtained through the use of glass in tubular form which provides a central void along the length of the rods. A more detailed discussion of the borosilicate glass BP rod design is found in WCAP 9000[4].

Based on available data on properties of Pyrex glass and on nuclear and thermal calculations for the rods, gross swelling or cracking of the glass tubing is not expected during operation. Some minor creep of the glass at the hot spot on the inner surface of the tube is expected to occur but continues only until the glass comes into contact with the inner liner. The inner liner is provided to maintain the central void along the length of the glass and to prevent the glass from slumping or creeping into the void as a result of softening at the hot spot. The wall thickness of the inner liner is sized to provide adequate support in the event of slumping but to collapse locally before rupture of the exterior cladding if large volume changes due to swelling or cracking should possibly occur. The top end of the inner liner is open to receive the helium which diffuses out of the glass.

To ensure the integrity of the burnable poison rods, the tubular cladding and end plugs are procured to the same specifications and standard of quality as is used for stainless steel fuel rod cladding and end plugs in other Westinghouse plants. In addition, the end plug seal welds are checked for integrity by visual inspection and x-ray. The finished rods are helium leak checked.

Removable Rod Assemblies

Four demonstration assemblies were loaded in Turkey Point Unit 4, Cycle 10. Each of the assemblies contains twenty-eight demonstration Integral Fuel Burnable Absorber (IFBA) fuel rods and one hundred and seventy-six unpoisoned fuel rods.

The mechanical design of the demonstration assemblies is identical to that of the other fuel assemblies in the reload region, except that the demonstration assemblies are the "removable rod" type, which will allow removal of some rods for post-irradiation inspections. Similar "removable rod" type Optimized Fuel Assemblies have been used in previous demonstration assembly programs at Farley, Salem, Beaver Valley and Point Beach reactors. The mechanical design of the assemblies has been evaluated and meets the same acceptance criteria as the standard fuel assembly design for steady state, transient, seismic and LOCA conditions.

The design of the fuel rods contained in the demonstration assemblies is identical to the fuel rod design of the other fuel rods in the reload region except that:

1. in each of the demonstration assemblies, there are fifty-two removable fuel rods (sixteen removable IFBA rods, 36 removable non-IFBA rods); these removable fuel rods have longer, more slender top end plugs to facilitate rod removal and a larger chamfer on their bottom end plugs to ease fuel rod reinsertion;

2. for the IFBA fuel rods only (sixteen removable IFBA fuel rods and twelve non-removable IFBA fuel rods per assembly), each fuel stack contains absorber material coated on the outside diameter of the $U0_2$ fuel pellets and distributed uniformly over the entire fuel stack; because the burnable absorber material releases additional helium into the fuel rod during depletion, the IFBA fuel rods are prepressurized to 200 psig during manufacture, whereas the non-IFBA fuel rods in the demonstration assemblies, and the standard fuel rods throughout the reload region, are prepressurized 350 psig.

3. the core locations of the IFBA demonstration assemblies were chosen such that the IFBA fuel rods are never the lead power rods.

Based on review of the appropriate phase diagram and on destructive examination after one reactor cycle of test rods incorporating coated pellets essentially identical in material and manufacture method, no adverse chemical interaction of the absorber material with either cladding or fuel pellet is predicted for the times and temperatures of operation.

The approved fuel rod model (PAD) [5] was used to assess in detail the fuel rod design criteria influenced by addition of the absorber material. Based upon a consideration of clad stress, fuel temperatures, and rod internal pressure, an allowable burnup for the demonstration rods in excess of the planned burnup of fuel assemblies was calculated. No adverse effects on fuel rod performance were predicted.

Evaluation of Core Components

Fuel Rod Evaluation

The fission gas release and the associated buildup of internal gas pressure in the fuel rods is calculated by the PAD code based on experimentally determined rates. The increase of internal pressure in the fuel rod due to this phenomenon is included in the determination of the maximum cladding stresses at the end of core life when the fission product gap inventory is a maximum.

The maximum allowable strain in the cladding, considering the combined effects of internal fission gas pressure, external coolant pressure, fuel pellet swelling and clad creep is limited to less than 1 percent throughout core life. The associated stresses are below the yield strength of the material under all normal operating and overpower conditions.

To assure that manufactured fuel rods meet a high standard of excellence from the standpoint of functional requirements, many inspections and tests are performed both on the raw material and the finished product. These tests and inspections include chemical analysis, tensile and ultrasonic testing of fuel tubes, dimensional inspection, ultrasonic test or x-ray of both end plug welds, gamma scanning and helium leak tests.

In the event of cladding defects, the high resistance of uranium dioxide fuel pellets to attack by hot water protects against fuel deterioration or decrease in fuel integrity. Thermal stress in the pellets, while causing some fracture of the bulk material during temperature cycling, does not result in pulverization or gross void formation in the fuel matrix. As shown by operating experience and extensive experimental work in the industry, the thermal design parameters conservatively account for any changes in the thermal performance of the fuel element due to pellet fracture.

The consequences of a breach of cladding are greatly reduced by the ability of uranium dioxide to retain fission products including those which are gaseous or highly volatile. This retentiveness decreases with increasing temperature or fuel burnup, but remains a significant factor even at full power operating temperature in the maximum burnup element.

A survey of fuel elements behavior in high burnup uranium dioxide[6] indicates that for an initial uranium dioxide void volume, which is a function of the fuel density, it is possible to conservatively define the fuel swelling as a function of burnup.

The evaluation of fuel densification and the treatment of fuel swelling are described by an empirical model developed with data from numerous operating Westinghouse reactors as described in Reference 10.

The integrity of the fuel rod cladding is directly related to cladding stresses and strains under normal and overpower conditions. The cladding stress is limited to the yield strength of the material. The steady-state tensile strain is limited to 1.0% and during power increases the cladding tensile strain is limited to 1.0% during the transient.

The cladding stresses at constant local fuel rod power are low. Compressive stresses are created by the pressure differential between the coolant pressure and the rod internal pressure. Tensile stresses could be created once the cladding has come into contact with the pellet which results from fuel swelling and cladding creepdown (thermal and irradiation induced creep as determined by the models of Reference 10). These stresses would be induced by

the fuel pellet swelling during irradiation. Fuel swelling can result in small cladding strains (<1%) for expected discharge burnups, but the associated cladding stresses are low because of cladding creep. Furthermore, the 1% strain criterion is extremely conservative for fuel swelling driven cladding strain because the strain rate associated with solid fission product swelling is very slow.

Pellet thermal expansion caused by power increases is considered the only mechanism by which significant stresses and strains can be imposed on the cladding. Radial, tangential, and axial stress components due to pressure differential and fuel cladding contact pressure which can occur during power increases the combined stress components into an effective stress using the maximum-distortion energy theory. The Von Mises criterion is used to evaluate if the yield strength has been exceeded. The effective stress is increased by an allowance for local non-uniformity effects before it is compared to the yield strength. The yield strength of the cladding is a function of the cladding temperature. The yield strength is that appropriate for irradiated cladding since the irradiated properties are attained at low exposure whereas the fuel-cladding contact which can lead to minimum margin to the yield strength occurs at much higher exposure. Slow transient power increases can result in large cladding strains without exceeding the yield strength because of cladding creep and stress relaxation. Therefore, the additional limitation of 1% cladding tensile strain during a transient is considered.

The internal gas pressure of the rods in the reactor is limited to a value below that which would cause the pellet-cladding diametral gap to increase due to outward cladding creep during steady-state operation, and which would cause extensive DNB propagation to occur. The safety evaluation of the fuel rod internal pressure design basis is presented in Reference 11. The fission gas release and the associated buildup of internal gas pressure inside the fuel rod is determined by the models of Reference 10. The increase of internal pressure in the fuel rod is included in the determination of the maximum cladding stresses and strains.

Cladding collapse is precluded during fuel rod design lifetime by appropriate control of pellet characteristics which control in-reactor fuel densification behavior, as described in References 7 and 12.

The use of chamfered fuel pellets in Optimized Fuel Assemblies results in a hot spot average fuel temperature increase of less than 20◦F compared to unchamfered pellets. Evaluation results show that all core design criteria and safety limits (including LOCA and non-LOCA transients) are satisfied when using chamfered pellets.

Evaluation of Burnable Poison Rods

The burnable poison rods are positioned in the core inside fuel assembly guide thimbles and held down in place by attachment to a plate assembly compressed beneath the upper core plate and hence cannot be the source of any reactivity transient. Due to the low heat generation rate, and the conservative design of the poison rods, there is no possibility for release of the poison as a result of helium pressure or clad heating during accident transients including loss of coolant.

Effects of Vibration and Thermal Cycling on Fuel Assemblies

Analyses of the effect of cyclic deflection of the fuel rods, grid spring fingers, RCCA's, and burnable poison rods due to hydraulically induced vibrations and thermal cycling show that the design of the components is good for an infinite number of cycles.

In the case of the fuel grid spring support, the amplitude of a hydraulically induced motion of the fuel rod is extremely small ($\approx$ .001) and the stress associated with the motion is significantly small (< 100 psi). Likewise, the reactions at the grid spring due to the motion is much less than the preload spring force and contact is maintained between the fuel clad and the grid spring and dimples. Fatigue of the clad and fretting between the clad and the grid support are not anticipated.

The effect of thermal cycling on the grid-clad support is merely a slight relative movement between the grid contact surfaces and the clad, which is gradual in nature during heat-up and cool-down. Since the number of cycles of the occurrence is small over the life of a fuel assembly ($\approx$ 6 years), negligible wear of the mating parts is expected.

In-core operation of assemblies in the Yankee Rowe and Saxton reactors using similar clad support have verified the calculated conclusions. Additional test results under simulated reactor environment in the Westinghouse Reactor Evaluation Channel also support these conclusions.

The dynamic deflection of the full length control rods and the burnable poison rods is limited by their fit with the inside diameter of either the upper portion of the guide thimble or the dashpot. With this limitation, the occurrence of truly cyclic motion is questionable. However, an assumed cyclic deflection through the available clearance gap results in an insignificantly low stress in either clad tubing or in the flexure joint at the spider or retainer plate. The above consideration assumes the rods are supported as cantilevers from the spider, or the retainer plate in the case of the burnable poison rods.

A calculation, assuming the rods are supported by the surface of the dashpots and at the upper end by the spider or retainer, results in a similar conclusion.

Control Rod Drive Mechanism

Full Length Rods

Design Description

The Control Rod Drive Mechanisms (CRDM) are used for withdrawal and insertion of the RCCA's into the reactor core and to provide sufficient holding power for stationary support.

Fast total insertion (reactor trip) is obtained by simply removing the electrical power allowing the rods to fall by gravity.

The complete drive mechanism, shown in Figure 3.2.3-12, consists of the internal (latch) assembly, the pressure vessel, the operating coil stack, the drive shaft assembly, and the position indicator coil stack.

Each assembly is an independent unit which can be dismantled or assembled separately. Each drive is threaded into an adaptor on top of the reactor pressure vessel and is connected to the control rod (directly below) by means of a grooved drive shaft. The upper section of the drive shaft is suspended from the working components of the drive mechanism. The drive shaft and control rod remain connected during reactor operation, including tripping of the rods.

For Unit 3, the reactor vessel head penetrations at two locations have been modified from the head adaptor plug design to a welded pipe cap design (Figures 3.2.3-15 and 3.2.3-16). At these locations, dummy CRDM cans are positioned over the vertical pipes to maintain proper air flow around the CRDMs. The dummy CRDM cans are secured by connecting them to adjacent CRDM housings.

For Unit 3, the canopy seal for spare CRDM locations D-4, D-12, J-7, J-9, M-4, and M-12 have been modified to include a Canopy Seal Clamp Assembly (CSCA).

For Unit 4, the canopy seal for spare CRDM locations D-4, D-12, G-7, J-7, J-9, M-4, and M-12 have been modified to include a Canopy Seal Clamp Assembly (CSCA).

Reactor coolant fills the pressure containing parts of the drive mechanism. All working components and the shaft are immersed in the reactor coolant.

Three magnetic coils, which form a removable electrical unit and surround the rod drive pressure housing induce magnetic flux through the housing wall to operate the working components. They move two sets of latches which lift or lower the grooved drive shaft.

The three magnets are turned on and off in a fixed sequence by solid-state switches for the full length rod assemblies.

The sequencing of the magnets produces step motion over the 144 inches of normal control rod travel.

The mechanism develops a lifting force approximately two times the static lifting load. Therefore, extra lift capacity is available for overcoming mechanical friction between the moving and the stationary parts. Gravity provides the drive force for rod insertion and the weight of the whole rod assembly is available to overcome any resistance.

The mechanisms are designed to operate in water at 650◦F and 2485 psig. The temperature at the mechanism head adaptor will be much less than 650◦F because it is located in a region where there is limited flow of water from the reactor core, while the pressure is the same as in the reactor pressure vessel.

A multi-conductor cable connects the mechanism operating coils to the 125 volt DC power supply. The power supply is described in Section 7.3.2.

Latch Assembly

The latch assembly contains the working components which withdraw and insert the drive shaft and attached control rod. It is located within the pressure housing and consists of the pole pieces for three electromagnets. They actuate two sets of latches which engage the grooved section of the drive shaft.

The upper set of latches moves up or down to raise or lower the drive rod by 5/8 inch. The lower set of latches has 1/16 inch axial movement to shift the weight of the control rod from the upper to the lower latches. The housings are designed in accordance with the requirements for Class A vessels of the ASME Nuclear Vessel Code.

Rod Drive Mechanism Housing

The pressure vessel consists of the pressure housing and rod travel housing. The pressure housing is the lower portion of the vessel and contains the latch assembly. The rod travel housing is the upper portion of the vessel. It provides space for the drive shaft during its upward movement as the control rod is withdrawn from the core.

Operating Coil Stack

The operating coil stack is an independent unit which is installed on the drive mechanism by sliding it over the outside of the pressure housing. It rests on a pressure housing flange without any mechanical attachment and can be removed or installed while the reactor is pressurized.

The operator coils (A, B and C) are made of wound copper wire which is insulated with a double layer of filament type glass yarn.

The design operating temperature of the coils is 232◦C (450◦F). Coil temperature can be determined by resistance measurement. Forced air cooling along the outside of the coil stack maintains a coil temperature below 200◦C (392◦F).

Drive Shaft Assembly

The main function of the drive shaft is to connect the control rod to the mechanism latches. Grooves for engagement and lifting by the latches are located throughout the 144 in. of control rod travel. The grooves are spaced 5/8 inch apart to coincide with the mechanism step length and have 45◦ angle sides.

The drive shaft is attached to the contol rod by the coupling. The coupling has two flexible arms which engage the grooves in the spider assembly.

A 1/4 inch diameter disconnect rod runs down the inside of the drive shaft. It utilizes a locking button at its lower end to lock the coupling and control rod. At its upper end, there is a disconnect assembly for remote disconnection of the drive shaft assembly from the control rod. During operation, the drive shaft assembly remains connected to the control rod at all times.

Position Indicator Coil Stack

The position indicator coil stack slides over the rod travel housing section of the pressure vessel. It detects drive rod position by means of cylindrically wound differential transformers which span the normal length of the rod travel (144 inches).

Drive Mechanism Materials

All parts exposed to reactor coolant, such as the pressure vessel, latch assembly and drive rod, are made of metals which resist the corrosive action of the water.

Three types of metals are used exclusively: stainless steels, Inconel X, and cobalt based alloys. Wherever magnetic flux is carried by parts exposed to the reactor coolant, stainless steel is used. Cobalt based alloys are used for the pins and latch tips.

Inconel X is used for the springs of both latch assemblies and 304 stainless steel is used for all pressure containment. Hard chrome plating provides wear surfaces on the sliding parts and prevents galling between mating parts (such as threads) during assembly.

Outside of the pressure vessel, where the metals are exposed only to the reactor containment environment and cannot contaminate the reactor coolant, carbon and stainless steels are used. Carbon steel, because of its high permeability, is used for flux return paths around the operating coils. It is zinc-plated 0.001 inch thick to prevent corrosion.

Principles of Operation

The drive mechanisms shown schematically in Figure 3.2.3-13 withdraw and insert their respective control rods as electrical pulses are received by the operator coils.

ON and OFF sequence, repeated by Silicon Controlled Rectifiers (SCR) in the power programmer causes either withdrawal or insertion of the control rod. Position of the control rod is indicated by the differential transformer action of the position indicator coil stack surrounding the rod travel housing. The differential transformer output changes as the top of the ferromagnetic drive shaft assembly moves up the rod travel housing.

Generally during operation, the stationary gripper coil of the drive mechanisms hold the control rods withdrawn from the core in a static position until the movable gripper coil is energized.

Control Rod Withdrawal

The control rod is withdrawn by repeating the following sequence:

(1) Movable Gripper Coil - ON

The movable gripper armature raises and swings the movable gripper latches into the drive shaft groove.

(2) Stationary Gripper Coil - OFF

Gravity causes the stationary gripper latches and armature to move downward until the load of the drive shaft is transferred to the movable gripper latches. Simultaneously, the stationary gripper latches swing out of the shaft groove.

(3) Lift Coil - ON

The 5/8 inch gap between the lift armature and the lift magnet pole closes and the drive rod rises one step length.

(4) Stationary Gripper Coil - ON

The stationary gripper armature rises and closes the gap below the stationary gripper magnetic pole, swings the stationary gripper latches into a drive shaft groove. The latches contact the shaft and lift it 1/16 inch. The load is so transferred from the movable to the stationary gripper latches.

(5) Movable Gripper Coil - OFF

The movable gripper armature separates from the lift armature under the force of three springs and gravity. Three links, pinned to the movable gripper armature, swing the three movable gripper latches out of the groove.

(6) Lift Coil - OFF

The gap between the lift armature and the lift magnet pole opens. The movable gripper latches drop 5/8 inch to a position adjacent to the next groove.

Control Rod Insertion

The sequence for control rod insertion is similar to that for control rod withdrawal:

(1) Lift Coil - ON

The movable gripper latches are raised to a position adjacent to a shaft groove.

(2) Movable Gripper Coil - ON

The movable gripper armature rises and swings the movable gripper latches into a groove.

(3) Stationary Gripper Coil - OFF

The stationary gripper armature moves downward and swings the stationary gripper latches out of the groove.

(4) Lift Coil - OFF

Gravity separates the lift armature from the lift magnet pole and the control rod drops down 5/8 inch.

(5) Stationary Gripper Coil - ON

(6) Movable Gripper Coil - OFF

The sequences described above are termed as one step or one cycle and the control rod moves 5/8 inch for each cycle. Each sequence can be repeated at a design rate of up to 72 steps per minute and the control rods can therefore be withdrawn or inserted at a design rate of up to 45 inches per minute.

Control Rod Tripping

If power to the movable gripper coil is cut off, as for tripping, the combined weight of the drive shaft and the rod cluster control assembly is sufficient to move the latches out of the shaft groove. The control rod falls by gravity into the core. The tripping occurs as the magnetic field, holding the movable gripper armature against the lift magnet, collapses and the movable gripper armature is forced down by the weight acting upon the latches.

Reactor Vessel Level Measuring System Probes

Two part length control rod mechanisms have been modified to accommodate the installation of thermocouple probes. A new shroud has been installed in place of the existing guide tubes. The new shroud will be used as the receptacle for the probe assembly. These shrouds are designed in accordance with the guide tube design criteria.

Fuel Assembly and RCCA Mechanical Evaluation

To confirm the mechanical adequacy of the fuel assembly and RCCA's, functional test programs have been conducted on full scale San Onofre mock-up version of the fuel assembly and control rods. Additional tests were run on two full scale prototype assemblies for a twelve-foot active core. One of the twelve-foot assemblies incorporated stainless steel guide tubes and other incorporated Zircaloy-4 tubes.

Reactor Evaluation Center (WREC) Tests

The prototype assemblies were tested under simulated reactor operating conditions (1875 psig, 575°F, and 17.8 fps flow velocity) in the Westinghouse Reactor Evaluation Center (WREC) for a total of more than 6400 hours.

Each prototype assembly was subjected to trip cycling equivalent to one or more plant lifetimes. The test history for each prototype is summarized below:

PROTOTYPE	TEST TIME, HOURS	NUMBER OF TRIPS	TOTAL OF TRAVEL, FT.	TOTAL DRIVEN TRAVEL, FT.	TOTAL TRIP TRAVEL, FT.
San Onofre, 10 ft. assy. stainless steel guide thimbles	4132	1461	38,927	27,217	11,710
12-ft. assembly stainless steel guide thimbles	1000	600	45,000	38,500	6,500
12-ft. assembly Zircaloy-4 guide thimbles	1277	600	124,200	117,700	6,500

Each of the three prototype fuel assemblies remained in excellent mechanical condition. No measurable signs of wear on the fuel tubes or control rod guide tubes were found.

The control rod was also found to be in excellent condition, having maximum wear measured on absorber cladding of approximately 0.001 in.

Loading and Handling Tests

Tests simulating the loading of the prototype fuel assembly into a core location were also successfully conducted to determine that proper provisions had been made for guidance of the fuel assembly during refueling operation.

Axial and Lateral Bending Tests

In addition, axial and lateral bending tests were performed in order to simulate mechanical loading of the assembly during refueling operation.

Although the maximum column load expected to be experienced in service is approximately 1000 lb. the fuel assembly can successfully be loaded to 2200 lb. axially with no damage resulting. This information is also used in the design of fuel handling equipment to establish the limits for inadvertent axial loads during refueling.

CRDM Housing Mechanical Failure Evaluation

An evaluation of the possibility of damage to adjacent control rod drive mechanism housings in the event of a circumferential or longitudinal failure or a rod housing located on the vessel head is presented.

A control rod drive mechanism schematic is shown in Figure 3.2.3-12 and 3.2.3-13. The operating coil stack assembly of this mechanism has a 10.718 inch by 10.718 inch cross section and a 39.875 inch length. The position indicator coil stack assembly (not shown in this figure) is located above the operating coil stack assembly. It surrounds the rod travel

housing over nearly its entire length. The rod travel housing outside diameter is 3.8 inches and the position indicator coil stack assembly consists of a 1/8" thick stainless steel tube surrounded by a continuous stack of copper wire coils. This assembly is held together by two end plates (the top end plate is square), an outer sleeve, and four axial tie rods.

Effect of Rod Travel Housing Longitudinal Failures

Should a longitudinal failure of the rod travel housing occur, the region of the stainless steel tube opposite the break would be stressed by the reactor coolant pressure of 2250 psia. The most probable leakage path would be provided by the radial deformation of the position indicator coil assembly, resulting in the growth of axial flow passages between the rod travel housing and the stainless steel tube. A radial free water jet is not expected to occur because of the small clearance between the stainless steel tube and the rod travel housing, and the considerable resistance of the combination of the stainless steel tube and the position indicator coils to internal pressure. Calculations based on the mechanical properties of stainless steel and copper at reactor operating temperature show that an internal pressure of at least 4000 psia would be necessary for the combination of the stainless steel tube and the coils to rupture.

Therefore, the combination of stainless steel tube and copper coils stack is more than adequate to prevent formation of a radial jet following a control rod housing split which assures the integrity of the adjacent rod housings.

Effect of Rod Travel Housing Circumferential Failures

If circumferential failure of a rod travel housing should occur, the broken-off section of the housing would be ejected vertically because the driving force is vertical and the position indicator coil stack assembly and the drive shaft would tend to guide the broken-off piece upwards during its travel. Travel is

limited to less than two feet by the missile shield, thereby limiting the projectile acceleration. When the projectile reaches the missile shield, it would partially penetrate the shield and dissipate its kinetic energy. The water jet from the break would push the broken-off piece against the missile shield.

If the broken-off piece were short enough to clear the break when fully ejected, it could rebound after impact with the missile shield. The top end plates of the position indicator coil stack assemblies would prevent the broken piece from directly hitting the rod travel housing of a second drive mechanism. Even if a direct hit by the rebounding piece were to occur, the low kinetic energy of the rebounding projectile would not be expected to cause significant damage.

Summary

The considerations given above lead to the conclusion that failure of a control rod housing due to either longitudinal or circumferential cracking would not cause damage to adjacent housings that would increase the severity of the initial accident.

REFERENCES

1. Letter from Uhrig, R. E., FP&L to Varga, S. A., NRC, Subject: Pressurized Thermal Shock, Letter No L-83-180, March 25, 1983.

2. Petrarca, D., et al, "Reload Transition Safety Report For Turkey Point Units 3 & 4," June, 1983.

3. Letter from Thomas, C. 0., NRC, to Rahe, E. P., Westinghouse, Subject: Acceptance for Referencing of Licensing Topical Report WCAP-10021 (P), Revision 1, and WCAP-10377 (NP), "Westinghouse Wet Annular Burnable Absorber Evaluation Report," August 9, 1983.

4. WCAP-9000 (1968), "Nuclear Design of Westinghouse Pressurized Water Reactor with Burnable Poison Rods," PROPRIETARY. A NON-PROPRIETARY version of this report is WCAP-7806, Revision 1.

5. WCAP-8720, Addendum-2, "Westinghouse Revised Pad Code Thermal Safety Model," October 27, 1982 (Proprietary).

6. Daniel, R. C., et al. "Effects of High Burnup on Zircaloy-Clad Bulk DO_2 Plate Fuel Element Samples," WAPD-263, (September, 1965).

7. Oelrich, R. L. and Kersting, P. J., "Assessment of Clad Flattening and Densification Power Spike Factor Elimination in Westinghouse Nuclear Fuel," WCAP-13589, January 1993.

8. XN-NF-85-12(P) Ford, K. L., et al "Mechanical Design Report For Turkey Point Units 3 & 4 Hafnium Vessel Flux Depression (HVFD) Cluster Assemblies," Proprietary.

9. WCAP-12346, "Turkey Point Units 3 and 4 - 15x15 Debris Resistant Fuel Assembly Design Report," July 1989.

10. Weiner, R. A. et. al., "Improved Fuel Performance Models for Westinghouse Fuel Rod Design and Safety Evaluations," WCAP-10851-P-A (Proprietary) and WCAP -11873-A (Non-Proprietary), August 1988.

11. Risher, D. H. (Editor), "Safety Analysis for the Revised Fuel Rod Internal Pressure Design Basis," WCAP-8963-P-A (Proprietary) and WCAP-8964-A (Non-Proprietary), August 1978.

12. Letter, G. M. Holohan (NRC) to N.J. Liparulo (W), Subject: Acceptance for Referencing of Topical Report WCAP-13589, "Assessment of Clad Flattening and Densification Power Spike Factor Elimination in Westinghouse Nuclear Fuel," (TAC NO. M85707), January 30, 1995.

13. WCAP-11027, “The Nuclear Design and Core Management of the Turkey Point Unit 4 Power Plant Cycle 11,” March 1986.

14. WCAP-10445-NP-A. “Reference Core Report Vantage 5 Fuel Assembly,” S.L. Davidson and W.R. Kramer, September 1995.

15. Letter from E. Rahe, Jr. (Westinghouse) to H. Berkow (NRC), NS-NRC-85-3090, Subject: Request for Addendum 1 to WCAP-10445-NP-A, December 1985.

16. Davidson, S.L., and Nufer, D.L., eds.,”Vantage+Fuel Assembly Reference Core Report,” WCAP-12610-P-A, and Appendices A through D, June 1990.

TABLE 3.2.3-1

CORE MECHANICAL DESIGN PARAMETERS(1)

Active Portion of the Core	
Equivalent Diameter, in.	119.7
Active Fuel Height, in - Unit 3	144.00, 144.00, 143.474
Unit 4	144.00, 143.40, 142.80
Length-to-Diameter Ration	1.2
Total Cross Section Area, Ft. ^{2}	78.1
Fuel Assemblies	
Number	157
Rod Array	15 x 15
Rods per Assembly	204 (2)
Rods Pitch, in.	0.563
Overall Dimensions, in.	8.426 x 8.426
Fuel Weight (as UO_2), pounds	176,000
Total Weight, pounds	225,000
Number of Grids per Assembly	7
Guide Thimble I.D. (Above Dashpot), in.	0.499
(at Dashpot), in.	0.455
Fuel Rods	
Number	32,028
Outside Diameter, in.	0.422
Diametral Gap, mils	7.5, 7.5, 8.5
Clad Thickness, in.	0.0243
Clad Material	Zircaloy-4 or ZIRLO
Overall Length, in. Unit 3	152.235 to <152.735
Unit 4	152.235 to <152.735
Fuel Pellets	
Material	UO_2 sintered
Density (% of Theoretical) - First Cycle (3)	
Region 1	94 (10.3 g/cc)
Region 2	93 (10.19 g/cc)
Region 3	92 (10.08 g/cc)(Unit 4-93)
Fuel Enrichments w/o - First Cycle (3)	
Region 1	1.85
Region 2	2.55
Region 3	3.10
Diameter, in. - Unit 3 (Regions 1, 2, 3)	0.3659, 0.3659, 0.3649
Unit 4 (All Regions)	0.3659
Length, in.	0.439

NOTES :

(1) All Dimensions are for cold conditions.
(2) Twenty-one rods are omitted: twenty to provide passage for control rods and one to contain in-core instrumentation.
(3) Values for current cycles are given in Appendixes 14A and 14B.

TABLE 3.2.3-1

Rod Cluster Control Assemblies	
Neutron Absorber	5% Cd, 15% In, 80% Ag
Cladding Material	Type 316L or 304 SS - Cold Worked
Clad Thickness, in.	0.019
Number of Clusters	45
Full Length	45
Number of Control Rods per Cluster	20
Weight in 60°F Water	
Full Length, pounds	147
Length of Rod Control, in.	158.454 (overall) 150.574 (insertion length)
Length of Absorber Section, in.	142.00
Core Structure	
Core Barrel, in.	
I.D.	133.875
O.D.	137.875
Thermal Shield, in.	
I.D.	142.625
O.D.	148.0
Burnable Poision Rods (4)	
Number	816
Material	Borosilicate Glass
Outside Diameter, in.	0.4395
Inner Tube, O.D. in.	0.2365
Clad Material	S.S.
Inner Tube Material	S.S.
Boron Loading (natural) gm/cm of glass rod	0.0429
Neutron Source Assemblies (5)	
Primary Source (typical)	Pu-Be
Secondary Source (typical)	Sb-Be

NOTES :

(4) Values for current cycles are given in Appendices 14A and 14B.

(5) Neutron sources are not installed in current cycles.

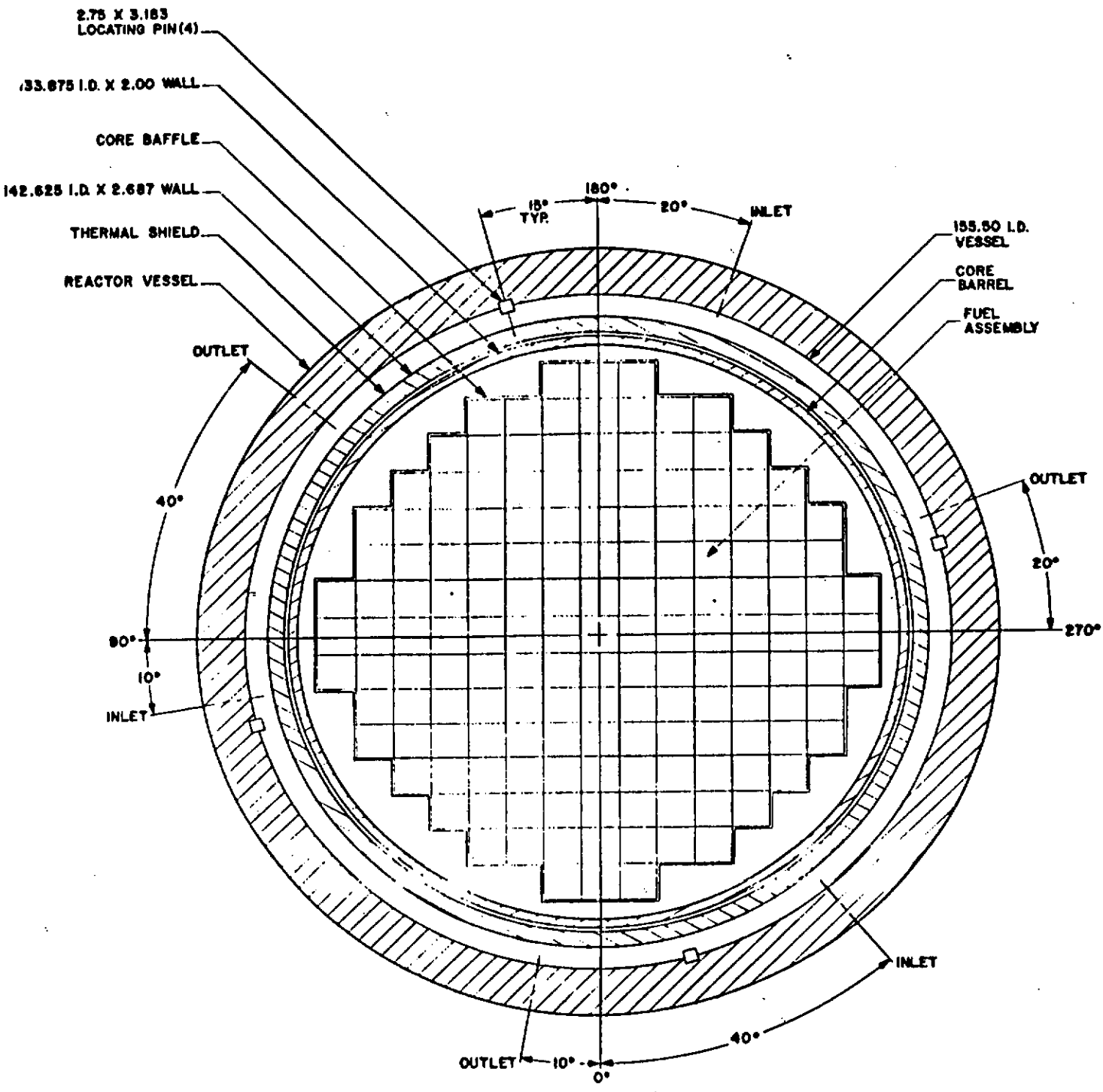

REACTOR CORE CROSS SECTION

FIG. 3.2.3-1

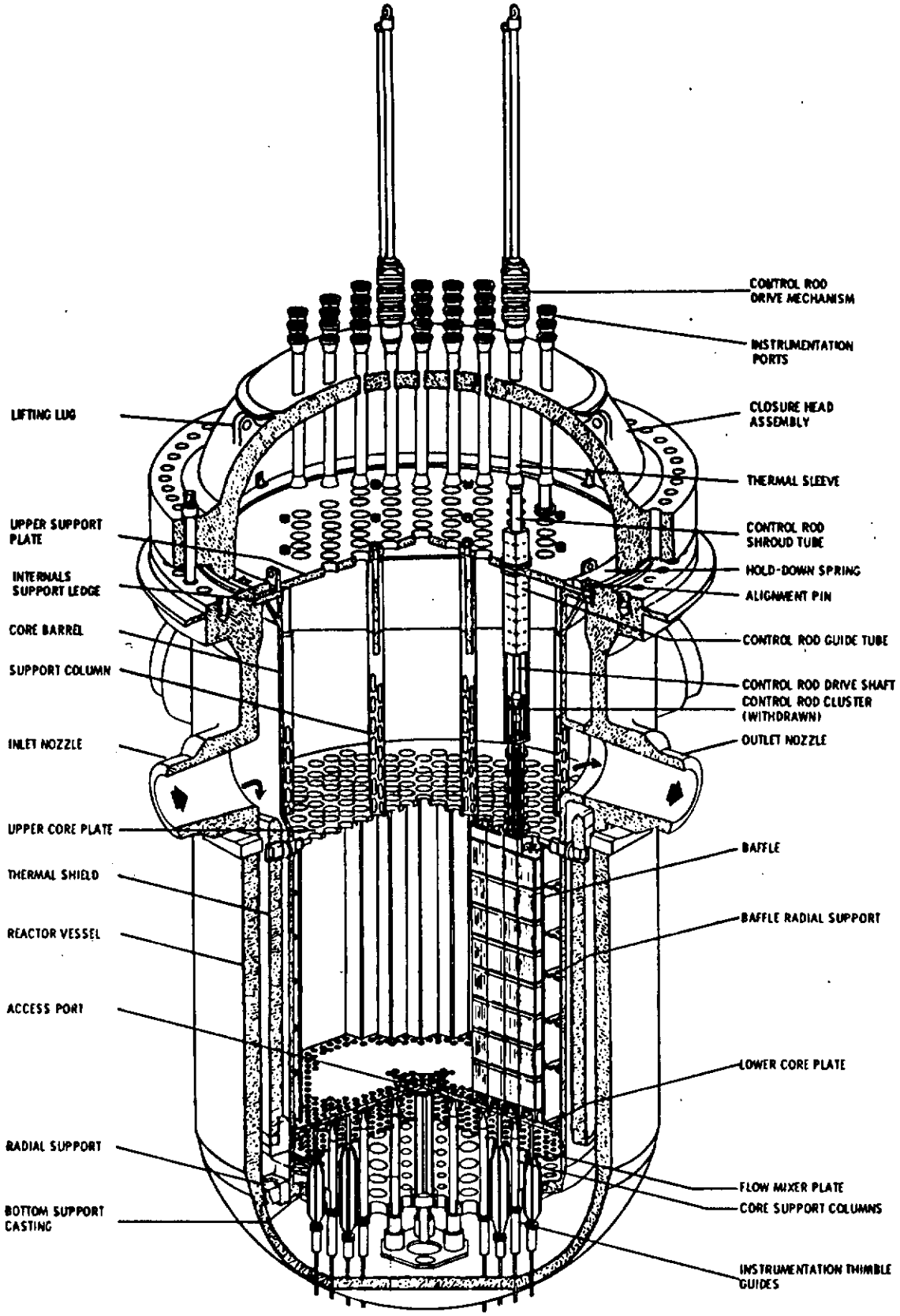

REACTOR VESSEL INTERNALS
FIG. 3.2.3-2

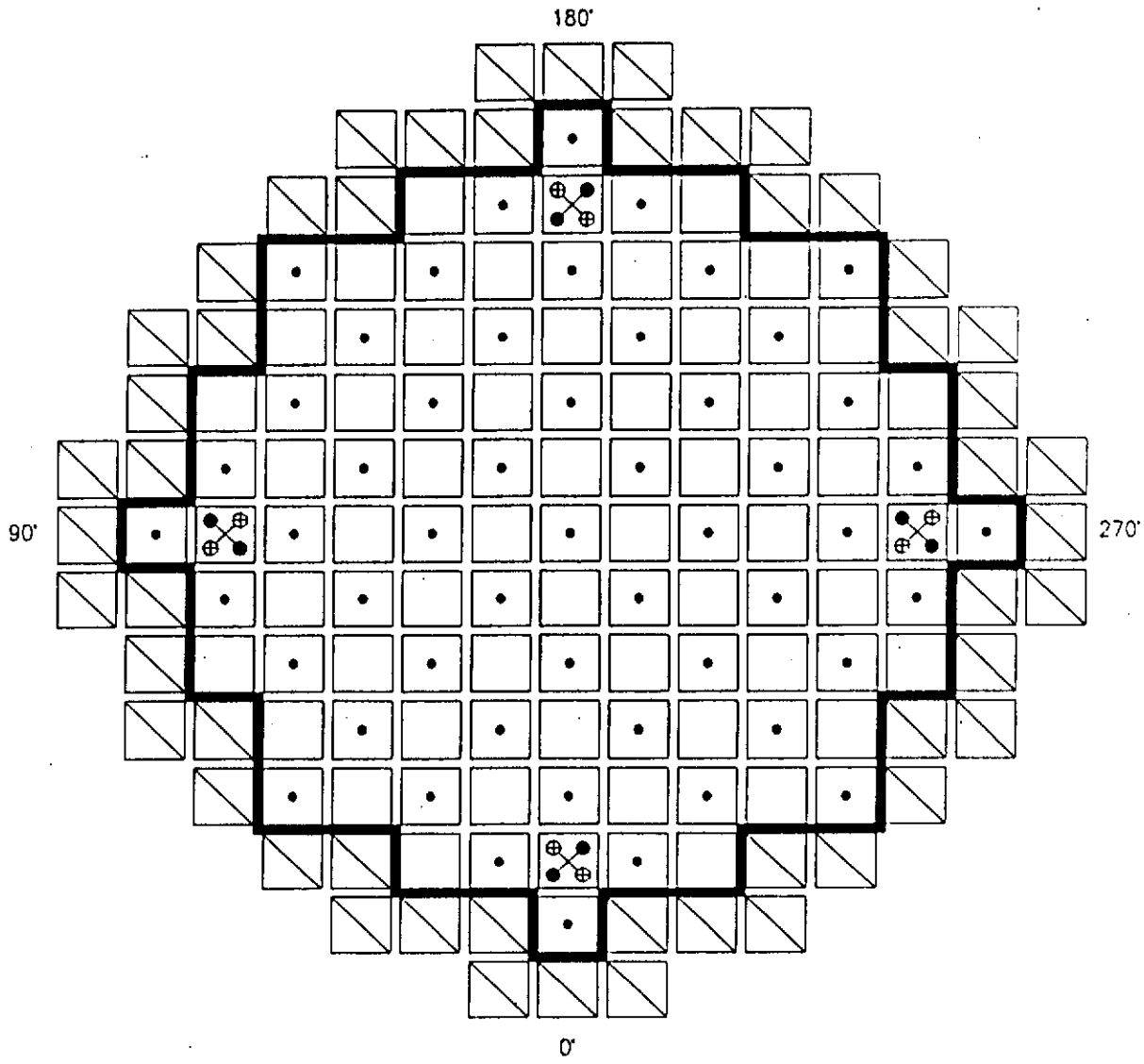

PRIMARY — SECONDARY

– PRIMARY SECONDARY SOURCE ASSEMBLY

– REGION 1 53 ASSEMBLIES

– REGION 2 52 ASSEMBLIES

– REGION 3 52 ASSEMBLIES

NOTE: CORRESPONDING LOCATIONS FOR CURRENT CYCLES ARE GIVEN IN THE APPENDICES 14A AND 14B.

REV. 15 (4/98)

FLORIDA POWER & LIGHT COMPANY
TURKEY POINT PLANT UNITS 3 & 4

THREE REGION CORE LOADING

FIGURE 3.2.3-3

FILE: FTM00258.DWG

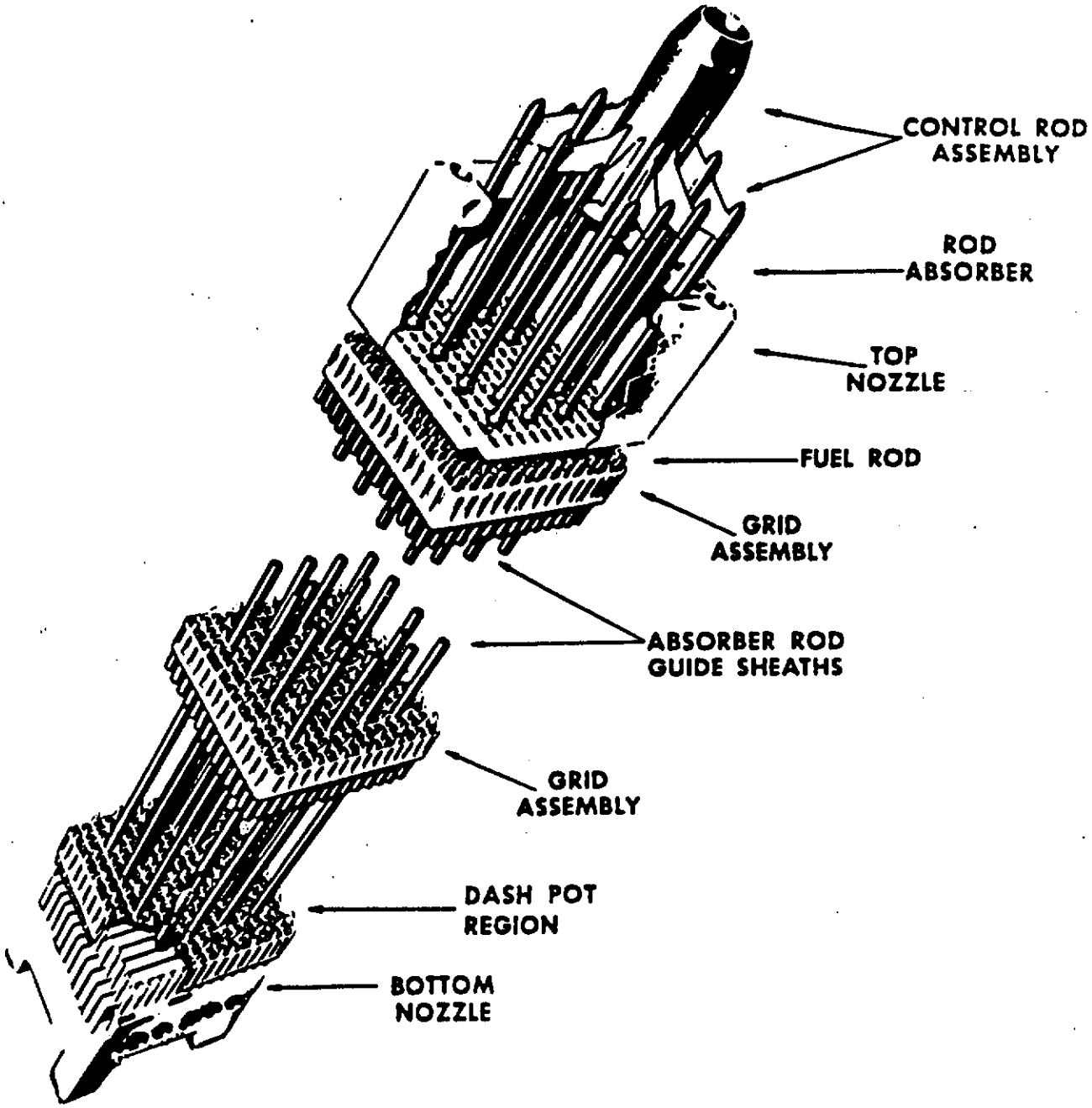

TYPICAL ROD CLUSTER CONTROL ASSEMBLY
FIG. 3.2.3-4

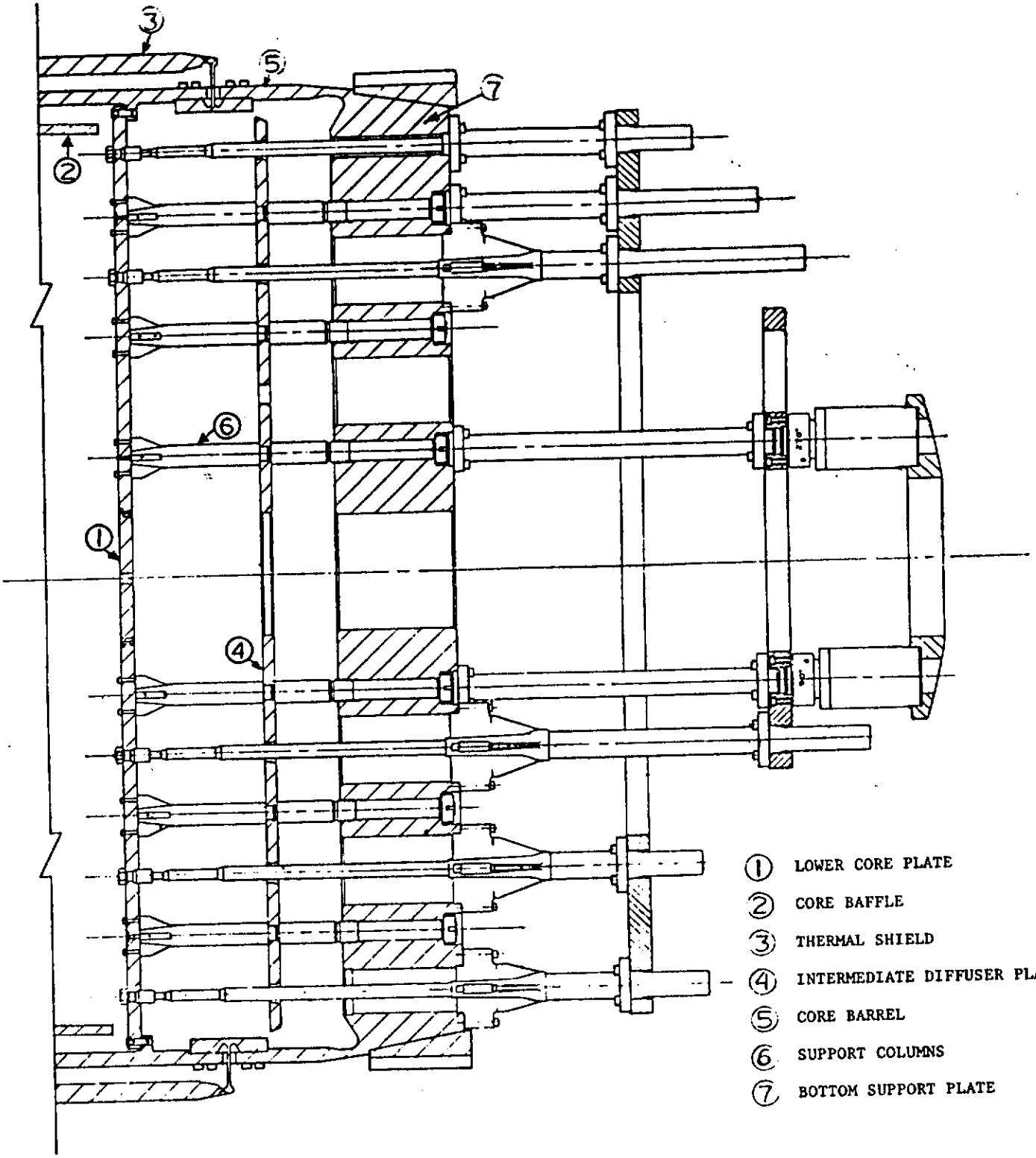

LOWER CORE SUPPORT ASSEMBLY
FIG. 3.2.3-5

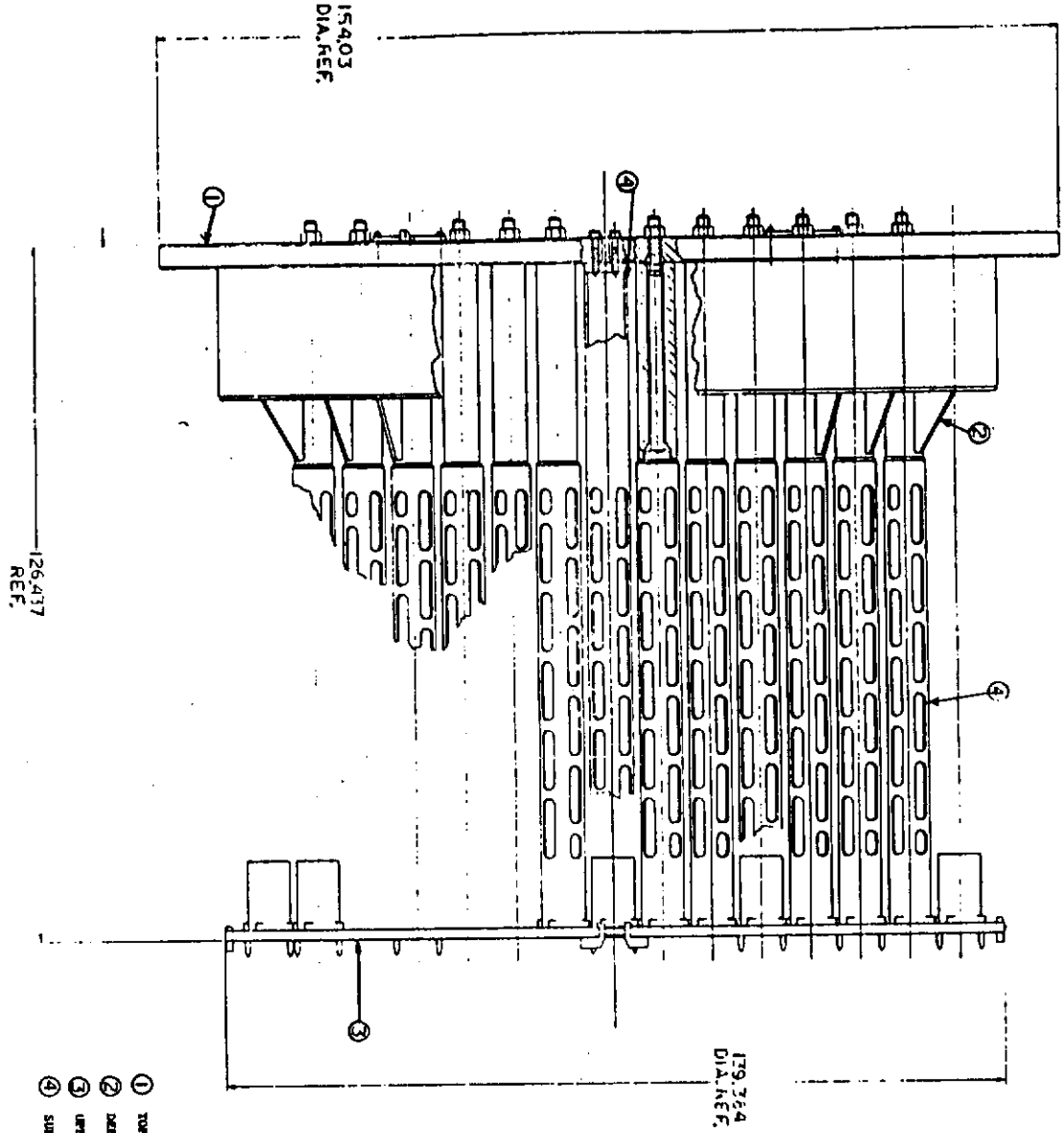

UPPER CORE SUPPORT ASSEMBLY
FIG. 3.2.3-6

UPPER CORE SUPPORT ASSEMBLY

FIG. 3.2.3-6

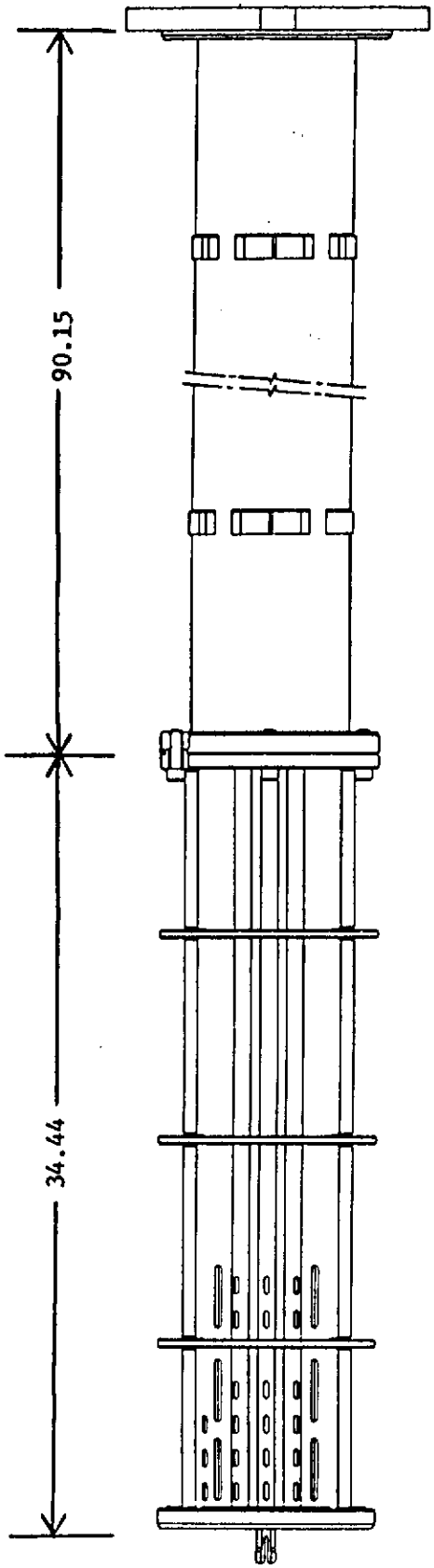

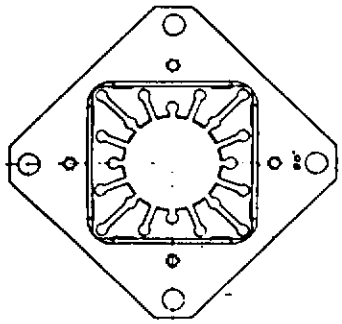

TOP VIEW

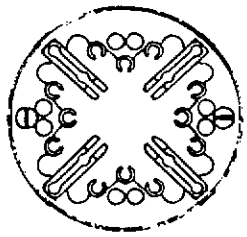

BOTTOM VIEW

GUIDE TUBE ASSEMBLY
FIG. 3.2.3-7

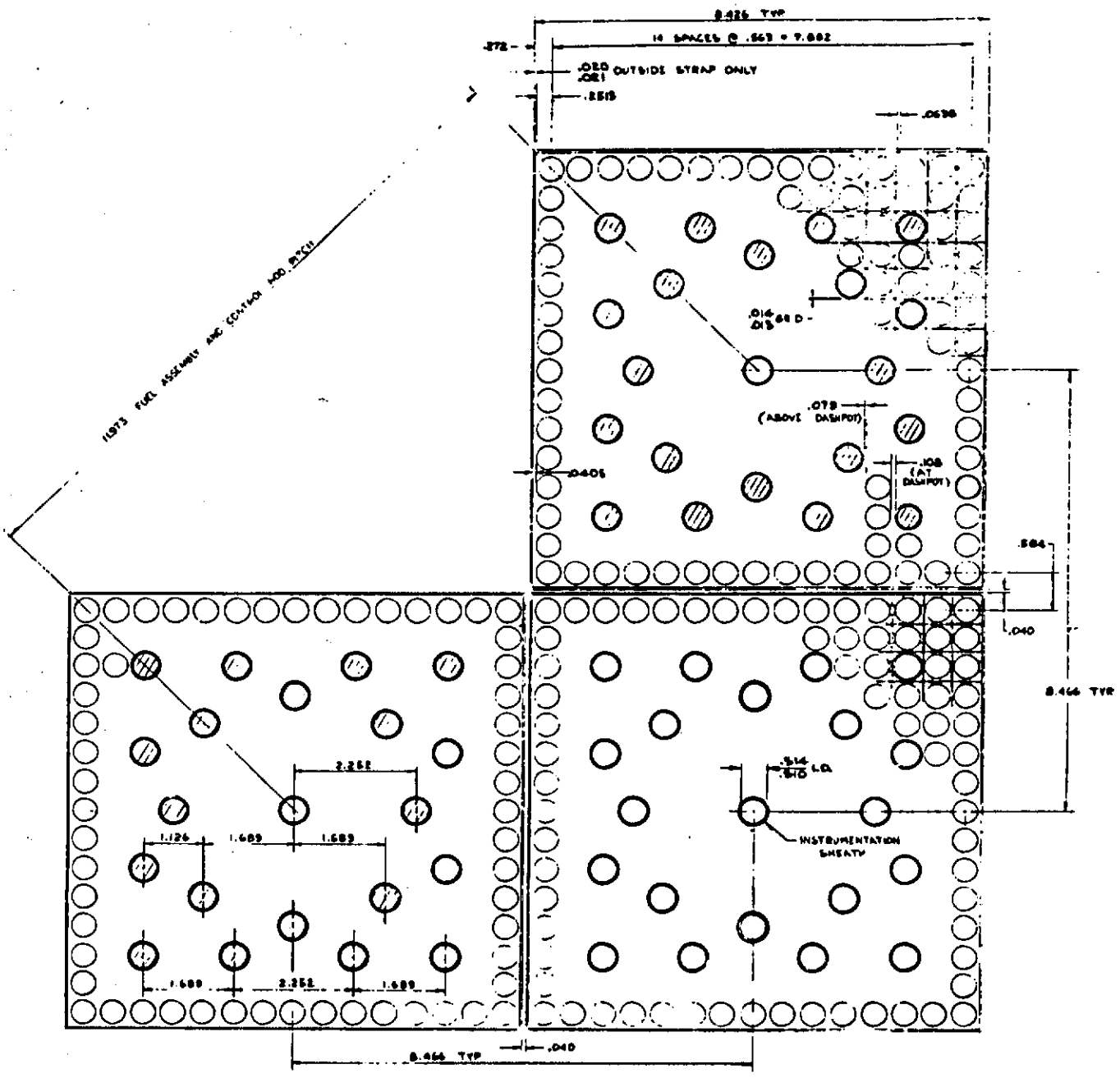

FUEL ASSEMBLY AND CONTROL CLUSTER CROSS SECTION
FIG. 3.2.3-8

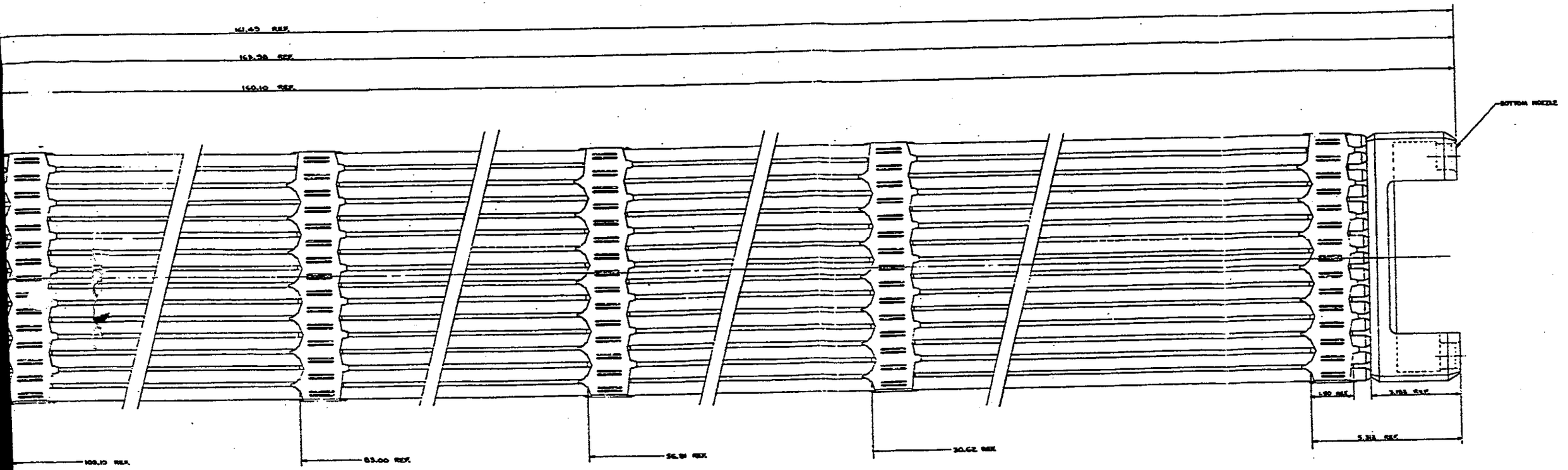

FUEL ASSEMBLY OUTLINE
FIGURE 3.2.3-9

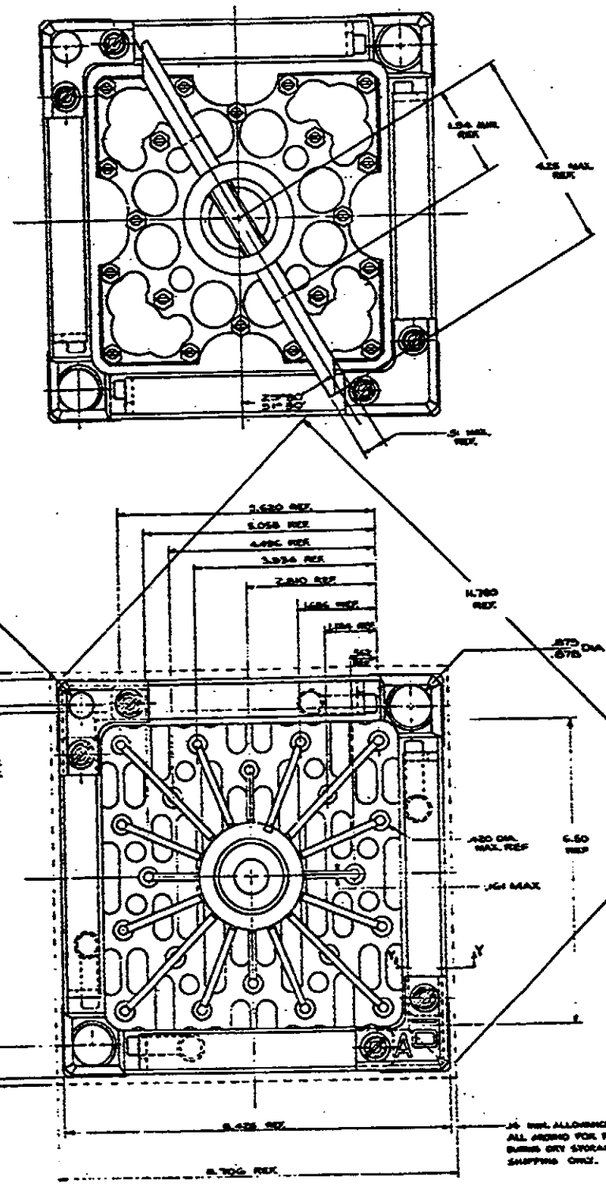
1.630 REF.
1.058 REF.
.447 DIA
.500
.370 REF.
.875 DIA
.878
.420 DIA MAX REF
6.50 REF
.434 MAX
6.706 REF.
6.436 REF.
.14 MIN. ALLOWANCE REQUIRED ALL AROUND FOR PROTECTIVE COVER DURING DRY STORAGE & DRY SHIPPING ONLY.

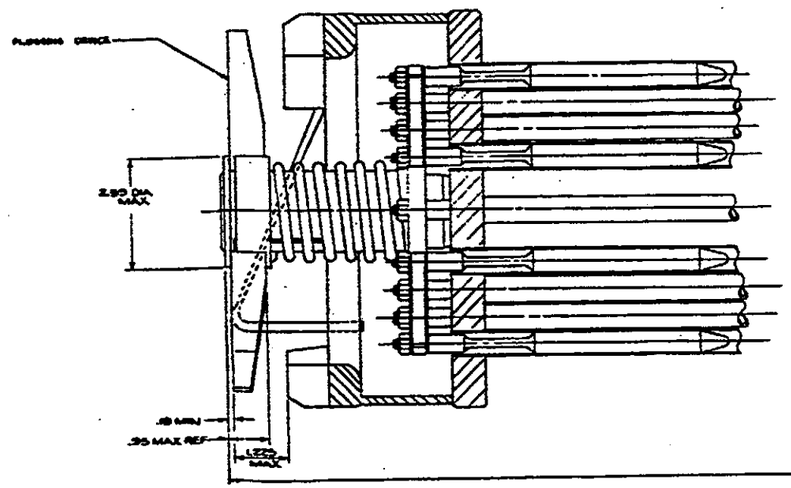
2.90 DIA MAX
.19 MIN
.95 MAX REF
1.222 MAX

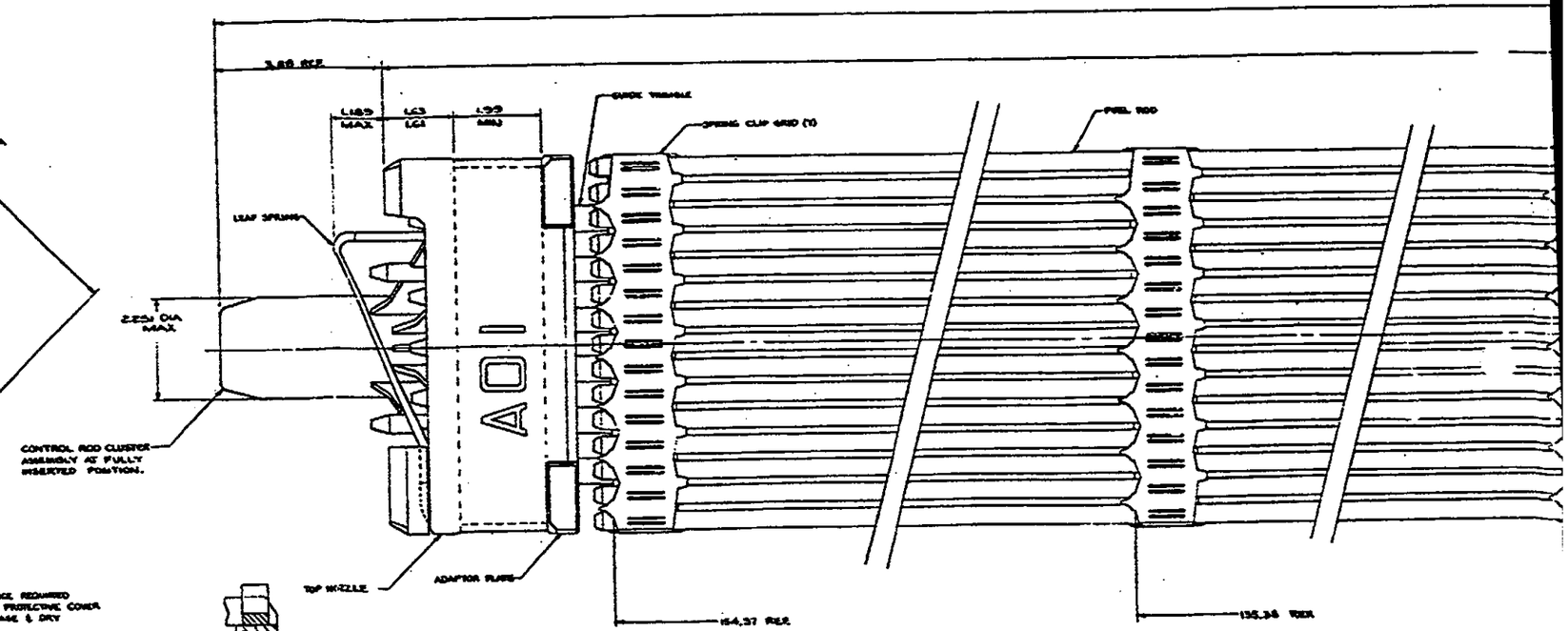
3.88 REF.
1.185 MAX
1.63 1.64
1.39 MIN
GUIDE THIMBLE
SPRING CLIP GRID (1)
FUEL ROD
LEAF SPRING
2.224 DIA MAX
CONTROL ROD CLUSTER ASSEMBLY AT FULLY INSERTED POSITION.
A01
TOP NOZZLE
ADAPTOR PLATE
154.37 REF.
135.34 REF.

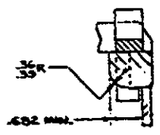
.36R .33
.682 MIN.

SECTION Y-Y

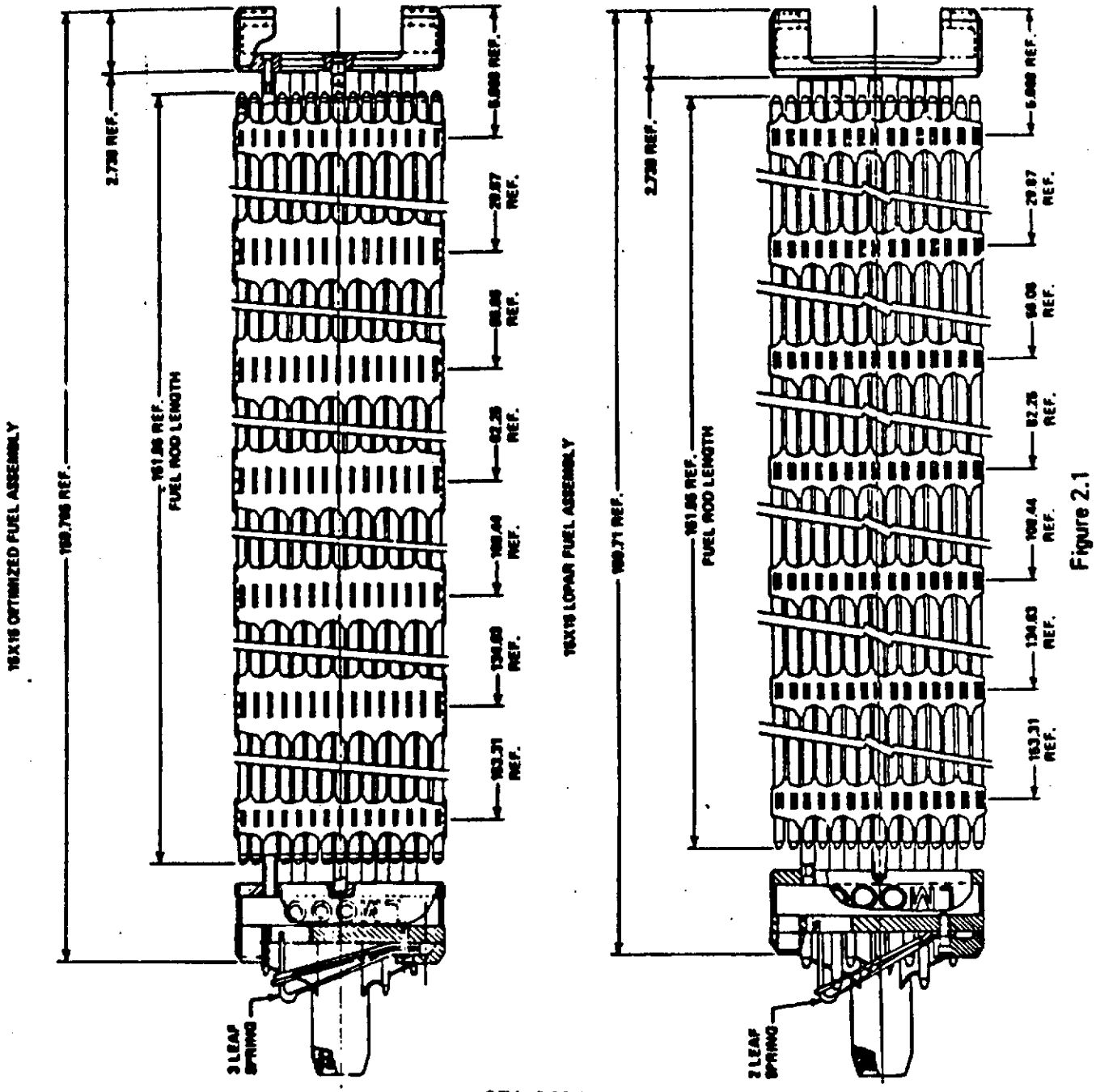

Figure 2.1

OFA-LOPAR FUEL
ASSEMBLY OUTLINES

FIG. 3.2.3-9A

Rev. 2-7/84

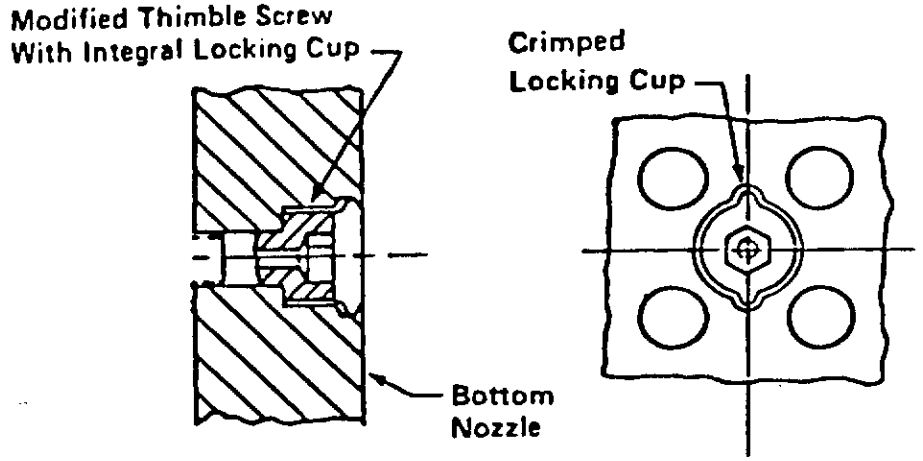

a) Reconstitutable Bottom Nozzle Design

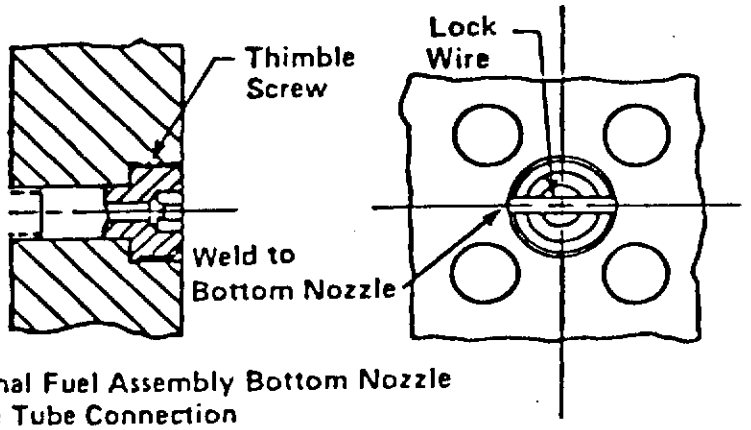

b) Conventional Fuel Assembly Bottom Nozzle
To Thimble Tube Connection

Rev. 4-7/86

BOTTOM NOZZLE TO THIMBLE
TUBE CONNECTION

FIG. 3.2.3-9B

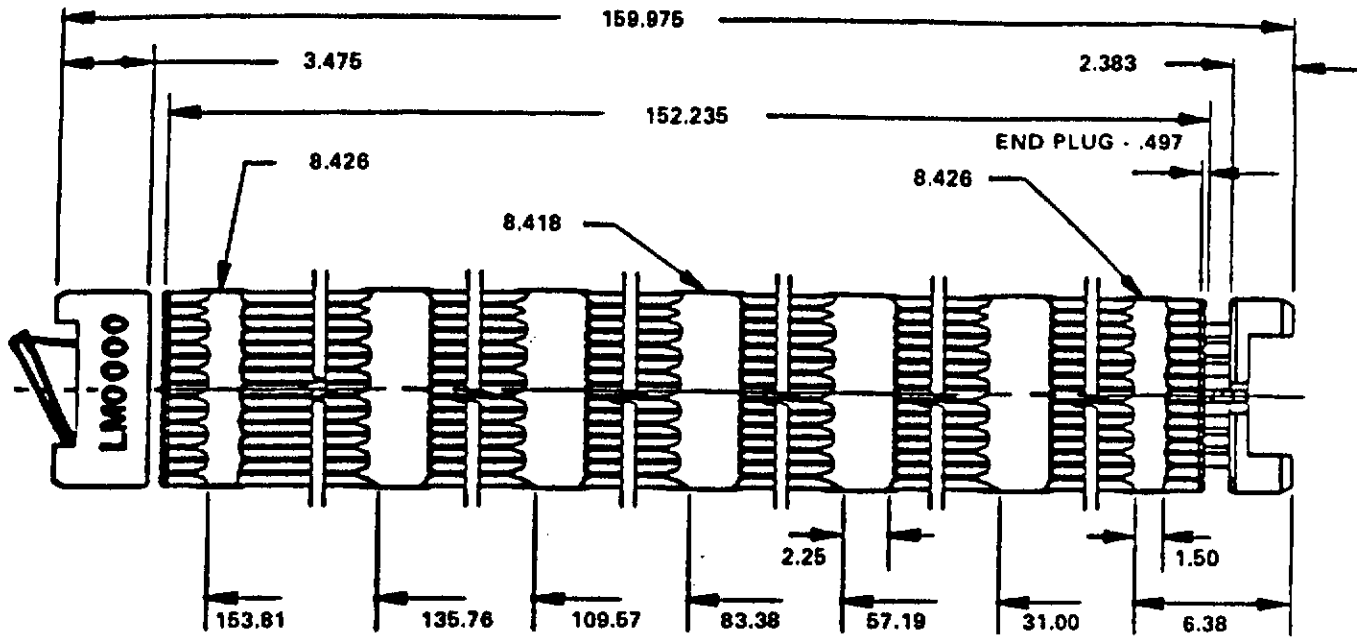

15X15 OFA FUEL ASSEMBLY

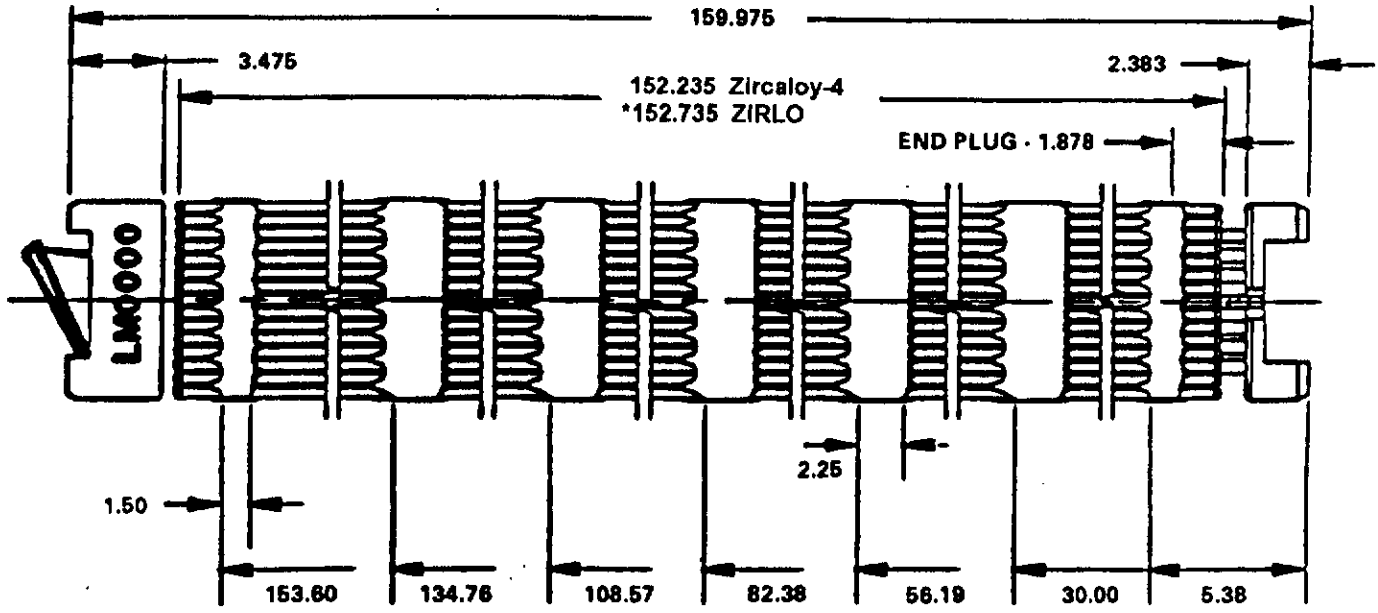

15X15 DEBRIS RESISTANT FUEL ASSEMBLY

* BEGINNING WITH UNIT 3 CYCLE 17

REV 16 (10/99)

FLORIDA POWER & LIGHT COMPANY
TURKEY POINT PLANT UNITS 3 & 4

15X15 OFA/DRFA
FUEL ASSEMBLY COMPARISON

FIGURE 3.2.3-9C

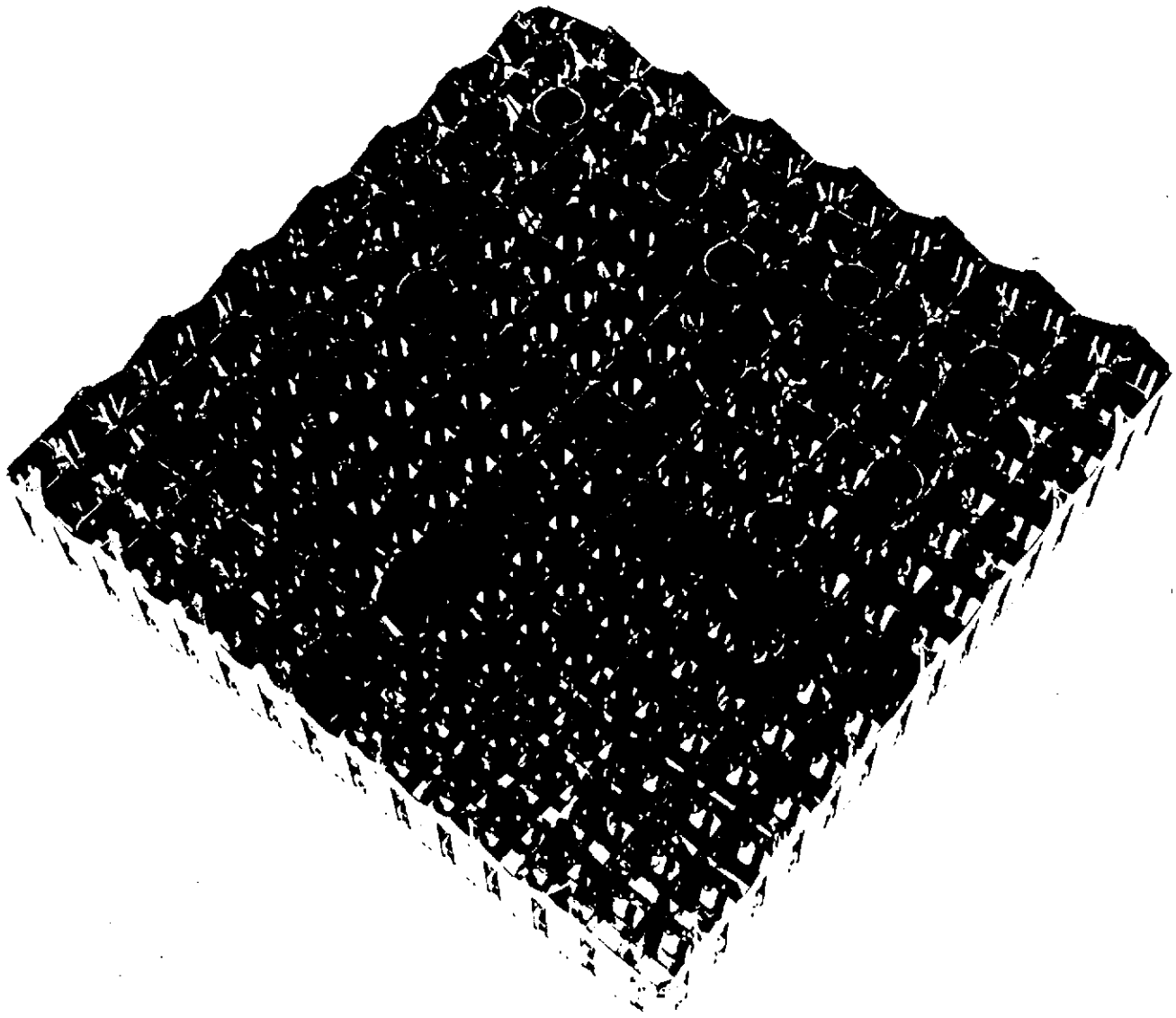

SPRING CLIP GRID ASSEMBLY

FIGURE 3.2.3-10

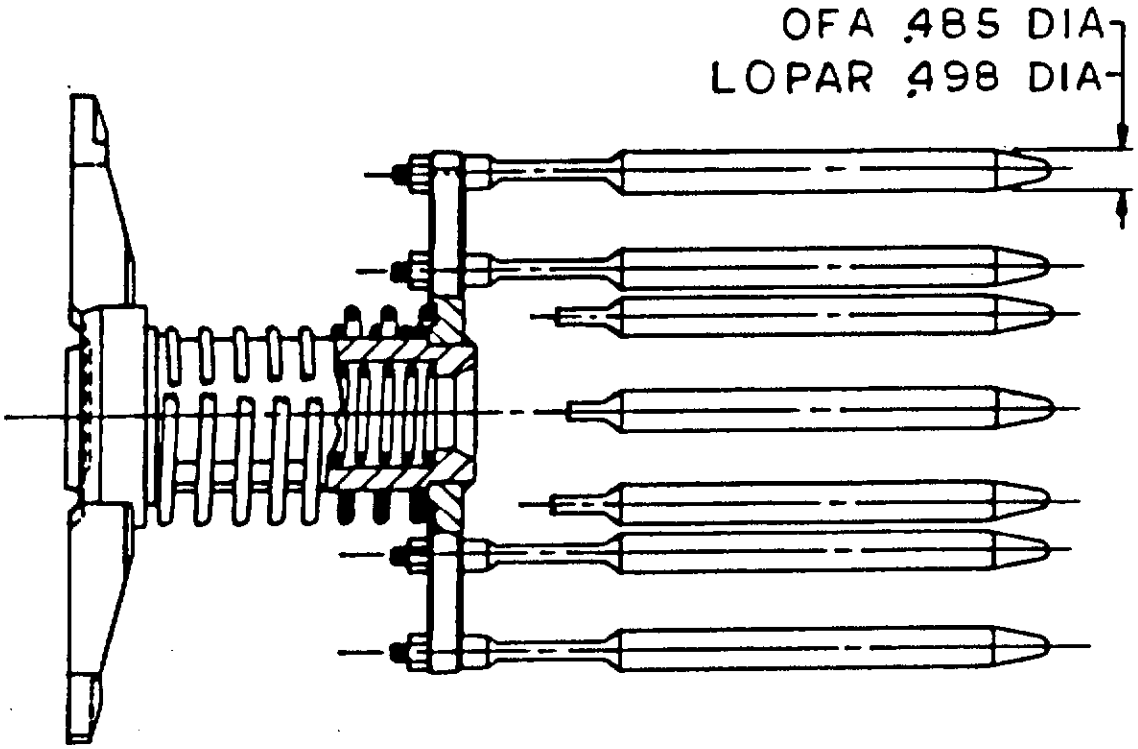

NOTE: ALL OR ANY COMBINATION OF THESE DEVICES CAN BE REMOVED FROM THE CORE.

Rev 8 7/90

COMPARISON OF OFA
AND LOPAR PLUGGING DEVICE

FIG. 3.2.3-10A

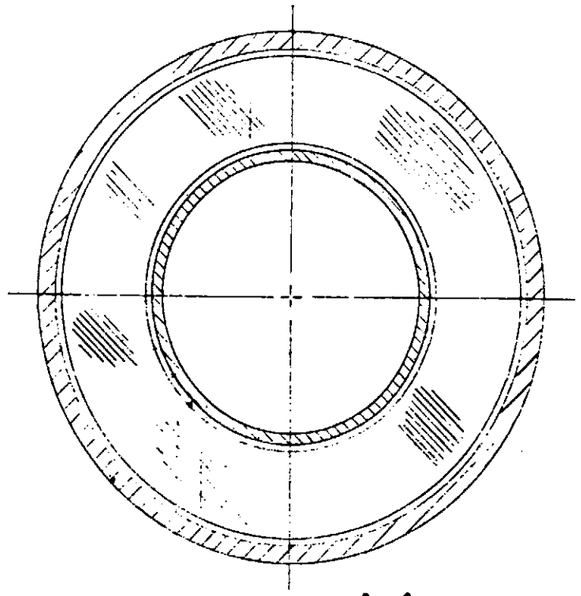

SECTION A-A
SCALE 10:1

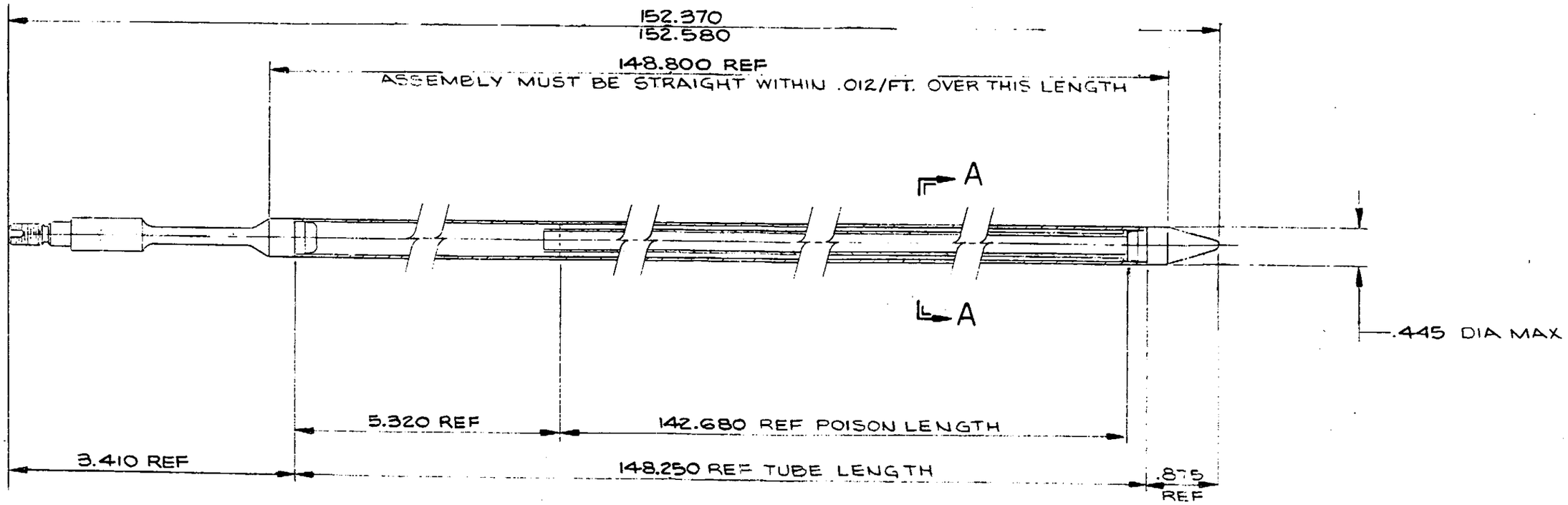

DETAIL OF BURNABLE POISON ROD
FIGURE 3.2.3-11

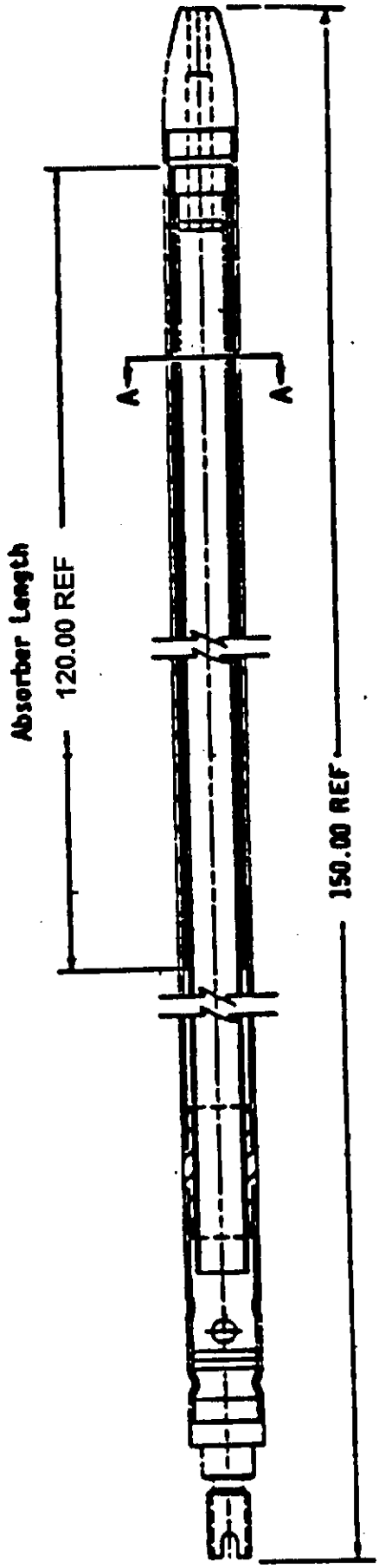

REV 16 (10/99)

WET ANNULAR BURNABLE
ABSORBER ROD

FIG. 3.2.3-11A

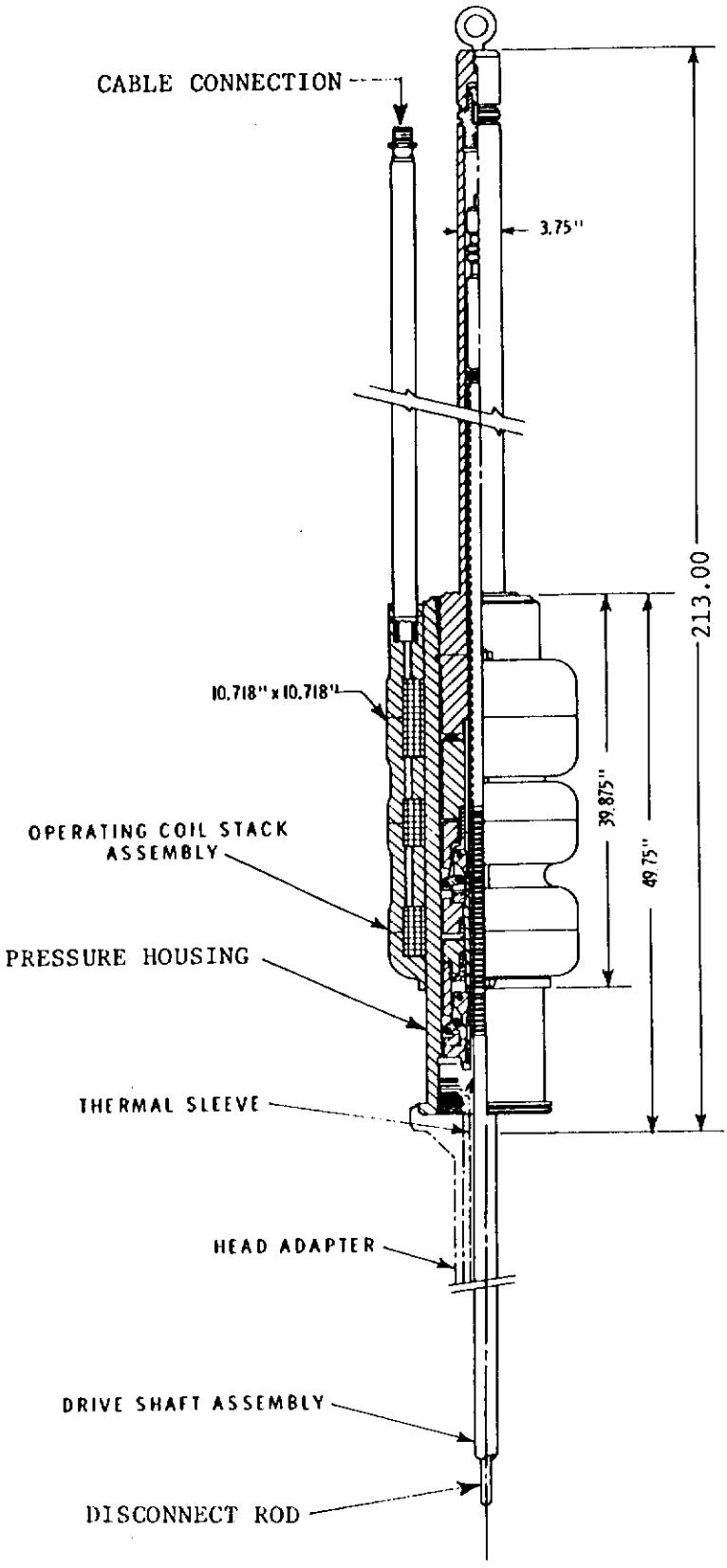

CONTROL ROD DRIVE MECHANISM ASSEMBLY

FIG. 3.2.3-12

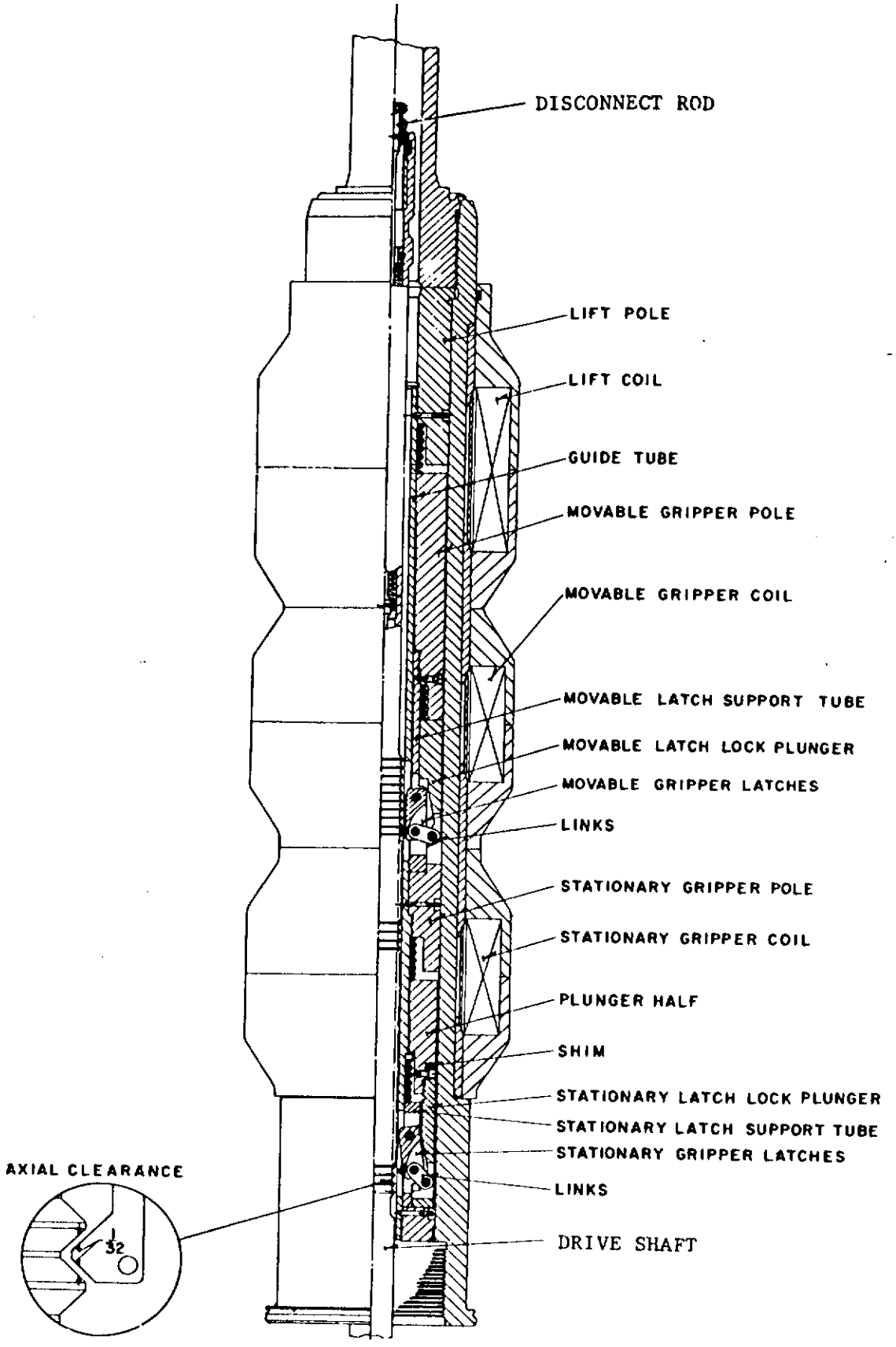

CONTROL ROD DRIVE MECHANISM SCHEMATIC
FIG. 3.2.3-13

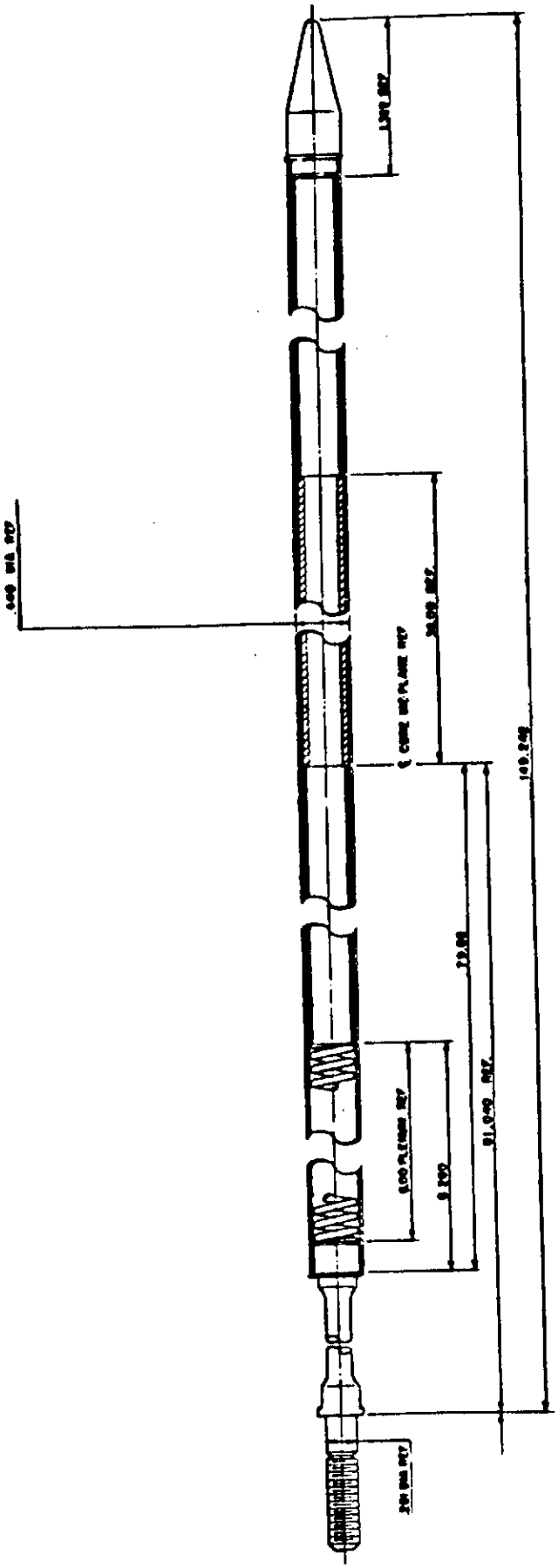

Rev. 4-7/86

REDUCED LENGTH HVFD
ABSORBER ROD

FIG. 3.2.3-14

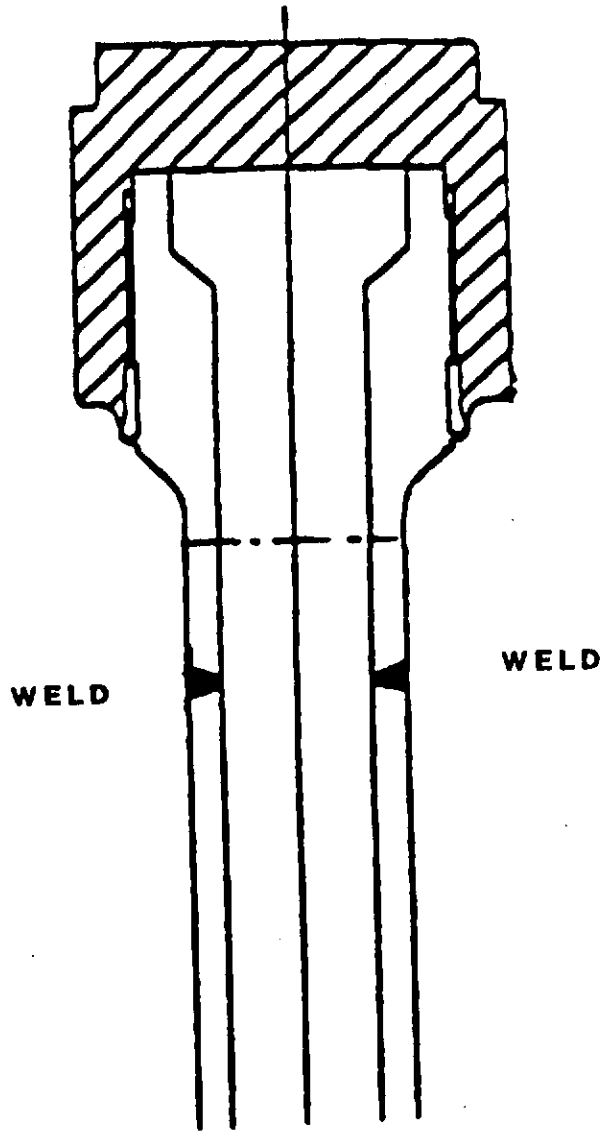

REV. 6 (7/88)

FLORIDA POWER & LIGHT COMPANY
TURKEY POINT PLANT UNITS 3 & 4

HEAD ADAPTER PLUG DESIGN

FIGURE 3.2.3-15

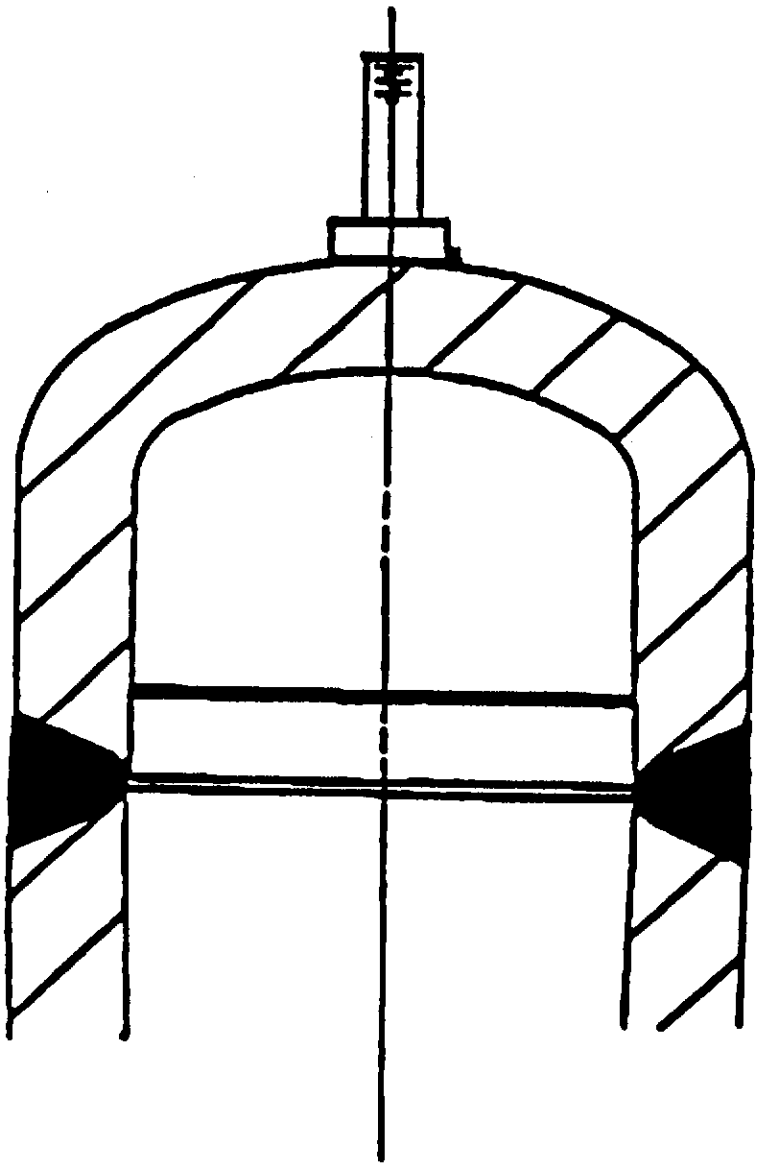

REV. 6 (7/88)

FLORIDA POWER & LIGHT COMPANY
TURKEY POINT PLANT UNITS 3 & 4

PIPE CAP DESIGN

FIGURE 3.2.3-16